Charles University in Prague
Faculty of Mathematics and Physics

MASTER'S THESIS

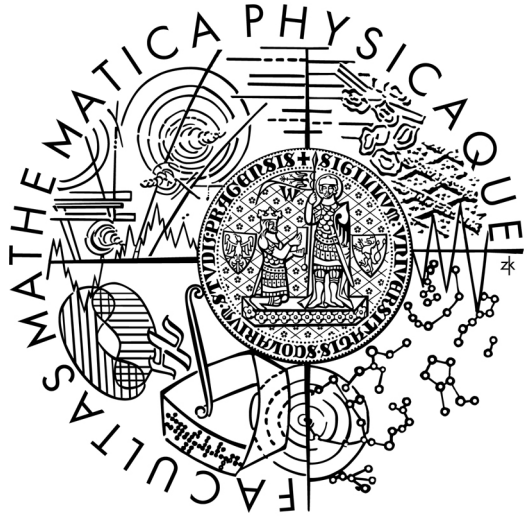

Lukáš Vermach

Mathematical modeling of magnetostrictive materials

Mathematical Institute of Charles University

Thesis advisor:

Priv.-Doz. Dr. habil. RNDr. Martin Kružík Ph.D.,
Institute of Information Theory and Automation of the ASCR, v.v.i.

Study program: Physics
Specialization: Mathematical and computational modelling
in physics and engineering

2011

Rád bych tímto poděkoval svém vedoucímu Priv.-Doz. Dr.habil.RNDr. Martinu Kružíkovi Ph.D.. Jsem mu vděčný za laskavé a trpělivé vedení po dobu necelých tří let mého univerzitního studia. Děkuji za mnoho cenných rozhovorů týkajících se diplomové práce i osobního života. Díky jeho vřelému přístupu bylo pro mě psaní diplomové práce velkým potěšením.

Děkuji své snoubence Lucii Drvotové za postupné přečtení celé práce a odhalení mnoha lingvistických chyb. Její pochopení, podpora a nekonečná trpělivost mi umožnily tuto práci dokončit.

I declare that I carried out this master thesis independently, and only with the cited sources, literature and other professional sources. I understand that my work relates to the rights and obligations under the Act No. 121/2000 Coll., the Copyright Act, as amended, in particular the fact that the Charles University in Prague has the right to conclude a license agreement on the use of this work as a school work pursuant to Section 60 paragraph 1 of the Copyright Act.

In Prague, 3rd August 2011 Lukáš Vermach

Název práce:	Matematické modelování magnetostriktních látek
Autor:	Lukáš Vermach
Katedra (ústav):	Matematický ústav Univerzity Karlovy
Vedoucí diplomové práce:	Priv.-Doz. Dr. habil. RNDr. Martin Kružík Ph.D., Ústav teorie informace a automatizace AV ČR, v.v.i.
e-mail vedoucího:	kruzik@utia.cas.cz

Abstrakt

V předložené práci je sestaven izotermický matematický model materiálů s feromagnetickou tvarovou pamětí (FSMA). FSMA jsou speciální třídou tzv. magnetostriktních látek, materiálů, u nichž lze měnit tvar vzorku aplikací magnetického pole a naopak vyvolávat změny magnetizace namáháním vzorku. Podstatou této vlastnosti jsou fázové přechody uvnitř materiálu, k nimž dochází během zatěžování vzorku.

Nejprve je zformulován stacionární model FSMA. Je sestaven termodynamický potenciál (zde Helmholzova volná energie) a je ukázáno, že není kvazikonvexní. Kvazikonvexifikace je provedena pomocí teorie relaxace, tj. konstrukcí kvazikonvexní obálky. Pro takto sestavený model je provedena existenční analýza.

Výsledky stacionárního modelu jsou následně využity k modelu časového vývoje, přičemž pozornost je věnována hystereznímu chování, které vzniká v důsledku disipace volné energie. Časová diskretizace vede na sekvenci hysterezí modifikovaných stacionárních úloh (koncept energetického řešení). S využitím existujících abstraktních výsledků je dokázána existence energetického řešení pro model FSMA. Model se opírá o experimentální skutečnost, že disipace energie během fázových přechodů nezávisí na rychlosti, s jakou fázové přechody probíhají.

Výhodou použitého přístupu je mj. i přímočará implementace modelu, která je popsána v závěru textu. Součástí práce jsou též konkrétní výsledky pro různé kombinace typů materiálu a zatížení.

Klíčová slova: Magnetická tvarová paměť'; magnetostriktní látky

Title: Mathematical modeling of magnetostrictive materials
Author: Lukáš Vermach
Department: Mathematical Institute of Charles University
Advisor: Priv.-Doz. Dr. habil. RNDr. Martin Kružík Ph.D.,
Institute of Information Theory and Automation,
Academy of Sciences of the Czech Republic
Advisor's e-mail address: kruzik@utia.cas.cz

Abstract

In the present work we introduce an isotermic mathematical model of ferromagnetic shape memory alloys (FSMAs). FSMAs are a special class of magnetostrictive materials, i.e. materials which deform their shape on account of external magnetic field or which change magnetization as a consequence of strain. This property originates from phase transformations that occur within the material when being exposed to external loading.

First, the stationary model of FSMA is formulated. The thermodynamical potential is composed (Helmholz free energy) and its non-quasiconvexity is discussed. The quasiconvexification is performed via the relaxation theory, i.e. quasiconvex envelope construction. For such a model the existence theory is built.

Then, taking advantage of the stationary case the evolutionary model is developed. The attention is drawn to hysteresis, which arises from energy dissipation. The time discretization leads to a sequence of hysteresis-modified stationary problems (the concept of energetic solution). Benefiting from the existing abstract results, the existence of the energetic solution for FSMA is shown. The model relies on the experimental fact that the energy dissipation is a rate-independent process.

The advantage of the formulated model is its straightforward numerical implementation. Numerical aspects of the model are discussed in the final part of the thesis. Several concrete results are included for various combinations of a material type and loading.

Keywords: Magnetic shape memory; Magnetostrictive materials

Contents

List of Figures

Chapter 1

Introduction

Magnetostriction can be defined as "the change in dimension of a piece of magnetic material induced by a change in its magnetic state[1]." Magnetostrictive materials, in general, are materials with the ability to change their shape due to an external magnetic field or embody change in magnetization when being deformed. It is one of the properties that accompanies ferromagnetism.

Although the phenomenon of magnetostriction is a relatively complex subject matter that arises from processes on the atomic level, it is very easy to get in touch with magnetostriction in daily life. The effect of magnetostriction is responsible for the characteristic hum of transformers and other high power electrical devices that we meet every day. As the transformer takes advantage of electromagnetic induction, there is a huge magnetic field surrounding the device. The iron material associated with the core of the transformer replies mechanically to the magnetic field and consequently produces the hum. Since the frequency of the AC electricity in EU is 50 Hz, the frequency of the characteristic (and also annoying) hum is 100 Hz.

The effect of magnetostriction could be understood through the domain structure of a ferromagnetic body and energy associated with this structure. Domains are regions of approximately constant magnetization. Dimension change is connected with redistribution of domain structures responding to an applied external magnetic field. Each of the magnetic domains is distorted by inter-atomic forces in a way so as to minimize the total energy of the sample.

Considering one of these domains, material with positive (negative) magnetostriction

[1] the definition introduced in BUSCHOW K.H.J., DE BOER F.R.: *Physics of Magnetism and Magnetic Materials,* Kluwer Academic/Plenum Publishers, New York, 2003.

embodies extension (contraction) of a domain along magnetization direction while the material simultaneously embodies contraction (extension) perpendicular to magnetization direction, keeping the volume unchanged (see the figure 1.1). The magnetostrictive body is a complex of many magnetostrictly distorted domains. Application of the external magnetic field causes dislocation of boundaries between magnetic domains and rotation of magnetization direction within a domain to achieve the "satisfactory" location (with lowest total energy). This process is accompanied with growth of domains with magnetization direction close to the field direction at the cost of domains whose magnetization direction differs more from the field direction. These two mechanisms result in macroscopic dimension change of the specimen. The process of reorientation of domains is far more complicated. However, the main idea remains: the rotation and the movement of magnetic domains cause deformation of the shape of the material (for more detailed discussion see e.g. [3] or [14]).

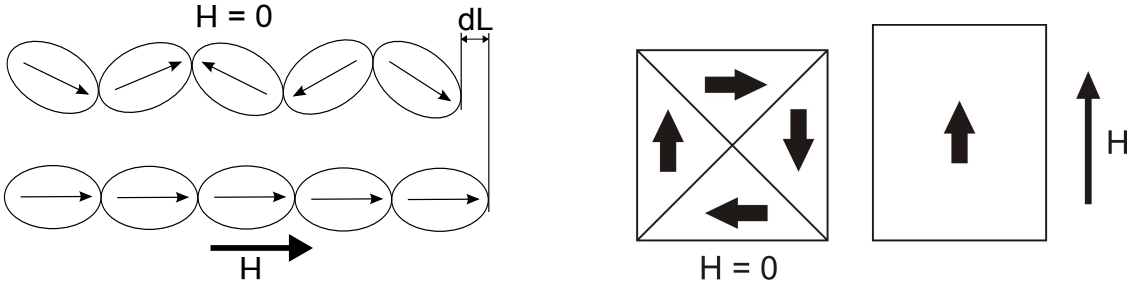

(a) Domain rotation (b) Domain wall motion

Figure 1.1: Schematic representation of principles that produce magnetostriction. When there is no magnetic field applied, the domains are distorted in order to reduce the magnetostatic energy. Magnetical loading of the sample causes dislocation of the domain boundaries which enables rotation of magnetization direction (1.1(a)) and consequently growth of domains that have magnetization aligned to the external field (1.1(b)).

The above described process is the most common type of magnetostriction and it is usually referred to as Joule[2] magnetostriction. Considering a single crystal, the deformation of the material will reflect symmetry of the crystal lattice. Let us describe a simple case of a cubic material. If tested, the prolongation of the sample depends on direction of loading as well as on initial and final direction of magnetization. As explained in [3], the strain (fractional length change) might be described by only two magnetostrictive constants λ_{100}

[2]Historically, it was James P. Joule who first described the phenomenon of magnetostriction in 1842. Joule studied a nickel sample.

and λ_{111} via

$$\frac{\Delta l}{l} = \frac{3}{2}\lambda_{100}\left(\alpha_x^2\beta_x^2 + \alpha_y^2\beta_y^2 + \alpha_z^2\beta_z^2 - \frac{1}{3}\right) + 3\lambda_{111}\left(\alpha_x\alpha_y\beta_x\beta_y + \alpha_x\alpha_z\beta_x\beta_z + \alpha_y\alpha_z\beta_y\beta_z\right).$$

The parameters α, β stand for direction cosines of the magnetization orientation and loading of the length-measurement direction, respectively. Magnetostrictive constants $\lambda_{100}(\lambda_{111})$ represent change in length or saturation magnetostriction in the [100]([111]) direction when the magnetization direction is also along the [100]([111]) direction after the material has been cooled through its Curie temperature. We provide values of magnetostrictive constants for several cubic materials in table 1. As one might see, magnetostriction constants in pure metals are on order of 10^{-6}. Thus, the resulting shape change is very small and so the application in engineering is limited.

Material	$\lambda_{100}(10^{-6})$	$\lambda_{111}(10^{-6})$
Fe	24	-22
Ni	-51	-23
$TbFe_2$	-	2460
$SmFe_2$	-	-2100

Table 1.1: The magnetostriction constants for particular cubic materials at room temperature. Data are taken from [3]. The negative values of the constants correspond to the shortening of the sample due to external magnetic field.

The effect of magnetostriction might be strengthened by alloying suitable elements. The highest magnetostriction was achieved in iron alloys containing rare earth elements Dysprosium and Terbium. The effect is more than 100 times stronger. Thus, it is referred to as giant magnetostriction. For illustration, see table 1 that also contains magnetostriction constants for $DyFe_2$ and $TbFe_2$. However, these alloys require large magnetic fields to embody magnetostriction since both (Terbium and Dysprosium) suffer from large anisotropy. Benefiting from the fact that anisotropies in these elements are in opposite directions, it was proposed to use an alloy incorporating Tb, Dy and Fe. The resulting material named TERFENOL-D[3] fullfiled the expectations. At room temperature it exhibits deformation up to 2000 microstrains (corresponds to 0.2% fractional length change) in the field of 2kOe[4]. The stoichiometric formula of TERFENOL-D is $Tb_xDy_{1-x}Fe_2$, with $x \approx 0.3$. This giant magnetostrictive material found its use in a great number of applications such as

[3]The material was devoloped in Naval Ordnance Labs, US. The name is abbreviation of terbium (TER), iron (FE), Naval Ordnance Labs (NOL), and Dysprosium (-D).

[4]Oe is the unit of magnetic field intensity in the CGS system of units. 1 Oe is equivalent to $1000/4\pi A/m$

magnetomechanical sensors, actuators, and acustic and ultrasonic transducers.

In this work we are interested in a special subclass of magnetostrictive materials called ferromagnetic shape memory alloys (FSMA). Besides domain wall motion and domain rotation, in FSMAs the magnetostriction is driven by shape memory effect - solid-to-solid phase transformation that occurs within the alloy. The shape memory effect represents strong contribution to Joule magnetostriction. Thus, FSMAs have exbited approximately five times larger strains than TERFENOL-D. Additionally, in these materials, magnetically induced strain is produced fast and without need of external temperature change (unlike classical shape memory alloys). This property together with large strains production make FSMA attractive for applications since FSMA-based devices (actuators, sensors) can operate in high frequencies. In order to introduce the matter of shape memory effect in more detail we devote the whole chapter 2 to this topic.

(Ferromagnetic) shape memory alloys represent extremely exciting category of materials that is worth studying. Modelling of FSMAs is interesting from physical as well as mathematical point of view. Mathematical modelling of such systems is rather complicated since the thermodynamic potentials describing the material are generally not (quasi)convex. Therefore, the stable configuration of the systems can not be found as an energy minimizer, but has to be described via construction of a minimizing sequence. Furthermore, considering the evolutionary model the effect of hysteresis has to be taken into account. Before we proceed to detail analysis of FSMAs, let us set up our goals first.

1.1 Tasks and objectives of the work

In the present work we study mathematical aspects of modelling of ferromagnetic shape memory alloys (FSMAs), a special class of magnetostrictive materials. The tasks of the thesis are as follows:

1. Become familiar with the mathematical and physical theory of micromagnetism. Put special emphasis on the theory describing ferromagnetic materials and the mechanism that gives rise to magnetic domains. Learn methods necessary for (F)SMA modelling.

2. Study the direct method of calculus of variations.

3. Formulate the stationary model of FSMA. Analyse the model with respect to solution existence.

4. Formulate the evolutionary model of FSMA. Analyse the model with respect to solution existence.

5. Based on the previous two items, implement 2D model of FSMA that would be useful for quantitative analysis.

6. Discuss the model and confront it with available experimental data.

The structure of the text naturally follows the aforementioned points. In the first part of the work we present physical and mathematical bases for our model. We start from the assumption that the material is continuous, neglecting microscopic consequences. Thus, considering small deformation, several results of continuum mechanics are introduced in chapter 3. In chapter 4, the fundamentals of magnetism as well as the mathematical model of micromagnetism are presented. Mathematical analysis is also included within the chapter.

In the second part, we formulate a model combining linear elasticity and micromagnetism. Chapter 5 introduces the stationary model combining mechanical and magnetical behaviour. First, the appropriate thermodynamical potential (Helmholz free energy) is constructed and the non-(quasi)convex properties are discussed. Then, the quasiconvexification is performed via standard methods of calculus of variations. Using the relaxation theorem we construct the quasiconvex envelope. The existence result is provided under certain conditions. Based on the analysis of the stationary model, the evolutionary model of FSMA is introduced in chapter 6. Taking advantage of the fact that the hysteresis is observed to be rate-independent, we construct the energetic model of the material and prove the existence result.

Additionally, we provide several (both stationary and evolutionary) numerical simulations in chapter 7. The aim is to demonstrate functionality and reasonable behaviour of the formulated mathematical model(s).

Chapter 2

Shape memory materials

In this chapter we present phenomenological description of FSMA and we provide physical information in sense of experimental data examples and figures. The aim of the chapter is to make the reader familiar with the discussed material. Additionally, we provide several applications of FSMA. Altogether, we wish to share the idea that topic of FSMA represents rather interesting matter.

When introducing FSMA, we naturally start with more famous class of active materials, the so called shape memory alloys. Later on we draw our attention back to the effect magnetostriction and FSMAs.

2.1 Shape memory alloys

Shape memory alloys (SMAs) are materials which are able to recover their original shape after having been deformed by applying heat to the alloy. Such extraordinary phenomenon is referred to as shape memory effect. Additionally, shape memory alloys exhibit other interesting properties - superelasticity and psedoplasticity.

Shape memory effect

The physical reason of the shape memory effect is presence of two stable solid phases in which the material can exist. The phase transformation between the phases within SMAs is evoked by change in temperature. The high-temperature phase with high-symmetry, usually cubic, is called austenite. The low-temperature phase, named martensite, exists in several symmetry-related variants. In NiTi for instance, there are 24 monoclinic variants.

Moreover, according to external loading, martensite can be produced in two forms, the deformed one and the un-deformed (twinned) one.

The martensitic transformation (austenite-to-martensite) is described by four values of temperature: A_s, A_f, M_s, M_f which determine the start and end of each phase, cf. figure 2.1. Having the sample in austenite phase, cooling increases free energy associated with the austenite phase. At certain temperature, free energy exceeds the value of martensite phase and it is no longer energetically suitable for the material to stay in the austenite. Let us denote T_{am} the temperature at which free energy of austenite is equal to free energy of martensite. At temperature $T_{am} > M_s$ the martensitic transformation starts. It is in motion until the temperature M_f is reached. Then the whole sample is in low-temperature phase. Similarly, the reverse (martensite-to-austenite) transformation is driven by heating. It starts at temperature $T_{am} < A_s$ and finishes at A_f. The equilibrium temperature lies just in the middle of M_s and A_s. The difference between M_s and A_f (M_f and A_s) is caused by energy dissipation.

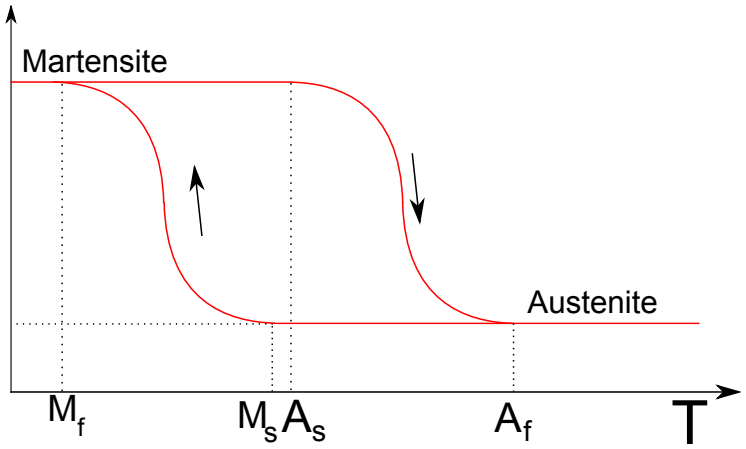

Figure 2.1: Temperature induced austenite-to-martensite transformation. There exist two stable solid phases for shape memory alloy: the high-temperature austenitic and low-temperature martensitic. The martensitic phase occurs in many geometry-related variants. The transformation is described via four temperatures which define beginning and ending of each of the phases.

If the sample is cooled in the absence of applied load, the alloy transforms from austenite into twinned (self-accommodated) martensite. At this stage, all variants are present in the twinned configuration. As a result of this phase transformation, no observable macroscopic shape change occurs, but at this state the material can be easily deformed. Applying external loading to the sample leads to reorientation (detwinning) of martensitic variants

and the specimen moves into a single deformed phase. A relatively large strain is produced via this procedure. The original shape of the body might be recovered by heating upon temperature A_f. The heat transmitted to the specimen is the energy driving the atomic rearrangement of the alloy, similar to heat that melts ice into water, but the SMAs stay solid. The deformed martensite is now transformed to the cubic austenite phase, which is configured in the original shape of the specimen. The situation is schematically shown in Figure 2.2.

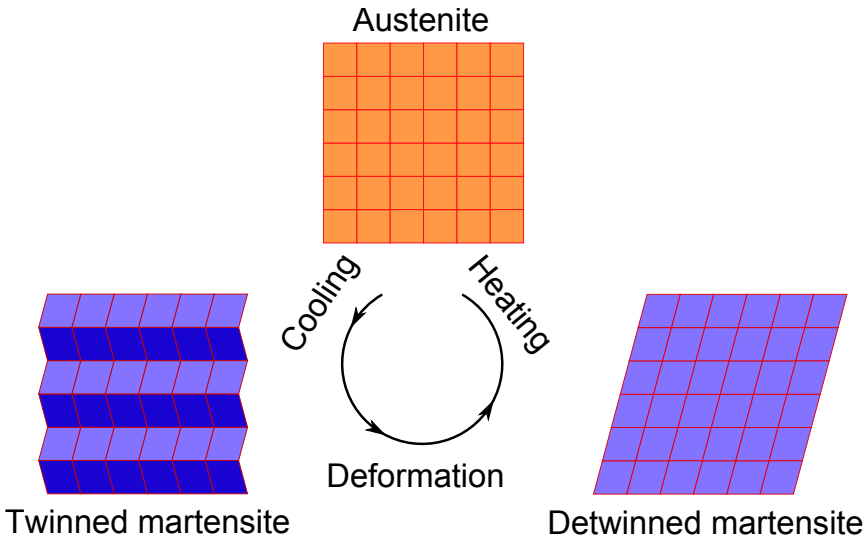

Figure 2.2: Shape memory effect diagram. When being cooled, the sample transforms from the austenitic phase to the martensitic phase. If there is no mechanical loading applied, the material forms a twinning structure (twinned martensite) and no macroscopic strain occurs. Subsequent loading of the sample causes movement of the twin boundaries and growth of a variant that fits the loading best. As a consequence of this process the macroscopic strain is observed. Heating of the sample initiates a reverse martensite-to-austentite transformation and the material returns to its original shape.

Superelasticity and Pseudoplasticity

The austenite-to-martensite transformation can be also reached without cooling. If the sample is loaded in the austenitic state (at temperature $T > A_f$), the material transforms into the most suitable martensitic variant (according to the applied stress). The resulting strain is naturally limited, however, it is fully reversible after the loading is removed (clarify the figure 2.3(a)). Contrary to elastic deformation in common metals, where the strains are relatively small (they rarely reach 0.7%), the elastic response induced by phase

transformation might reach 10%. Such huge elastic deformation is called superelasticity.In contrast to elasticity, the stress-strain curve of superelastic response is nonlinear and always accompanied with hysteresis.

Another interesting feature of SMAs is pseudoplasticity. Like superelasticity, it is also a direct consequence of the phase transformation that might occure in the material. As schematically shown at the figure **??**,in the case of loading in the martensitic phase (at temperature $T < M_s$), the sample is easily deformed within the range of about 5%. In the material are formed such martensitic variants that are in accordance with the loading (tensing or compressing). After creating a suitable variant, the material behaves elastically. The resulting strain might then be plastic. However, when the opposite loading is applied, the initial state might be recovered.

Although the stress vs. strain diagram might resemble behaviour of a common metal, in SMAs there occur no shear dislocations that would cause unrecoverable deformations. It causes only the movement of twin boundaries. Consequently, the material transforms from one martensitic variant to another. Therefore, the plastic deformation of SMAs might reach up to 10% without making irreversible changes in the micro-structure of the alloy.

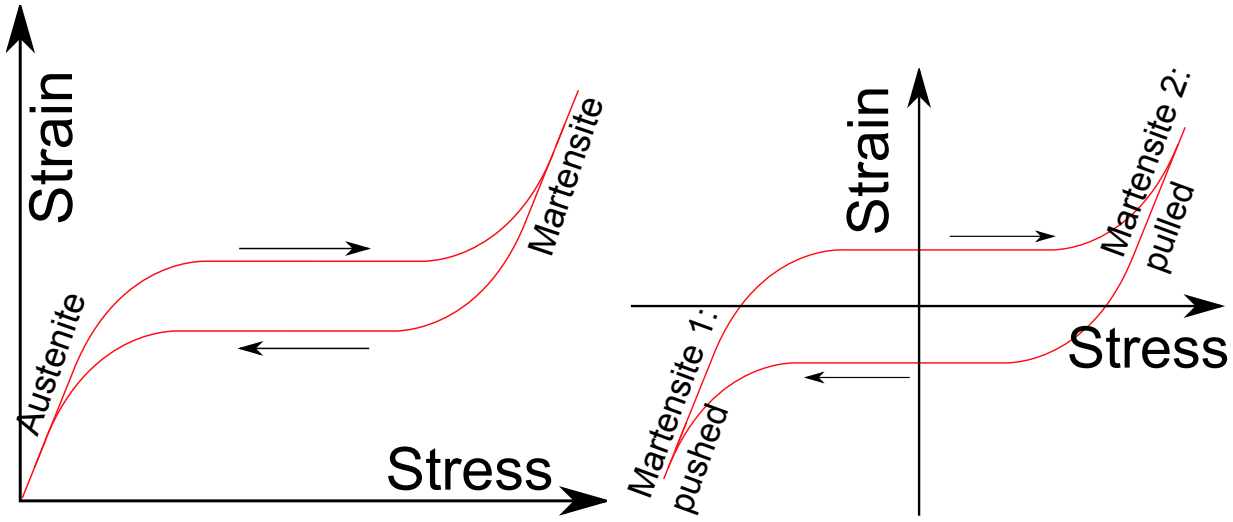

(a) Superelasticity (b) Pseudoplasticity

Figure 2.3: The effect of superelasticity and pseudoplasticity. The possibility of stress-induced austenite-to-martensite and martensite-to-martensite phase transformation within SMAs causes interesting mechanical properties called superelasticity and pseudoplasticity.

Commonly used SMAs are typically made of copper-zinc-nickel (Cu-Zn-Ni), copper-aluminium-nickel (Cu-Al-Ni) or nickel-titanium (Ni-Ti). The unusual properties of the

shape memory offer a wide range of applications, among others in aeronautics[1] and medicine[2].

2.2 Ferromagnetic shape memory alloys

Ferromagnetic Shape Memory Alloy Materials (FSMAs), often also referred to as Magnetic Shape Memory Alloys (MSMAs) represent magnetic extension of SMAs. They embody twinning mechanism, as observed in SMA materials, however, the difference lies in causation of the phase change. Besides temperature and stress-induced strains, in FSMA large strains can be produced by magnetic field application. Each of the martensitic variant is associated with preferred direction of magnetization. Therefore, the phase transformation between particular martensitic variants and so macroscopic strain can be initiated by external magnetic field. FSMAs are ferromagnetic alloys. Thus also phenomena described in previous chapter contribute to the magnetostrictive behaviour. Altogether, there are three mechanisms in FSMAs that give rise to magneto-mechanical coupling: domain wall motion, domain rotation and martensitic variants reorientation. The field-induced strain response of FSMA is nonlinear, hysteretic and strongly stress-dependent.

Ferromagnetic shape memory alloys are interesting materials due to their application potential. Magnitude of magnetic-field-induced strains produced by FSMAs is nearly of two orders higher than in giant-magnetostrictive materials such as Terfenol-D or Galfenol, clarify e.g. [17], [33]. Additionaly, compared to conventional shape memory alloys, FSMAs can be operated in higher frequency range up to 1kHz. The respose of the material is caused by magnetic-field-activated reorientation of martensitic variants and so it is not limited by the speed of heat transfer. Thus, the reaction of the alloy is much faster. On the other hand, the main disadvantage of FSMAs is relatively low blocking stress - minimal stress needed for complete suppression of the magnetic field induced strain.

FSMAs may be used in construction of sensors and transducing components in modern machineries. The actuation mechanism is always provided by energy transformation

[1]For example, SMAs enable construction of variable geometry chevron that helps to reduce engine noise of commercial aeroplanes. Morphing chevrons located at the trailing edge of the jet engine create vortexes that influence the mixing rate of adjacent stream lines. Optimizing of the mixing ration enables to decrease jet engine noise. More information about SMA implementation into jet engine design might be found in [4].

[2]Nitinol (nickel-titanium based alloy developed in Naval Ordnance Laboratory) is commonly used for cardiovascular stent construction. The deformed stent is inserted into a vein. Being heated (by the body) the stent expands into the designed shape and consequently improves the blood flow, for more details about stent design see e.g. [36]

(electric/magnetic, thermal) into the mechanical work. The component needs to combine large strains, high-force production and fast dynamic response during an actuation event. FSMAs have potential to satisfy these requirements. Hence, they are attractive for application in actuators[3] and sensors, see [16], [32]. Due to unique and adjustable magnetic properties ferromagnetic shape memory alloys might be also suitable materials for construction of solenoid transducers [21] or voltage generators [15]. There is a rich set of various applications of FSMAs introduced in related literature. For further and more detailed description about state-of-art applications see e.g. [31], [5].

The class of ferromagnetic shape memory alloys contains many materials such as Fe-Pd, Fe-Ni-Co-Ti, Fe-Pt, Co-Ni-Ga, Ni-Mn-Al or Co-Ni-Al. However, materials that enjoy the greatest interest are with no doubts Ni-Mn-Ga alloys [18]. Optimizing the ratio between Ni, Mn and Ga elements, we have gained field-induced strains up to 10%. In the following section we use Ni-Mn-Ga to demonstrate the characteristic behaviour of FSMAs. We also provide examples of experimental data for two particular alloys.

2.3 Characteristic behaviour of NiMnGA

The Ni-Mn-Ga compounds are commonly the most investigated ferromagnetic shape memory alloys. Therefore, we use this material to describe qualitatively the characteristic behaviour of FSMAs. Naturally, quantitative properties are strongly dependent on particular stoichiometry of the alloy. Thus, we provide experimental result for two concrete alloys.

The austenitic phase of Ni-Mn-Ga alloy of stoichimetry close to Ni_2MnGa adopts the $L2_1$ Heusler structure, see figure 2.10(a). The high temperature phase of compounds closer to stoichiometric NiMnGa exhibits similar $C1_b$ structure (sometimes called the semi-Heusler), illustrated in figure 2.10(b). The austenite is in a paramagnetic state above the Curie temperature and in a ferromagnetic state below it. The Curie temperature has value of 376K for the Ni_2MnGa and it seems to be almost compositional-independent[4]. Contrary to the Curie temperature, the martensitic start temperature M_s depends on the particular elements'ratio. For the stoichimetric Ni_2MnGa the value is 202K.

[3]For illustration let us mention the membrane actuator based on FSMA composite for synthetic jet applications proposed in [37]

[4]The compositions $Ni_{2+x}Mn_{1+y}Ga_{1+z}$ with x+y+z = 0 were studied in [10]. Authors state that "moving away from the stoichiometric composition, a slight variation, a large reduction, and a marked enhancement, were, respectively, observed for the Curie temperature, the magnetic anisotropy, and the structural (martensitic–austenitic) transformation temperatures".

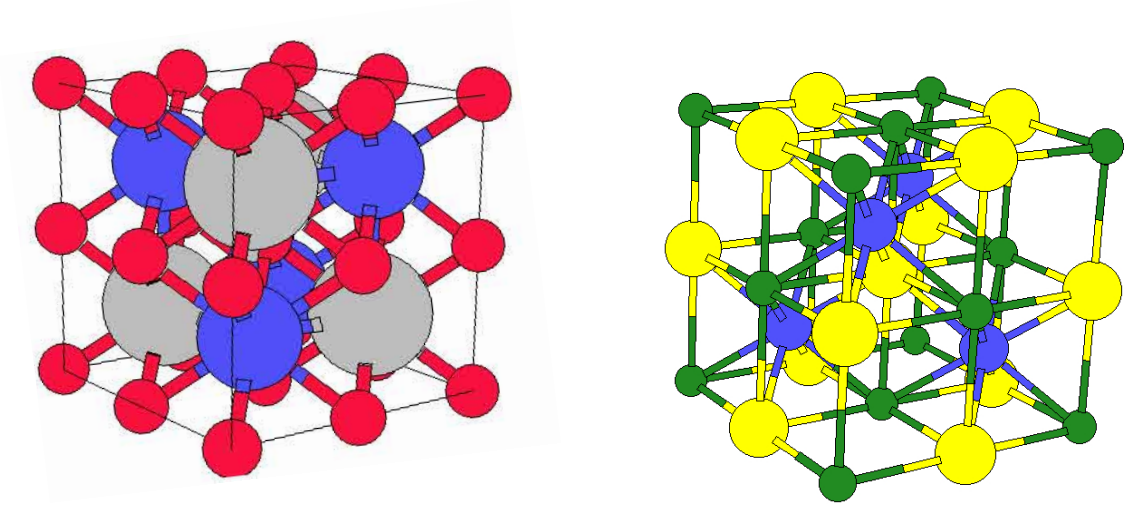

(a) $L2_1$ structure (b) $C1_b$ structure

Figure 2.4: Heusler and semi-Heusler structure. Stoichiometric Ni_2MnGa and NiMnGa are Heusler and semi-Heusler alloys. Thus they crystallize in $L2_1$ and $C1_b$ structure respectively. Unit cell of $L2_1$ structure consists of 4 intersecting f.c.c. sublattices with positions (000), $(\frac{1}{2}\frac{1}{2}\frac{1}{2})$ for Ni, $(\frac{1}{4}\frac{1}{4}\frac{1}{4})$ for Mn and $(\frac{3}{4}\frac{3}{4}\frac{3}{4})$ for Ga. The $C1_b$ structure misses the second Ni sublattice. In case all atoms are of the same type, the structure would become bcc. The figures are taken from [22].

Depending on composition, the martensitic phase can exhibit five-layered tetragonal (5M), seven-layered orthorombic (7M) or non-modulated tetragonal (NM) morphology [13]. We consider the most common tetragonal martensite configuration. For illustration see 2.5. Regarding the fact that the temperature M_f is below the Curie point, the material is in a ferromagnetic state and so the martensitic variants are spontaneously magnetized. The local magnetization in each variant is oriented in particular easy axis direction.

In figure 2.6 we schematically show the typical loading sequence of FSMA that enables us to measure the field-induced strain. The sample is cooled below M_s first, so the martensitic phase transformation occurs. Then the external compressive stress is applied in direction of x-axis. Since the mechanical loading causes shortening in x-direction, martensitic variant 1 is favoured (compare with 2.5). The stress is then reduced to desired test level which remains constant during the whole test. The value of stress that suppresses any variant reorientation is named the blocking stress.

Consequently, when the single variant state is accommodated, the fine micro-structure of magnetic domains is developed. Magnezitation within domains is in accordance with the easy axis of the variant 1. However, the domains with magnetization in direction [100]

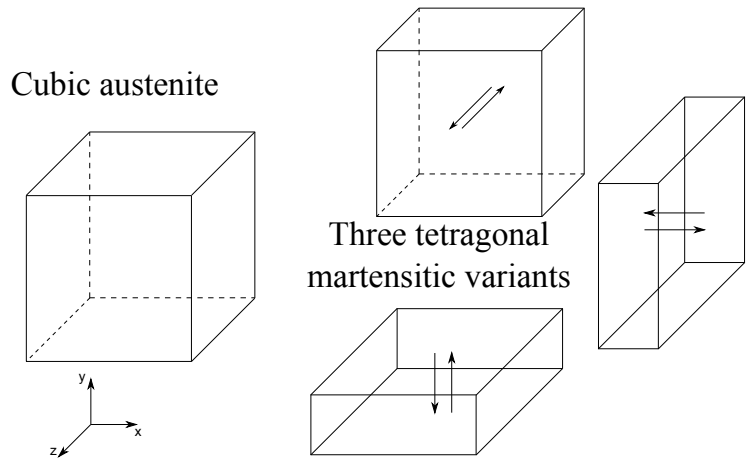

Figure 2.5: A simplified representation of FSMA crystal structure that is adopted in the thesis. We consider a cubic austenite and three tetragonal martensitic variants. Arrows denote directions of easy magnetization.

alternate with those with magnetization in opposite direction ([-100]). This happens in order to minimize the magnetostatic energy. Since no magnetic field is applied, neither of the domains is preferred and both occur in equal ratio. No macroscopic magnetization is produced.

The magnetic field application in direction perpendicular to the compressive stress (y-axis direction in the figure 2.6) gives rise to the variant 2 once a critical value of the field intensity $H_y^{s(1,2)}$ is reached. The variant 2 occurs in the microstructure because its easy axis lies in the direction of the applied field. As H_y increases, the variant 2 grows at the expense of variant 1 and so twin boundaries are created. Since the variant 2 is spatially oriented in a different way than the variant 1, its growth naturally brings along macroscopic strain of the sample. Further strengthening of the magnetic field decreases the volume fraction of the variant 1 and from the critical value $H_y^{f(1,2)}$ the variant 1 is completely eliminated. Consequently, maximal field-induced strain is reached.

Characteristic strain vs. magnetic field curves for four different stress levels are plotted in figure 2.11. Values $H_y^{s(1,2)}$ and $H_y^{f(1,2)}$ denote the start and the end of the process of transition from the variant 1 to the variant 2. Similarly, $H_y^{s(2,1)}$ and $H_y^{f(2,1)}$ stand for corresponding values for transition from the variant 2 to the variant 1. On the way from one martensitic variant to another the material forms the twin structure. Depending on the field intensity, the proportion between the variants is not balanced. Thus, non-zero magnetization is observed. The schematic arrangement of the twinned martensite at field level $H_y^{s(1,2)} < H_y < H_y^{f(1,2)}$ is depicted in sector II. of the figure 2.6. The martensitic

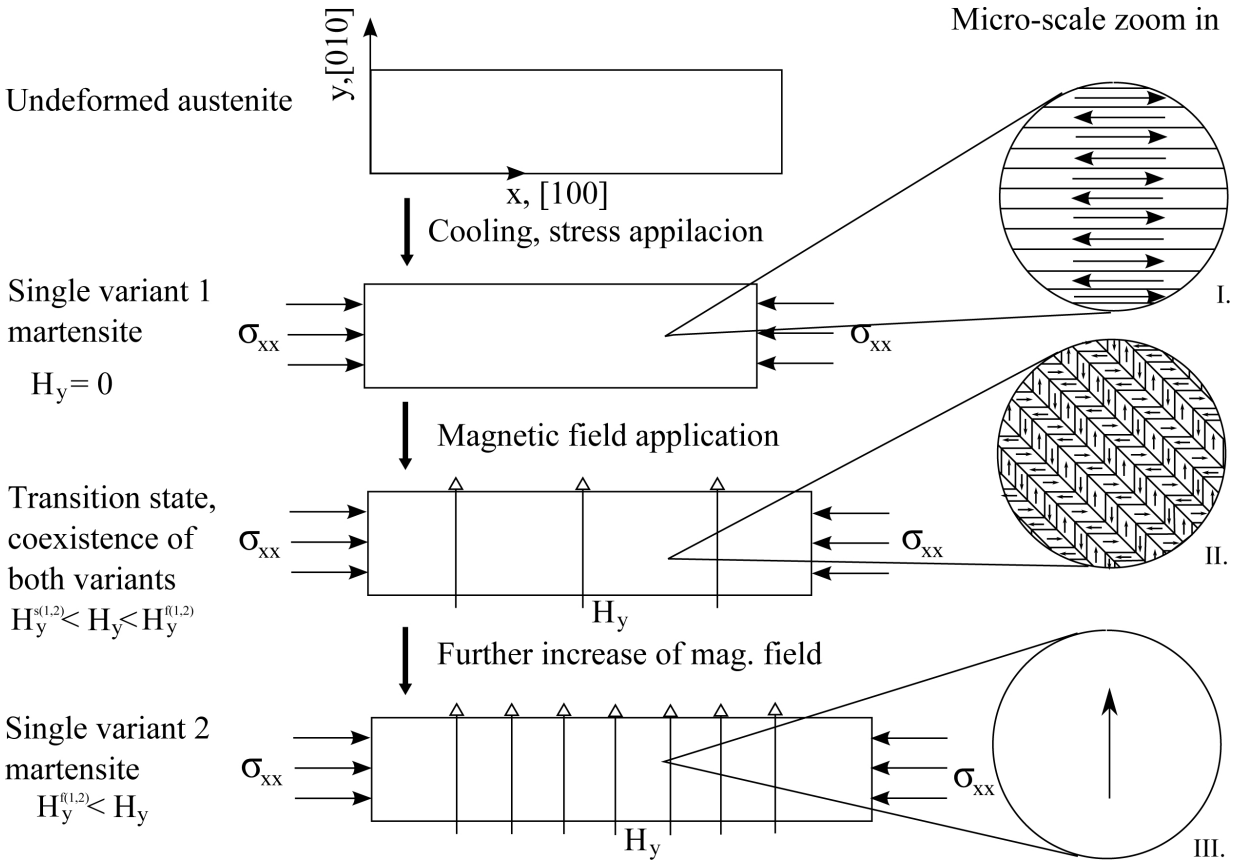

Figure 2.6: Characteristic loading sequence for field-induced strain production in FSMA. The zoom-in sectors illustrate the arrangement of martensitic variants during the rise in magnetic filed.

variants are separated by skew lines; vertical and horizontal lines denote the domain walls. within each variant two domain types with mutually opposite magnetization are present. As one can see, the transition from one variant to another might be also understood as a motion of the twin boundaries.

Alloy	Ni	Mn	Ga	Ms	Mf	As	Af	Tc
Alloy A	49.2	29.6	21.2	304	301	308	311	373
Alloy B	52.1	27.3	20.6	405	385	375	395	390-400

Table 2.1: Composition and characteristic temperatures of the investigated Ni-Mn-Ga alloys. Experimental data are taken from [35].

The tests were carried out at room temperature. The stress-strain curves for both alloys are shown in figure 2.8. The minimal stress that evokes the twin boundaries motion in the

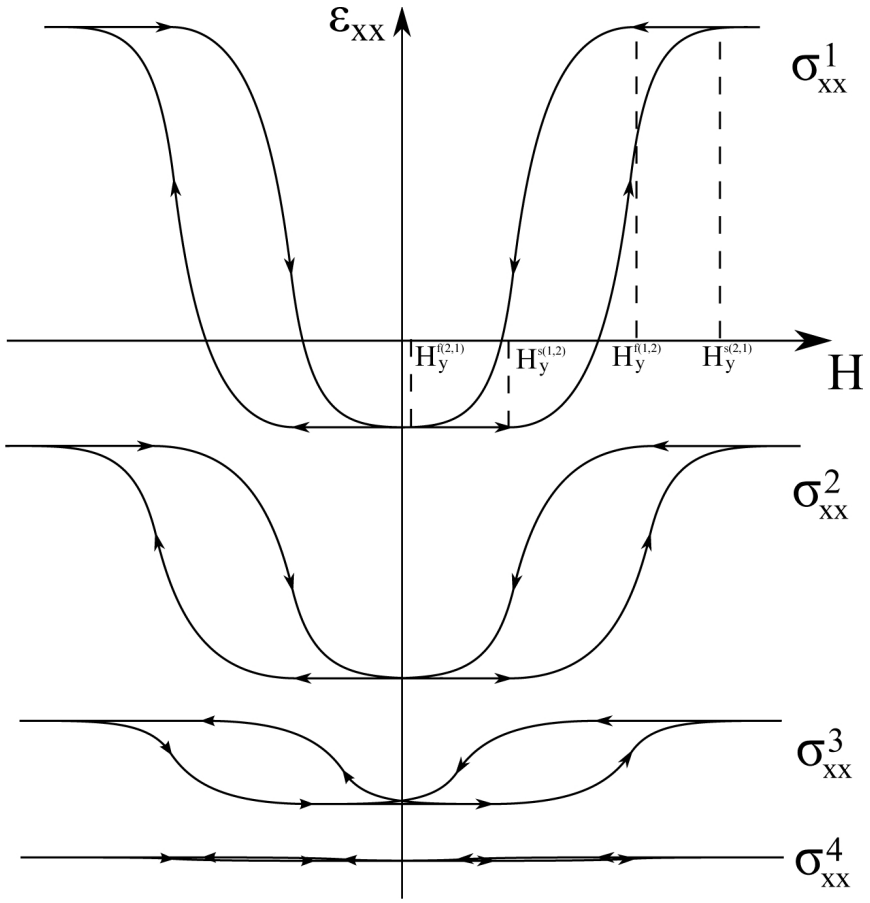

Figure 2.7: Characteristic strain vs. magnetic field curves for FSMA. Four different stresses $\sigma^1_{xx} < \sigma^2_{xx} < \sigma^3_{xx} < \sigma^4_{xx} < \sigma_{block}$ were applied.

alloy A is approximately 2 MPa. The twinning stress in the alloy B is of one order higher. The optical image in polarized light of the twinning structure is depicted in 2.9. The image was taken when the strain took value of 3% and 10% for alloy A and B respectively.

The results from measuring of the magnetic properties are plotted in figure 2.10. During the measurements the samples were mechanically loaded in order to prevent martensitic variant reorientation. As can assume from the results, in the alloy A the c-direction is the easy axis of magnetization. The hard axis is a perpendicular plane to the c-axis. Contrary to the first alloy, in the alloy B the c-axis is the hard axis. The saturation magnetization of both alloys is approximately the same ($\mu_0 H = 0.6$).

Finally, the figure 2.11 shows the magnetic field-induced strain of the alloy A. The sample was prestressed to generate the single variant configuration. The c-axis of the resulting variant was oriented in normal direction to the applied stress. The maximal

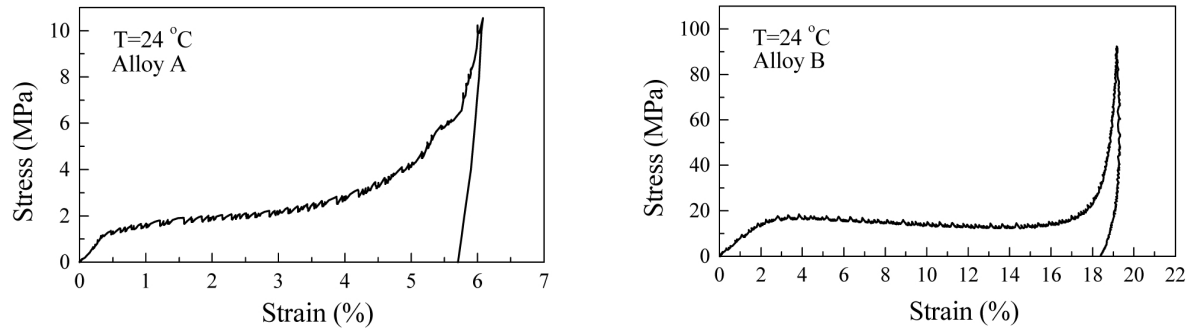

(a) Alloy A (b) Alloy B

Figure 2.8: Stress vs. strain diagram of Ni-Mn-Ga alloys. Experimental data are taken from [35].

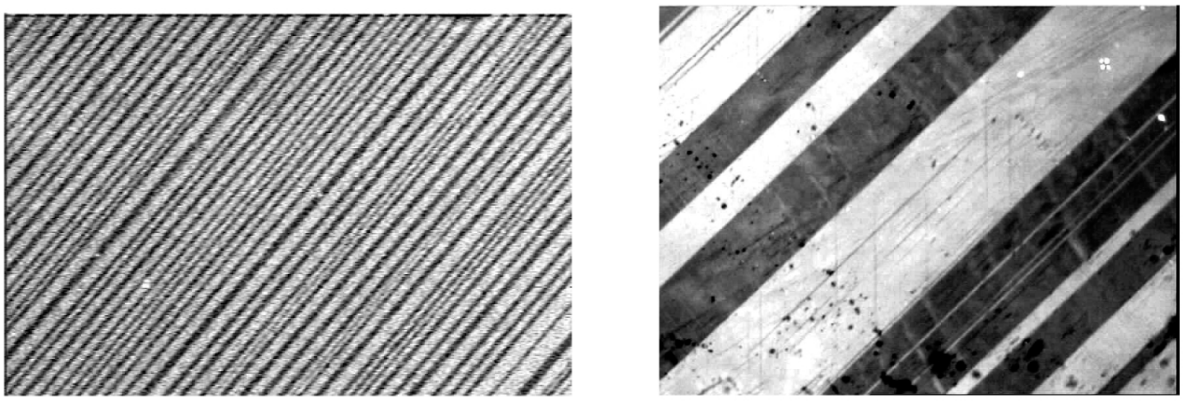

(a) Alloy A (b) Alloy B

Figure 2.9: Twinning structure of Ni-Mn-Ga alloys. Experimental data are taken from [35].

strain produced in the first cycle was 4.78% in the field 1.05 T.

The alloy B did not produce any field-induced strain (with respect to precision stated by authors, it is lower than $2 \cdot 10^{-2}\%$). As authors explain, this happens due to the high twinning stress.

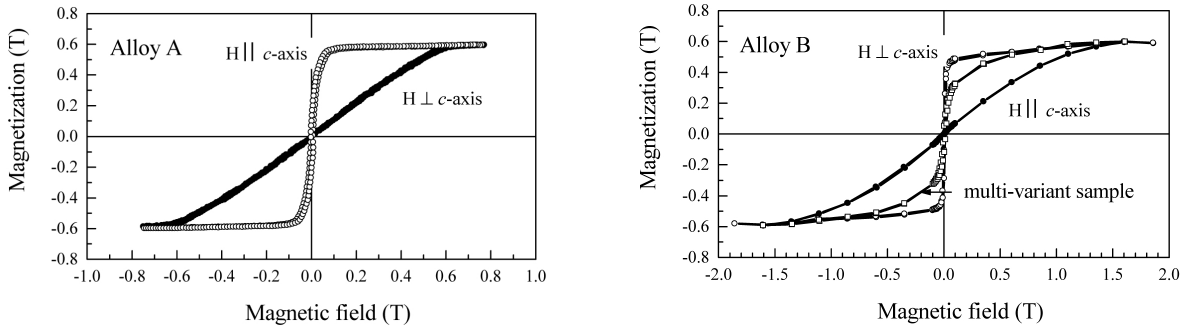

(a) Alloy A (b) Alloy B

Figure 2.10: Magnetization vs. field intensity diagram of Ni-Mn-Ga alloys. Experimental data are taken from [35].

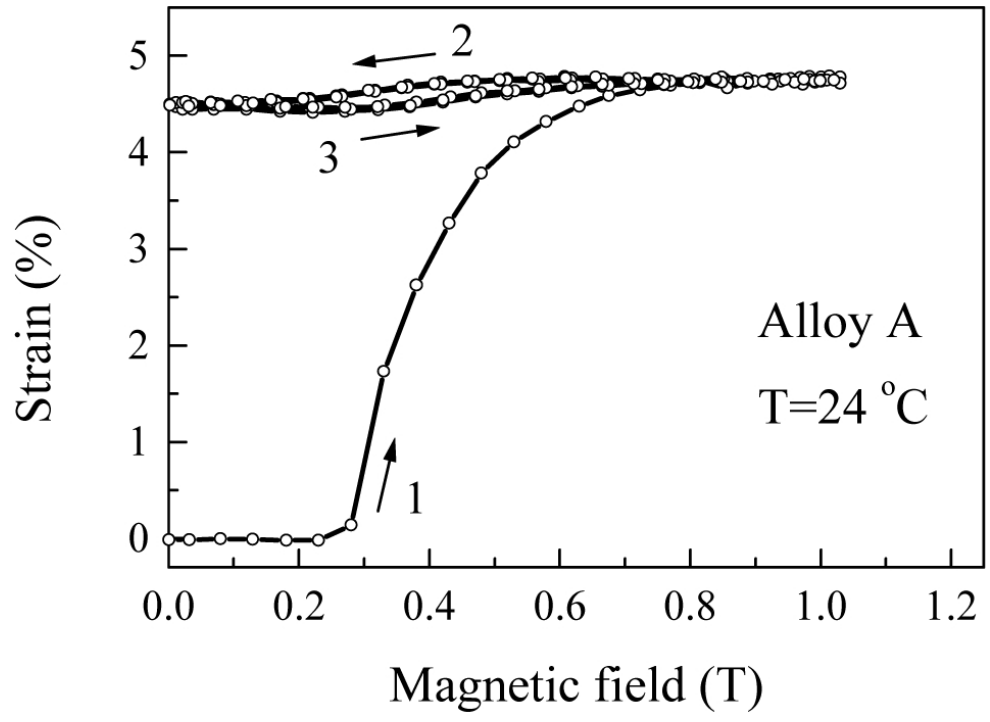

Figure 2.11: Characteristic strain vs. magnetic field curves for FSMA. Experimental data are taken from [35].

Chapter 3

Continuum mechanics overview

In this chapter, we review some results derived in continuum mechanics, which are important for the description of magnetostrictive material. In Section 3.1, we focus on a mathematical representation of continuum body and its motion (kinematics). Section 3.2 deals with the description of motion causer (stress) and its relation to the change of state (Hooke's law). In Section 3.3, the classical formulation of the linear elasticity problem is given as well as derivation of minimum total potential energy principle. Finally in Section 4.7, the existence of minimizing problem set in section 3.3 is presented. For comprehensive theory of linear elasticity see [12] or [30].

3.1 Kinematics

In continuum mechanics, we model a body as a set of mass points identified with the part of space $\Omega \subset \mathbb{R}^3$ that it occupies in certain time. Let Ω be open, bounded set. When the observed body is moving, the domain Ω is changing in time. Further more we assume that the body is homogeneous and Ω has a Lipschitz boundary.

Definition 3.1.1. *Let Ω be a domain. The boundary Γ of Ω is said to by Lipschitz if there exist numbers $\alpha > 0$ and $\beta > 0$ so that for $\forall x^0 \in \Gamma$ the frame of reference could be translated and rotated to the point x^0 such that the following is valid. If we denote*

$$k_{n-1} = \{x \in \mathbb{R}^n, |x_i| \leq \alpha \quad \text{for } \forall\ i = 1, ..., n-1, \}$$

then there exists a Lipschitz function $a : K_{n-1} \to x_n$, such that $a(x_1, ..., x_{n-1}) = x_n$. And all $x = (x_1, ..., x_{n-1}, x_n) \equiv (x', x_n)$ having $x' \in K_{n-1}$ and $a(x') < x_n < a(x') + \beta$ lay in Ω

and all $x = (x', x_n)$ *having* $x' \in K_{n-1}$ *and* $a(x') - \beta < x_n < a(x')$ *lay outside* $\bar{\Omega}$.

Let us consider a one-to-one mapping $\chi : \Omega \to \mathbb{R}^3$ called configuration, assigning every point $\tilde{X} \in \Omega$ its position x in $\mathbb{R}^3$. Then the motion is one-parameter configuration class $\chi_t : \Omega \to \mathbb{R}^3,\ t \in \mathbb{R}$:

$$x = \chi_t(\tilde{X}) = \chi(\tilde{X}, t),$$

where t represents time.

Choosing one configuration as a referential one and denoting points $\tilde{X}$ with positions of X in referential configuration ($X = \chi_0(\tilde{X})$, $\Omega = \chi_0(\Omega X)$), we may get a useful description of motion (deformation) of the body

$$x = \chi(\tilde{X}, t) = \chi(\chi_0^{-1}(X), t) = \chi(X, t).$$

Then the one-to-one mapping $x = \chi(X, t)$ is called the deformation function with respect to referential configuration and it is known as the Lagrange representation.

In this text, we will be interested in changes between referential configuration Ω and current configuration Ω, but not in the way in which the change occurs. This means that time evolution is not relevant for us and we may write $x = \chi(X, t) = \chi(X)$.

In view of the description above, the local geometrical transition surrounding of an arbitrary point of the body is defined by the deformation gradient

$$F = \nabla\chi \ = \nabla x \quad F_{ij} = \frac{\partial \chi_i}{\partial X_j} = \frac{\partial x_i}{\partial X_j}.$$

To avoid the disappearance of the mass, we assume $\det F > 0$. Thus, the deformation of any linear element dX is given by $dx = FdX$, and for the square of the change of length of this element we obtain

$$|dx|^2 - |dX|^2 = |FdX|^2 - |dX|^2 = dXFF^TdX - dXdX = dX(FF^T - 1)dX.$$

The term $E = \frac{1}{2}(F^TF - 1)$ is called the tensor of finite deformation. It is useful in introducing field quantity $u : \Omega_0 \to \Omega$ as $u(X) = \chi(X) - X$ describing the displacement of points from referential to current configuration. Then $\nabla u = F - 1$ and the tensor of finite deformation looks as follows:

$$E = \frac{1}{2}\left[(\nabla u + 1)^T(\nabla u + 1) - 1\right] = \frac{1}{2}\left[\nabla u + (\nabla u)^T + (\nabla u)^T(\nabla u)\right]$$

If we restrict our attention to small deformations $|\nabla u| << 1$ and neglect the last term in the last equation, we obtain the so-called small deformation tensor

$$e = \frac{1}{2}\left[\nabla u + (\nabla u)^T\right],$$

which also gives the precise meaning of the displacement gradient. Considering the decomposition of the displacement gradient into the symmetric and antisymmetric parts, we see that each transformation could be represented by composition of a pure deformation and a pure rotation:

$$\nabla u = \underbrace{\frac{1}{2}\left[\nabla u + (\nabla u)^T\right]}_{deformation} + \underbrace{\frac{1}{2}\left[\nabla u - (\nabla u)^T\right]}_{infinite rotation}.$$

3.2 Primal problem of linear elasticity formulation

The state of continuum subjected to an applied external force is well described by Cauchy's stress tensor. Forces acting within the body could be divided into body forces (e.g. gravitation) and contact forces (e.g. press, friction).

Let $\Omega^0 \subset \Omega$ with Lipschitz boundary Γ^0, $x \in \Gamma^0$ and ν be the outer normal to Γ^0 in x. The stress vector $g(x, \nu)$, $g : \Omega \times S \to \mathbb{R}^3$, where S denotes unit sphere, characterizes the density of contact forces acting from $\Omega - \Omega^0$ to $\bar{\Omega}^0$ in point x. Then the relation between stress and outer normal is intended by Cauchy's theorem.

Theorem 3.2.1. *Let us assume $g \in C(\bar{\Omega} \times S)$. Then $g(x, \nu)$ is linearly dependent on ν in x, i.e. there exists tensor τ such as*

$$g(x, \nu) = \tau(x)\nu(x)$$

for $\forall x \in \Omega^0$ and any $\nu(x)$ in x.

We use the Einstein summation convention. Proof of the statement can be found in [30]. The following equilibrium equations shows important properties of stress tensor.

Theorem 3.2.2. *Let us assume $\tau \in C^1(\Omega)$. Let $f : \Omega \to \mathbb{R}^3$ be a body force density. Let $x^0 \in \Omega$ and $\Omega_h \subset \Omega$ be a ball with Lipschitz boundary with center in x^0 and radius h. Then*

1. *(force equilibrium)*

$$\frac{\partial \tau_{ij}}{\partial x_j}(x^0) + f_i(x^0) = 0, \quad \text{for } i = 1, 2, 3 \text{ and } \forall x^0 \in \Omega \tag{3.1}$$

2. (force momentum equilibrium)

$$\tau_{ij} = \tau_{ji}, \quad \text{for } \forall i, j \text{ and } \forall x^0 \in \Omega \tag{3.2}$$

Generally in mechanics, we are concerned with a position change (characterized by the deformation tensor) of the body in relation to applied external forces (described by the stress tensor). The response of one material to a loading may vary according to the measure of applied stress. Therefore we distinguish plastic deformation, where the specimen stays deformed after unloading and elastic deformation, whereas the body takes back its own shape after removing the stress. In this text, we restrict our attention to the situation when the stress depends linearly to the deformation of a specimen. This is usually called the linear theory of elasticity. The assumption set above may be expressed by Hooke's law

$$\tau_{ij}(x) = \mathbb{C}_{ijkl}(x)e_{kl}(x) \quad \text{for} \quad i, j = 1, 2, 3. \tag{3.3}$$

for $\forall x \in \Omega$, where $\mathbb{C}_{ijkl} \in \mathbb{R}$. In this equation, no absolute term occurs since we assume, that if the deformation tensor equates to zero, then the stress vanishes as well. From symmetry of τ and e, we obtain

$$\mathbb{C}_{ijkl} = \mathbb{C}_{jikl} \quad \text{and} \quad \mathbb{C}_{ijkl} = \mathbb{C}_{ijlk}.$$

In addition to this, energy considerations give

$$\mathbb{C}_{ijkl} = \mathbb{C}_{klij}.$$

Generally, there are 21 constants describing the material. This number could be cut down for some materials, but for example copper sulphate has 21 independent constants.

Definition 3.2.3. *The material is said to be homogenous, if $\mathbb{C}_{ijkl}(x) = \mathbb{C}_{ijkl}$ for $\forall x \in \Omega$. The material is said to be isotropic in $x \in \Omega$, if $\mathbb{C}_{ijkl}(x)$ is independent of the choice of coordinates.*

For isotropic materials the Generalized Hooke's law holds:

$$\tau(x) = \lambda \mathrm{Tr}(e(x)) + 2\mu e(x) \tag{3.4}$$

or written in components

$$\tau_{ij}(x) = \lambda e_{ij}\delta_{ij} + 2\mu e_{ij}(x), \tag{3.5}$$

where λ, μ are so-called Lame's constants.

Remark 3.2.4. $\lambda = \mathbb{C}_{1122}$, $\mu = \mathbb{C}_{1212}$.

If we assume $u \in C^2(\Omega)$, $F \in C^1(\bar{\Omega})$ and that the equilibrium equations are satisfied in Ω, we may then formulate the linear elasticity primal problem. Substituting the equation into the force equilibrium from the Generalized Hooke's law, we obtain

$$\frac{\partial}{\partial x_i}(\lambda e_{ii}) + \frac{\partial}{\partial x_i}\left(\mu\frac{\partial u_i}{\partial x_j}\right) + \frac{\partial}{\partial x_i}\left(\mu\frac{\partial u_j}{\partial x_i}\right) + f_i = 0 \tag{3.6}$$

$$(\lambda+\mu)\frac{\partial e_{ii}}{\partial x_i} + \mu\Delta u_i + f_i = 0 \tag{3.7}$$

for i = 1,2,3, where we used the homogeneity of the body. The two sets of equations are the so-called general Lame's equations and Lame's equations for homogenous and isotropic bodies.

Definition 3.2.5. *Let Ω be a domain with Lipschitz boundary Γ. Let Γ_1, Γ_2 be disjoint and open in Γ such that $\Gamma = \Gamma_1 \cup \Gamma_2 \cup \tilde{\Gamma}$, where $\tilde{\Gamma}$ has zero surface measure. There are contact forces $T : \Gamma_1 \to \mathbb{R}^3$ given on Γ_1 and boundary displacement $u^0 : \Gamma_2 \to \mathbb{R}^3$ given on Γ_2. λ, μ are Lame's constants. Then the primal problem of the linear elasticity is to find*

$$u \in C^1(\Omega \cup \Gamma_1) \cap C(\Omega \cup \Gamma_2) \cap C^2(\Omega)$$

satisfying (2.4) and

$$\tau_{ij}\nu_j = g_i \quad \text{on } \Gamma_1, \tag{3.8}$$

$$u = u^0 \quad \text{on } \Gamma_2, \tag{3.9}$$

where $g \in C(\Gamma_1)$ and $u^0 \in C(\Gamma_2)$.

The boundary condition (2.4) can be expressed using generalized Hooke's law

$$\lambda e_{ii}\nu_i + 2\mu e_{ij}\nu_j = g_i \quad \text{on } \Gamma_1. \tag{3.10}$$

3.3 The minimum free energy principle

The equilibrium equations presented in Theorem (3.2.2) enable us to describe the stability of any part of the body. These differential equations holds for every point of the specimen and have a local character. The equilibrium can also be described by integral relations using the energy balance or a variational principle for energy. This way of characterization turns out to be very useful for mathematical analysis and approximative solutions.

Let us consider $\tau(x)$ and $u(x)$ satisfying conditions (3.8), (3.9) and the force equilibrium equation. We assume, that $\tau(x)$ and $u(x)$ are smooth enough so that the Green's Theorem is valid and all differential relations and boundary conditions make sense.

If we then rewrite (3.1) in integral formulation and apply Green's Theorem, we obtain

$$\int_\Omega \tau \cdot e(u)\,\mathrm{d}x = \int_\Omega fu\,\mathrm{d}x + \int_{\Gamma_1} gu\,\mathrm{d}S + \int_{\Gamma_2} \nu^T \tau u^0\,\mathrm{d}S. \tag{3.11}$$

The equation above can be interpreted in such a way, that (virtual) work of inner forces equates to the (virtual) work of outer (body and contact) forces. This is the so-called virtual work principle.

Furthermore, we may consider τ_0 and fields of displacement u_0, $u_0 + \delta u$ all complying with the primal problem of linear elasticity. If we put these into (3.11) and deduct the equations from each other, we get

$$\int_\Omega \tau_0 \cdot e(\delta u)\,\mathrm{d}x = \int_\Omega f\delta u\,\mathrm{d}x + \int_{\Gamma_1} g\delta u\,\mathrm{d}S. \tag{3.12}$$

We reflect $\delta e(u) = e(\delta u)$, where δu stands for variation of u (virtual displacement). Relation (3.12) expresses the virtual displacement principle.

For deriving the minimum energy principle, it is enough to use Hooke's law for anisotropic material (3.3) and substitute it into the virtual displacement principle. We presume that $\mathbb{C}$ is positive definite, which is to say, there exist $c_0 > 0$ such that

$$\langle \mathbb{C}e(u), e(u)\rangle \geq c_0 e(u) \cdot e(u),$$

$\forall e:\ e = e^T$. Let τ_0, u_0 satisfy the primal problem of linear elasticity. Since

$$\frac{1}{2}\delta \left\langle \mathbb{C}e(u_0), e(u_0)\right\rangle = \frac{1}{2}\frac{\mathrm{d}}{\mathrm{d}t}\left\langle \mathbb{C}e(u_0 + t\delta), e(u_0 + t\delta u)\right\rangle |_{t=0} = \left\langle \mathbb{C}e(u_0), e(\delta u)\right\rangle,$$

where $\langle , \rangle$ stands for the dot product, we obtain

$$\frac{1}{2}\int_\Omega \langle \mathbb{C}e(u_0), \delta e(u)\rangle \, \mathrm{d}x - \int_\Omega f\delta u \, \mathrm{d}x - \int_{\Gamma_1} g\delta u \, \mathrm{d}S = 0,$$

which can be rewritten as

$$\delta\left\{\frac{1}{2}\int_\Omega \langle \mathbb{C}e(u), e(u)\rangle \, \mathrm{d}x - \int_\Omega fu \, \mathrm{d}x - \int_{\Gamma_1} gu \, \mathrm{d}S\right\}_{u=u_0} = 0. \tag{3.13}$$

Let us denote the term in the vinculums $I(u)$ and call it the potential energy of an elastic body. It is obvious that for $u = u_0$, the functional $I(u)$ satisfies Euler's necessary condition for being the extremizer. For proof that $I(u_0)$ is minimizer see [30].

The minimum energy minimizer could be then formulated. If u_0 is the solution of the linear elasticity primal problem then u^0 gives

$$I(u) = \frac{1}{2}\int_\Omega \langle \mathbb{C}e(u), e(u)\rangle \, \mathrm{d}x - \int_\Omega fu \, \mathrm{d}x - \int_{\Gamma_1} gu \, \mathrm{d}S,$$

the lowest value amongst u complying with (3.8), (3.8). At this point, the question of existence of such a minimizer arises. We will return to this matter later in Chapter 4 .

Chapter 4

Magnetism

4.1 Introduction

In the previous chapter, we built up a formalism in order to describe the behavior of a continuous body subjected to external body and contact forces, and we justified the energy approach to the problem. In this chapter, we develop our concept considering magnetically active body. We review basics of magnetism as well as the physical framework of such phenomena.

Magnetism describes the response of the material to the applied magnetic field. All materials show some degree of magnetic activity as a reply to an external field. Some materials exhibit a magnetic field attracted to an applied field (paramagnetic materials), however some produce a field that is repulsed by an external field (diamagnetic materials). Ferromagnetic materials are those which exhibit their own magnetic field without any external magnetic activity. The magnetic properties are strongly temperature dependant, so it is also important to examine how characteristic values behave with respect to temperature.

On the microscopic level magnetism may arise from two different sources:

- Localized magnetic moments. The carrier of magnetism is a spin or an angular momentum. This type of magnetism is usual for free atoms, molecules or single ions in solids. In metallic solids, the localized magnetic moments are present within f-electrons of the rare-earths.

- Itinerant magnetic moments. The magnetic properties are carried by conducting (itinerant) electrons which can travel through the material and are present in the

metallic solids.

It is a feature of nature to keep things complicated and these two phenomena are usually in some degree combined. However, in this text we would like to examine basic magnetic principles and so we will treat them separately. Futher and more detailed information may be found in e.g. [29], [2] or [19].

Diamagnetic and paramagnetic responses of a material to an applied magnetic field are explained in section 4.2. In section 4.3 we consider the different types of magnetic interaction, which play the key role in producing the long range order of solids. In section 4.4 two physical models of ferromagnetism are introduced, whereas only localized magnetic moments are taken into consideration. The presence of conducting electrons is discussed in section 4.5 as well as the principle that gives rise to the magnetic properties. Finally, in section 4.6 we introduce the continuous approximation, which will be used in further sections. Within the last section we present the term of the free energy of a magnetic material. Moreover, we introduce the direct proof of the existence of energy minimizer.

4.2 Diamagnetism and Paramagnetism

Let us consider a single atom with Z electrons described by the hamiltonian $\hat{\mathcal{H}}_0$

$$\hat{\mathcal{H}}_0 = \sum_{i=1}^{Z} \left(\frac{p_i^2}{2m_e} + V_i \right).$$

The sumation index i runs over all electrons in the atom with kinetic energy $\frac{p_i^2}{2m_e}$ and potential V_i.

We expose the atom to an external magnetic field B given by

$$B = \mathrm{rot} A,$$

where A stands for the magnetic vector potential, which we choose (according to the fact that A is not uniquely determinated) such that $A = \frac{1}{2}(B \times r)$. The hamiltonian of the

system is then changed into

$$\begin{aligned}\hat{\mathcal{H}} &= \sum_{i=1}^{Z}\left(\frac{[p_i + eA(r_i)]^2}{2m_e} + V_i\right) + g\mu_B B\cdot S \\ &= \sum_{i=1}^{Z}\left(\frac{p_i^2}{2m_e} + V_i\right) + \mu_B(L+gS)\cdot B + \frac{e^2}{8m_e}\sum_{i=1}^{Z}(B\times r_i)^2 \\ &= \hat{\mathcal{H}}_0 + \mu_B(L+gS)\cdot B + \frac{e^2}{8m_e}\sum_{i=1}^{Z}(B\times r_i)^2\,, \end{aligned} \tag{4.1}$$

where L and S stand for the orbital angular momentum and the spin angular momentum and g is known as the g-factor. The second term of 4.1, which is usually the dominant perturbation to the original hamiltonian $\hat{\mathcal{H}}_0$, is called the Paramagnetic term. The third one is a consequence of the diamagnetic moment. We discuss both contributions in more detail.

Diamagnetism

We say that a material is diamagnetic if it exhibits weak, negative susceptibility. That is to say, the applied magnetic field generates a conversely oriented magnetic moment within the material. To illustrate such an effect let us consider an atom with completely filled electronic shells so that the paramagnetic term in equation 4.1 may be neglected. Considering the magnetic field B oriented parallely to the z axis implies $(B\times r_i)^2 = B^2(x_i^2+y_i^2)$ and the first-order correction of the ground state energy is

$$\Delta E_0 = \frac{e^2B^2}{8m_e}\sum_{i=1}^{Z}\left\langle 0|x_i^2+y_i^2|0\right\rangle = \frac{e^2B^2}{12m_e}\sum_{i=1}^{Z}\left\langle 0|r_i^2|0\right\rangle.$$

For the last equation we assume spherical symmetry of the atom[1] $\langle x_i^2\rangle = \langle y_i^2\rangle = \frac{1}{3}\langle r_i^2\rangle$. Let us assume a solid formed by N ions by Z electrons occupying volume V. Using termodynamic results we may evaluate the magnetization as

$$M = -\left(\frac{\partial F}{\partial B}\right)_{T,V} = -\frac{N}{V}\frac{\partial \Delta E_0}{\partial B} = -\frac{N}{V}\frac{e^2B}{6m_e}\sum_{i=1}^{Z}\left\langle r_i^2\right\rangle,$$

[1]Such a presumption is eligible since the total angular momentum J is zero.

where F stands for the Helmholz free energy. Furthermore, we pressume[2] $\frac{\partial M}{\partial H} \approx \mu_0 \frac{\partial M}{\partial B}$. Hence we arrive for the diamagnetic susceptibility with

$$\chi = -\frac{N}{V}\frac{e^2\mu_0}{6m_e}\sum_{i=1}^{Z}\left\langle r_i^2\right\rangle .$$

This is a classical Langevin's result. The effect of diamagnetism (the negativ contribution to the susceptibility) is present in all materials, however it is considered as a very weak effect and therefore can be neglected or taken as a tiny correction to other dominant effects.

Paramagnetism

Compared to Diamagnetism, Paramagnetic materials are those with positive susceptibility. So that the applied magnetic field evokes magnetization aligned parallely with the magnetic field direction. Paramagnetism corresponds to the presence of unpaired electrons within the atoms, by another name presence of non-zero magnetic moments (both orbital and spin). When no magnetic field is applied, these moments are randomly oriented since neighbouring atoms interact weakly and may be considered as independent. The application of an external field aligns them, the level of lining up (and so the induced magnetization) depends on the strength of the applied magnetic field.

The magnetic moment on an atom is measured by total angular momentum J, which is defined as a sum of the orbital angular momentum L and the spin angular momentum S

$$J = L + S.$$

Throughout this text, we measure these quantities in multiples of $\hbar$. One would naturally anticipate that the induced magnetization of the paramagnetic material is directly proportional to the magnitude of the applied field and inversly proportional to the temperature which supports the randomization of spins within the material. We wish to examine this crucial behaviour as well as temperature dependance of the paramagnetic susceptibility.

We consider a quantum mechanical system with magnetic moments J of any integer or half-integer value. Without loss of generity, we assume the applied magnetic field to be parallel with z axis. We will compute $\langle m_J \rangle$ the average value of the z component of J,

[2]For small fields, $\chi << 1$,so $B \approx \mu_0 H$

which determines the magnetization. The partition function is given by

$$Z(B) = \sum_{m_J=-J}^{J} \exp\left(m_J g_J \mu_B / k_B T\right), \tag{4.2}$$

where μ_B denotes the Bohr magneton, k_B the Bolzman constant a g_J is the appropriate g-factor. If we substitute $x = g_J \mu_B B / k_B T$, we may write (according to Bolzman statistics)

$$\langle m_J \rangle = \frac{\sum_{m_J=-J}^{J} m_J \exp\left(m_J x\right)}{\sum_{m_J=-J}^{J} \exp\left(m_J x\right)} = \frac{1}{Z} \frac{\partial Z(B)}{\partial x}.$$

Considering that $F = -nk_B \ln Z$ (n stands for the concentration of magnetic moments) and $M = -\left(\frac{\partial F}{\partial B}\right)_{T,V}$, we may write

$$M = n g_J \mu_B \langle m_J \rangle = \frac{n g_J \mu_B}{Z} \frac{\partial Z}{\partial B} \frac{\partial B}{\partial x} = n k_B T \frac{\partial \ln Z}{\partial B}. \tag{4.3}$$

It is easy to compute the partition function since it means to tot up the geometric progression. Using cyclometric functions we arrive at

$$Z = \frac{\sinh((2J+1)x/2)}{\sinh(x/2)}.$$

So if we perform the computations of 4.3 and resubstitute $y = xJ = n g_J \mu_B J B / k_B T$, we find that

$$M = M_s B_J(y),$$

where the saturation magnetization M_s is

$$M_s = n g_J \mu_B J$$

and $B_J(y)$ is known as Brillouin function given by

$$B_J(y) = \frac{2J+1}{2J} \coth\left(\frac{2J+1}{2J} y\right) - \frac{1}{2J} \coth\left(\frac{y}{2J}\right). \tag{4.4}$$

The course of the Brillouin function for several values may be found in figure 4.1.

Let us assume that $y << 1$, which corresponds to very low temperatures or very weak

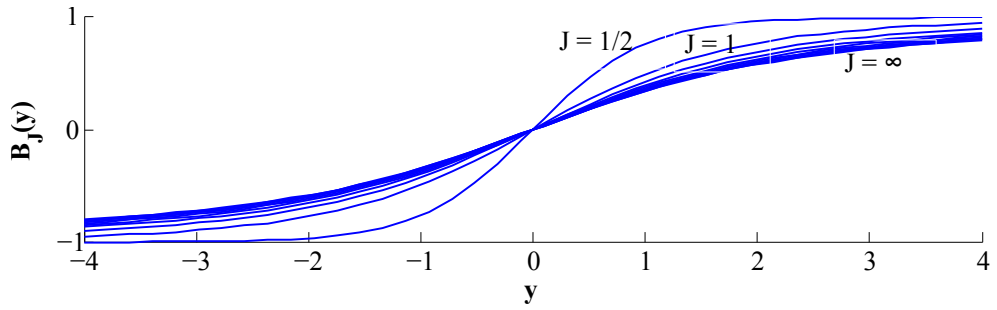

Figure 4.1: The magnetization of the paramagnetic material with magnetic moment J is governed by Brillouin function $B_J(y)$, which is plotted for several values of J.

fields. Then we may expand $B_J(y)$ into Taylor series

$$B_J(y) = \frac{(J+1)y}{3J} + O(y^3).$$

Hence for paramagnetic susceptibility holds

$$\chi = \frac{M}{H} \approx \mu_0 \frac{M}{B} = \frac{n\mu_0\mu_{\text{eff}}^2}{3k_BT}, \tag{4.5}$$

where μ_{eff} denotes the effective moment

$$\mu_{\text{eff}} = g_J\mu_B\sqrt{J(J+1)}.$$

The equation 4.5 is known as the Curie Law.

4.3 Interactions

The aim of our interest is to describe magnetic ordering within the material. In order to obtain any magnetic structure, the means of "communication" between individual magnetic moments (that all together induce magnetization) needs to be introduced. Such a communication between the magnetic moments is mediated by different magnetic interaction and it forms a crucial condition for presence of any long range order.

Magnetic dipolar interaction

The magnetic dipolar interaction is a classical mediator of the interplay of two dipoles. Let us consider two magnetic dipoles μ_1 and μ_2 which are separated by vector r. Then the

potential energy of such a system is

$$E = \frac{\mu_0}{4\pi r^3}\left(\mu_1 \cdot \mu_2 - \frac{3}{r^2}(\mu_1 \cdot r)(\mu_2 \cdot r)\right).$$

To estimate the importance of this interaction, notice that we are dealing with moments of magnitude degree of $|\mu| \approx 1\mu_B$ separated by distance of $|r| \approx 1$Å. Such interaction is represented by energy of 10^{-23}J which is equivalent to about 1K in temperature. However, materials usually order at higher temperature. Hence the effect of the magnetic dipolar interaction is minor and may be neglected.

Exchange interaction

The exchange interaction is the key effect thatenables the rise of magnetism. It is a purely quantum mechanism contributing to the total potential energy of the body with a spin-spin interaction between every pair of particles with non-zero spin. In fact, the exchange interaction reflects fact that the wave function of the system of two undistinguishable particals is subjected to exchange symmetry, it is to say the wave function is either symmetric (bosons) or antisymmetric (fermions, liable to Pauli exclusive principle).

To demostrate such an effect, let us consider two electrons placed at r_1 and r_2. The wave function of the joint state is a product of the two single-state wave functions $\psi_a(r_1)$ and $\psi_b(r_2)$

$$\Psi = \psi_a(r_1)\psi_b(r_2). \tag{4.6}$$

However, the equation 4.6 does not respect the exchange symmetry. Since we are dealing with electrons, only antisymmetric wave function is allowed. So the spin part of the wave function has to be either antisymmetric χ_S for the case of symmetric spatial part, or symmetric for the antisymmetric spatial part χ_T

$$\Psi_S = \frac{1}{\sqrt{2}}[\psi_a(r_1)\psi_b(r_2) + \psi_a(r_2)\psi_b(r_1)]\chi_S \tag{4.7}$$

$$\Psi_T = \frac{1}{\sqrt{2}}[\psi_a(r_1)\psi_b(r_2) - \psi_a(r_2)\psi_b(r_1)]\chi_T.. \tag{4.8}$$

The situation of 4.7 corresponds to a singlet state and 4.8 to a triplet state. The energies

of these two states are

$$E_S = \int \Psi_S^* \hat{\mathcal{H}} \Psi_S \, \mathrm{d}r_1 \, \mathrm{d}r_2$$
$$E_T = \int \Psi_T^* \hat{\mathcal{H}} \Psi_T \, \mathrm{d}r_1 \, \mathrm{d}r_2,$$

where we suppose the normalization of the wave function. So the energy difference is

$$E_S - E_T = 2 \int \psi_a(r_1)^* \psi_b(r_2)^* \hat{\mathcal{H}} \psi_a(r_2) \psi_b(r_1) \, \mathrm{d}r_1 \, \mathrm{d}r_2 = 2J. \tag{4.9}$$

The equation is also a definition of the value J, which is usually called the exchange integral. The eigenvalues of the joint operator $\hat{\mathcal{S}}_1 \hat{\mathcal{S}}_2$ are $-\frac{3}{4}$ (singlet) and $\frac{1}{4}$ (triplet), hence the hamiltonian can be rewritten as 'effective hamiltonian'

$$\hat{\mathcal{H}} = \frac{1}{4}(E_S + 3E_T) - (E_S - E_T)\hat{\mathcal{S}}_1 \hat{\mathcal{S}}_2. \tag{4.10}$$

The first part of 4.10 is constant, however, the second part is function of the spin. Using the exchange integral we may write the spin contribution to the hamiltonian of the system

$$\hat{\mathcal{H}}^{spin} = -2J \hat{\mathcal{S}}_1 \hat{\mathcal{S}}_2.$$

As $J > 0$ the triplet state with the total spin $S = 1$ is preferred, however if $J < 0$ the singlet state with the total spin $S = 0$ is favoured. Naturally in many electron systems the situation is more complicated, however there is no interaction among three particles (they always interact in pairs). Therefore Heisenberg proposed in his model the Hamiltonian of the form

$$\hat{\mathcal{H}} = -\sum_{ij} J_{ij} \hat{\mathcal{S}}_i \hat{\mathcal{S}}_j, \tag{4.11}$$

whereas the summation runs over all pairs of the interacting spins. J_{ij} stands for the exchange integral of the i^{th} and j^{th} spin.

There are different kinds of the exchange interaction. When there is interaction between electrons of the neighbouring magnetic atoms and no intermediator is needed, we talk about direct interaction. However, this kind of interaction is not of high importance for magnetic properties, as it is subjected to sufficient overlap of neighbouring electron orbitals (e.g. in rare earths the $4f$ electrons are very localized and even in transition metals the contribution of the direct exchange interaction is probably not the key effect). Another kind of exchange

interaction is usual for many ionic solids, such as MnO, MnF_2. So-called superexchange is the exchange interaction between non-neighbouring magnetic ions mediated by non-magnetic ion placed in between. In metals the exchanged interaction is often mediated by conducting electrons (it is usually called RKKY interaction). The ferromagnetic exchange interaction may occur within some oxides as the magnetic ions exhibit mixed valency. The more detailed analysis of different types of the exchange interaction is beyond the focus of this work. To find more see [2].

4.4 Ferromagnetism of the localized moments

We say that a material is ferromagnetic if it exhibits spontanoeus magnetization, even when no external magnetic field is present. As mentioned in the introduction, there are two phenomena that give rise to magnetic behaviour. Within this section we explain ferromagnetism as a global alignment of the (localized) atomic moments.

The level of spontaneous magnetization naturally depends on the temperature. With increasing temperature the thermal motion of the magnetic dipoles competes with the tendency of dipoles to align (due to the exchange interaction). When the temperature reaches a certain point so-called Curie temperature, a second-order phase transition occurs and the spontaneous magnetization vanishes, however, the material still responds paramagnetically to the external field.

Material	T_C [K]	magnetic moment [μ_B/ formula unit]
Fe	1043	2.22
Co	1394	1.715
Ni	631	0.605
Gd	289	7.5
MnSb	587	3.5
EuO	70	6.9

Table 4.1: The common ferromagnetic materials and their properties

Some common ferromagnetic materials as well as their magnetic properties are given in table 4.1.

We introduce two models of ferromagnetism of the localized moments. The first one, Weiss model, is in a way generalization of the paramagnetism by using the concept of mean field. The second one, Heisenberg model, then recognizes that the mean field is in reality

consequence of the exchange interaction.

Weiss molecular field model

In order to explain the spontaneous magnetization within the material, Pierre Weiss presumed (without knowing any physical interpretation) the presence of the internal magnetic field, the so-called molecular field B_{mf}. Since the molecular field is a measure of system magnetization, we may assume

$$B_{\mathrm{mf}} = \lambda M,$$

where $\lambda > 0$ is a molecular field constant. The problem can be now treated as a paramagnetic system placed in a magnetic field $B + B_{\mathrm{mf}}$. Hence, repeating the procedure from the section 4.2, we have to solve simultaneously equations

$$\frac{M}{M_s} = B_J(\tilde{y}) = \frac{2J+1}{2J}\coth\left(\frac{2J+1}{2J}\tilde{y}\right) - \frac{1}{2J}\coth\left(\frac{\tilde{y}}{2J}\right),$$

$$\tilde{y} = \frac{g_J \mu_B J(B + \lambda M)}{k_B T}. \tag{4.12}$$

For $\tilde{y} << 1$ we may use Taylor series for Brillouin function and write again

$$B_J(y) = \frac{(J+1)\tilde{y}}{3J} + O(\tilde{y}^3).$$

If we consider zero external field $B = 0$, the expression for the Curie temperature (the temperature at which M vanishes) may be derived. We seek for non-trivial intersection point of the plot of $B_J(\tilde{y})$ with $M(\tilde{y})$, which is given in 4.12. Hence

$$\frac{M}{M_s} = \frac{(J+1)}{3J}\frac{J g_J \mu_B \lambda M}{k_B T} \tag{4.13}$$

$$\Longrightarrow T_C = \frac{(J+1) g_J \mu_B \lambda M_s}{3k_B} = \frac{n\lambda\mu_{\mathrm{eff}}^2}{3k_B}. \tag{4.14}$$

Magnetization is a continuous function, positive for $T < T_C$ and identically zero for $T > T_C$ with a jump in the first derivative at point $T = T_C$. Therefore the transition between ferromagnetic and paramagnetic state is the second-order phase transition. When a weak

[3] field B is applied, the magnetization of the material follows the equation

$$\begin{aligned}\frac{M}{M_s} &= \frac{(J+1)}{3J}\frac{Jg_J\mu_B}{k_BT}\left(B+\lambda M\right),\\ &= \frac{(J+1)}{3J}\frac{Jg_J\mu_B}{k_BT}\left(B+\frac{3k_BT_cM}{(J+1)g_J\mu_BM_s}\right).\end{aligned}$$

After several manipulations we arrive at

$$\frac{M}{M_s}\left(1-\frac{T}{T_C}\right) = \frac{(J+1)g_J\mu_B}{3k_BT}B,$$

and so for the magnetic susceptibility stands

$$\chi = \frac{C}{T-T_C} \quad \text{where} \quad C = \frac{(J+1)g_J\mu_BM_s}{3k_B}. \tag{4.15}$$

The equation 4.15 is known as the Curie-Weiss law.

Heisenberg model

Another model of magnetic behaviour of solids is the (nearest neighbour) Heisenberg model. In contrast with Weiss model, where the interaction is approximated by molecular (mean) field, Heisenberg considers pairwise interaction between spins. With respect to the exchange interaction the model introduces a contribution to the hamiltonian of the system

$$\hat{\mathcal{H}} = -J\sum_{j,\delta}\hat{\mathcal{S}}_j\hat{\mathcal{S}}_\delta - g_J\mu_B\sum_l H_{ext}\hat{\mathcal{S}}_j. \tag{4.16}$$

The index j runs over all spin positions and δ denotes the nearest spins placed in δ-neighbourhood of the j^{th} spin.

The eigenstates of the hamiltonian describe the excitation of the whole spin system. These excitations are called spin waves or magnons. At temperature 0K all spins are (due to the exchange interaction) perfectly aligned in direction of magnetization. As the temperature increases, excitation of the system occurs. The excitation is in fact a perturbation of the perfect order which decreases the net magnetization. It is possible to determine the magnon dispersion relation from the Heisenberg model and so calculate the reduction of

[3] so that the assumtion $\tilde{y} << 1$ is still satisfied

the spontaneous magnetization at low temperature.

To demonstrate this, we use semiclassical approach to derive the magnon dispersion relation in one-dimension. Let us consider one-dimensional spin chain in no external field. Each spin has two neighbours in distance δ, so the hamiltonian reduces to

$$\hat{\mathcal{H}} = -2J \sum_j \hat{\mathcal{S}}_j \hat{\mathcal{S}}_{J+1}$$

We calculate the time dependance of $\left\langle \hat{\mathcal{S}}_j \right\rangle$

$$\begin{aligned}
\frac{\mathrm{d}}{\mathrm{d}t} \left\langle \hat{\mathcal{S}}_j \right\rangle &= \frac{1}{i\hbar} \left\langle \left[\hat{\mathcal{S}}_j, \hat{\mathcal{H}} \right] \right\rangle \\
&= -\frac{2J}{i\hbar} \left\langle [\hat{\mathcal{S}}_j, ...\hat{\mathcal{S}}_{j-1}\hat{\mathcal{S}}_j + \hat{\mathcal{S}}_j\hat{\mathcal{S}}_{j+1} + ...] \right\rangle \\
&= -\frac{2J}{i\hbar} \left\langle [\hat{\mathcal{S}}_j, \hat{\mathcal{S}}_{j-1}\hat{\mathcal{S}}_j] + [\hat{\mathcal{S}}_j, \hat{\mathcal{S}}_j\hat{\mathcal{S}}_{j+1}] \right\rangle \\
&= \frac{2J}{\hbar} \left\langle \hat{\mathcal{S}}_j \times (\hat{\mathcal{S}}_{j-1} + \hat{\mathcal{S}}_{j+1}) \right\rangle . \qquad (4.17)
\end{aligned}$$

We will treat spin as a classical vector of magnitude S. At the ground state all spins are aligned in z direction. If we assume that the amplitude of excitation is sufficiently small ($S_j^x, S_j^y << S, S_j^z \approx S$), we may linearize equation 4.17

$$\begin{aligned}
\frac{\mathrm{d}S_j^x}{\mathrm{d}t} &= \frac{2J}{\hbar}(2S_j^y - S_{j-1}^y - S_{j+1}^y) \\
\frac{\mathrm{d}S_j^y}{\mathrm{d}t} &= \frac{2J}{\hbar}(2S_j^x - S_{j-1}^x - S_{j+1}^x) \\
\frac{\mathrm{d}S_j^z}{\mathrm{d}t} &= 0.
\end{aligned}$$

We search for a solution in form of normal mode,i.e. we use ansatz

$$S_j^x = A \exp[i(kj\delta - \omega t)] \qquad S_j^y = B \exp[i(kj\delta - \omega t)],$$

where k stands for the wave vector. By instituting into linearized equations and from demanding solvability of the resulting equation system, we obtain

$$\hbar\omega = 4JS\left(1 - \cos(k\delta)\right),$$

which represents the dispersion relation for the one-dimensional case. For the illustration

see figure 4.4.

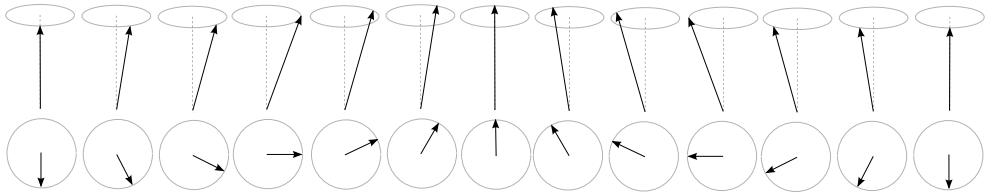

Figure 4.2: The spin wave in a line of spins. The perspective view (upper) and the view from above (lower).

In general the dispersion relation takes form

$$\hbar\omega = 2JSm\left(1 - \frac{1}{m}\sum_{\delta}\cos(k\delta)\right),$$

where m denotes the number of the closest neighbours. Since we are concerned with low energy excitations, we may use Taylor series for cosine

$$\hbar\omega = 2JS\delta^2k^2 \propto k^2. \tag{4.18}$$

To calculate Curie temperature, the fact that magnons are bosons needs to be taken into consideration. Therefore the Bose-Einstein statistics has to be used. In three dimensions, since

$$\frac{\mathrm{d}\omega}{\mathrm{d}k} = \frac{4JS\delta^2k}{\hbar} \propto \omega^{\frac{1}{2}},$$

the density of states is given by

$$g(\omega)\,\mathrm{d}\omega \propto \omega^{\frac{1}{2}}\,\mathrm{d}\omega.$$

Therefore the number of magnons is

$$n = \int_0^\infty \frac{g(\omega)}{\exp(\hbar\omega/k_BT) - 1}\,\mathrm{d}\omega = \left(\frac{k_BT}{\hbar}\right)^{\frac{3}{2}}\int_0^\infty \frac{x^{\frac{1}{2}}}{\exp(x) - 1}\,\mathrm{d}x \propto T^{\frac{3}{2}}.$$

Consider that each magnon mode is a delocalized single reversed spin and reduces the total magnetization by factor $S = 1$. Then the reduction of spontaneous magnetization at low temperature is

$$\frac{M(0) - M(T)}{M(0)} \propto T^{\frac{3}{2}}. \tag{4.19}$$

The equation 4.19 is known as Bloch $T^{\frac{3}{2}}$ law.

4.5 Magnetism of the itinerant electrons

Till now, we have been concerned with the localized magnetic moments, however, regarding metals the origin of magnetism is different. In metals the magnetic moments are carried by conducting electrons which can freely travel within the material. These are usually known as itinerant electrons. We approximate the behaviour of the itinerant electrons by the simplest model, the free electron model, and we introduce mechanisms that give rise to the paramagnetic and ferromagnetic behaviour.

The free electron model

In the free electron model, the electrons are supposed to behave as molecules of the ideal gass. That is to say electron-electron interactions are neglected as well as the periodical potential due to the lattice. With no loss of generality, we asssume that the electrons are placed in a cube of volume $V = L^3$. The electrons occupy states up to the Fermi wave vector k_F. States in the k-space are separated by $2\pi/L$. The number of states between k and $k + \mathrm{d}k$ is equal to proportion of the volume of a spherical shell of radious r and width $\mathrm{d}k$ and volume corresponding to the one state in k-space. Since each state can be occupied by two electrons, the state density is given by

$$g(k)\,\mathrm{d}k = 2\frac{4\pi k^2}{(2\pi/L)^3}\,\mathrm{d}k = \frac{Vk^2}{\pi^2}\,\mathrm{d}k.$$

At temperature $0K$ the electrons fill up the states up to k_F so for the numer of electrons implies

$$N = \int_0^{k_F} g(k)\,\mathrm{d}k = \frac{Vk_F^3}{3\pi^2}. \tag{4.20}$$

The Fermi energy is given by

$$E_F = \frac{\hbar^2 k_F^2}{2m_e}.$$

Since the energy is proportional to the square of the wave vector i.e. $E \propto k^2$, the states density is proportional to $\sqrt{E}$. That is to say

$$g(E) = \mathrm{d}n\,\mathrm{d}E \propto \sqrt{E},$$

where we defined $n = N/V$ as the electron density. By substituting in the equation 4.20 we obtain

$$n = \int_0^{E_F} g(E)\,\mathrm{d}E \propto E_F^{\frac{3}{2}}$$

and therefore for the state density at Fermi energy stands

$$g(E_F) = \left(\frac{\mathrm{d}n}{\mathrm{d}E}\right)_{E=E_F} = \frac{3}{2}\frac{n}{E_F} = \frac{m_e k_F}{(\pi\hbar)^2}.$$

The last equation holds due to the 4.20 and 4.5.

If the temperature is higher than zero, Fermi-Dirac distribution needs to be considered. The density stays unchanged, however the occupancy of each state is modified by Fermi function $f(E)$

$$f(E) = \frac{1}{e^{(E-\mu)/k_B T} + 1},$$

where μ stands for the chemical potential. The Fermi function results from Pauli exclusion principle, which holds for electrons. At $T = 0$ the function $f(E)$ is the Haeviside function with a step at μ. With increasing temperature the step smooths up. Usually, for most metals the Fermi function is very close to a step function at wide range of temperatures and we talk about degenerated limit. However, one can show that for large energies $E >> k_B T$ the Fermi-Dirac distribution meets the Maxwell-Boltzmann form $e^{(E-\mu)/k_B T}$, that is called the non-degenerated limit. The Fermi function for the various temperatures is plotted at figure4.3(a).

At zero temperature the Fermi energy is the highest energy occupied by an electron. That means

$$\int_0^{E_F} f(E)g(E)\,\mathrm{d}E = n.$$

Function $f(E)g(E)$ is plotted at figure 4.3(c). At $T = 0$ the Fermi energy equates with the chemical potential. If the temperature is increased, the two values slightly differ.

Pauli paramagnetism

Within the metal materials each k-state is double occupied (spin up and down). When the external magnetic field is applied, the energy of the electrons increases or decreases according to the spin direction. This effect causes a paramagnetic susceptibility and is known as Pauli paramagnetism.

To derive the susceptibility, we neglect the orbital contribution. The electron density

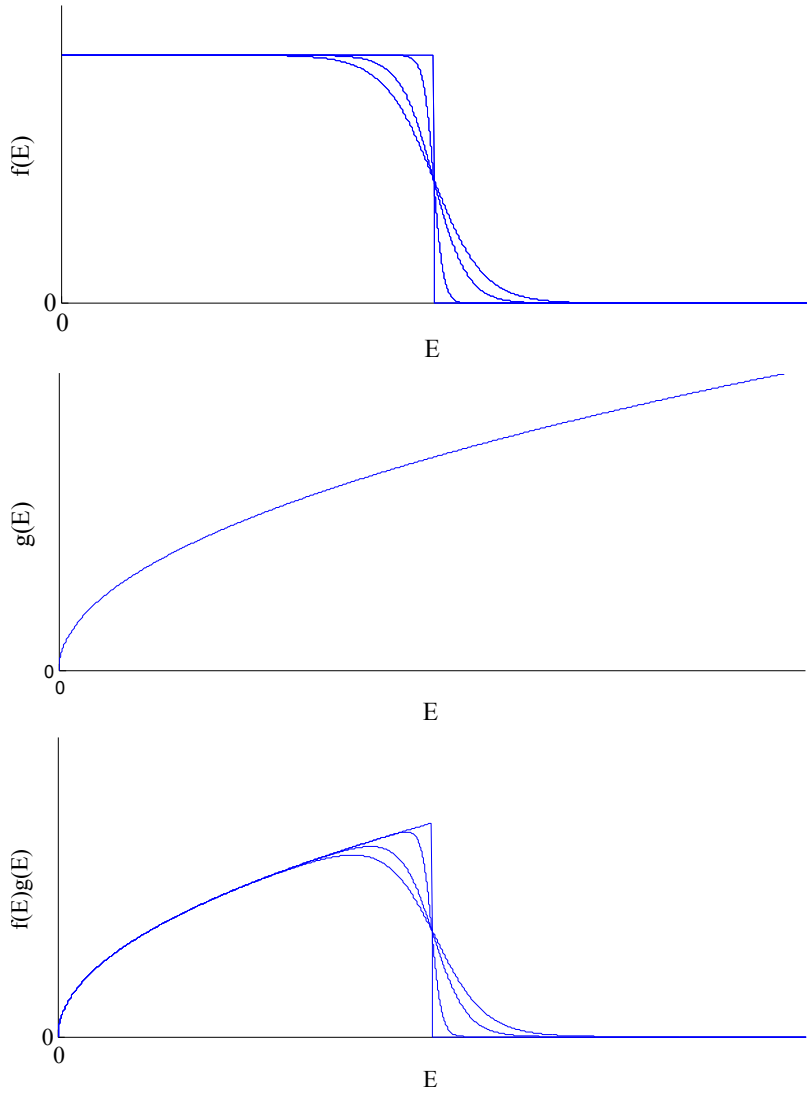

Figure 4.3: Fermi-Dirac distribution

for each spin orientation is

$$n_\uparrow = \frac{1}{2}\int_0^\infty g(E+\mu_B B)f(E)\,\mathrm{d}E$$
$$n_\downarrow = \frac{1}{2}\int_0^\infty g(E-\mu_B B)f(E)\,\mathrm{d}E$$

Considering small external field B, the magnetization of the material is given by $M =$

$\mu_B(n_\uparrow - n_\downarrow)$. Hence using the mean value theorem and the integration by parts, we get

$$M \approx \mu_B^2 B \int_0^\infty \frac{\mathrm{d}g}{\mathrm{d}E} f(E)\,\mathrm{d}E = \mu_B^2 B \left([g(E)f(E)]_0^\infty - \int_0^\infty \frac{\mathrm{d}f}{\mathrm{d}E} g(E)\,\mathrm{d}E \right).$$

If we consider that $g(0) = 0$ and $\lim_{E\to\infty} f(E) = 0$, the border term vanishes and we arrive at

$$M \approx \mu_B^2 B \int_0^\infty \left(-\frac{\mathrm{d}f}{\mathrm{d}E} \right) g(E)\,\mathrm{d}E.$$

In order to handle the diferential of the Fermi function, we consider two limits.

At $T = 0$ (the degenerate limit), the diferential of Haeviside function is a delta function at point E_F. That is to say

$$-\frac{\mathrm{d}f}{\mathrm{d}E} = \delta_{E_F}.$$

Hence we obtain

$$M = \mu_B^2 B g(E_F) \quad \text{and} \quad \chi_P = \mu_0 \mu_B^2 g(E_F).$$

However, in the non-degenerate limit $f(E) \approx e^{(E-\mu)/k_B T}$ which yields to

$$M = \frac{\mu_B^2 B}{k_B T} \int_0^\infty f(E) g(E)\,\mathrm{d}E = \frac{n\mu_B^2 B}{k_B T}$$

and so

$$\chi = \frac{n\mu_0\mu_B^2}{k_B T}. \tag{4.21}$$

One can see that 4.21 is in good agreement with 4.5. For most metals E_F takes the value of a few eV, therefore the degenerated limit holds well at all temperatures below the melting point.

Itinerant ferromagnetism

In the previous model of ferromagnetism we assume presence of the molecular field λM that affects all spins. Regarding the Pauli paramagnetism χ this field may magnetize the electron gas in the metals. However the resulting magnetisation M can be in return the causer of the molecular field. Such "chicken-egg" mechanism may give rise to spontaneous ferromagnetism if both λ and χ? are large enough. The key criterion is whether the ferromagnetic state is favourable with the view of energy.

To examine this, let us assume that no magnetic field is applied and let us virtually

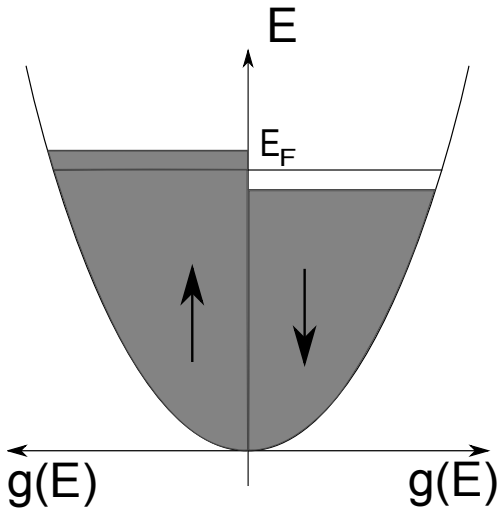

Figure 4.4: States-density of spin-up and spin-down bands showing spontaneous energy splitting.

remove small amount of electrons at the Fermi energy level from the spin-down band to the spin-up band. More precisely, we take spin-down electrons from the energy range $[E_F, E_F - \delta E]$, flip their spins and put them into the spin-up band to the energy range $[E_F, E_F + \delta E]$ as illustrated in Figure 4.4. The electron rearrangement causes increase of total energy since the kinetic energy of the electrons grows. On the other hand the interaction between resulting magnetization and the molecular field produces reduction of the potential energy. Consider that the number of moved electrons is $g(E_F)\delta E/2$ and the energy growth is δE, then the change of the total kinetic energy is given by

$$\Delta E_k = \frac{1}{2} g(E_F)(\delta E)^2.$$

The developed magnetization is $M = \mu_B(n_\uparrow - n_\downarrow)$, where spin-up and spin-down densities are

$$n_\uparrow = \frac{1}{2}(n + g(E_F)\delta E)$$
$$n_\downarrow = \frac{1}{2}(n - g(E_F)\delta E).$$

The total change of the molecular field energy is

$$\begin{aligned}\Delta E_p &= -\int_0^M \mu_0(\lambda M')\,\mathrm{d}M' = -\Delta 12\mu_0\lambda M^2 \\ &= -\frac{1}{2}\mu_0\mu_B^2\lambda(n_\uparrow - n_\downarrow)^2 = -\frac{1}{2}U\left(g(E_F)\delta E\right)^2. \end{aligned} \tag{4.22}$$

In the last identity we substitute $U = \mu_0\mu_B^2\lambda$, which is a measure of Coulomb energy. Hence the total change of energy is

$$\Delta E = \frac{1}{2}g(E_F)(\delta E)^2\left(1 - U\left(g(E_F)\delta E\right)^2\right).$$

So one can see that the spontaneous ferromagnetism is favourable if $\Delta E < 0$. That is to say

$$Ug(E_F) \geq 1, \tag{4.23}$$

which is the famous Stoner criterion. The presence of the spontaneous ferromagnetization requires strong Coulomb effects and large state density at the Fermi energy. Let us remark that the situation may be interesting even if the Stoner criterion is not satisfied, since the magnetic susceptibility is influenced. It may be derived that the presence of the Coulomb interaction increases the Pauli paramagnetic susceptibility as follows

$$\chi = \frac{\chi_P}{1 - Ug(E_F)}.$$

This is known as the Stoner enhancement of χ_P.

As one can see, the describtion of magnetism is rather complicted. However, we wish to develop medel that represent material as a macroscopic object. That is to say, we are not interested in behaviour of particular magnetic dipols. We are fully satisfied with describtion via mean values of relevant physical quantities. Thus, we can step back from the atomic level an take advanatege of the physical model developed by Landau and Lifschitz ussually called micromagnetism. It is based on a variational principle stating that those states are preferred which minimize the total stored energy functional. Such an approach is very convenient since it is coherent with variational principle introduced in section 3.3. The concept is discussed in the following section.

4.6 Continuum approximation for magnetism

Problem formulation

We study behavior of a ferromagnetic body placed in an external magnetic field H. We assume a rigid, homogeneous body identified with the part of space $\Omega \subset \mathbb{R}^3$ that it occupies. Let Ω be an open, bounded set with a Lipschitz boundary. The state of a ferromagnetic body at a fixed temperature below the Curie point is described by vector field called the magnetization m: $\Omega \to \mathbb{R}^3$, which corresponds to volume density of the macroscopic magnetic moment. This means that m generates a magnetic field u at all points of space. We assume that a ferromagnetic body could be locally saturated, i.e. there exists a value m_s, so that

$$0 < |m(\mathbf{x})| \;=\; m_s \qquad \text{almost everywere in } \Omega, \tag{4.24}$$

so that a specimen can reach a demagnetized state only in the sense of mean value. The value m_s is called saturation magnetization and in general, is a function of temperature. For the purposes of this text put $m_s = 1$. We suppose that $m(x) \in L^2(\Omega, \mathbb{R}^3)$.

The total potential energy of a ferromagnetic body exposed to an external magnetic field is composed from several contributions originating from the microscopic structure of the specimen and the properties of applied outer field. The respective components are called exchange energy, anisotropy energy, interaction energy and magnetostatic energy.

The principle of magnetism is the existence of current loops of electrons "orbiting" about a nucleus and the existence of electron spin. The exchange interaction is a quantum mechanical effect contributing to the total potential energy of the body with a spin-spin interaction between every pair of particles having non-zero spin. There is no classical analogy for such an effect in classical mechanics. The exchange interaction contributes to the Hamiltonian of the system by term

$$H_{ex} = -\sum_{i,j} J_{ij} S_i \cdot S_j.$$

where J_{ij} is the exchange integral and S_i, S_j stand for the spin operators. The summation runs over all couples (i, j) of particles taking part in the spin-spin interaction. Computation of J is based on wave function properties of the concerned particles. For more detailed information see [14]. Hence J_{ij} decreases rapidly with an increasing distance of particles we may write J instead of J_{ij}. If we substitute the spin operators with vectors and rewrite

the dot product, we obtain the term for the exchange energy

$$E_{ex} = -JS^2 \sum \cos \varphi_{ij}$$

where φ denotes the angle between the concerned vectors. Since only small values of φ are supposed, the Taylor's series for the cosine can be used. After shifting the zero value of energy (in order to remove any absolute term), we obtain

$$E_{ex} = JS^2 \sum \varphi_{ij}^2.$$

Notice that we take each interacting pair only once. If considered

$$|\varphi_{ij}| \approx |m_i - m_j| \approx |(r_{ij} \cdot \nabla)m|,$$

where r_{ij} stands for position vector from the lattice point i to j, then

$$E_{ex} = JS^2 \sum_i \sum_{r_{ij}} |(r_{ij} \cdot \nabla)m|^2.$$

Passing from the first summation to integration over the ferromagnetic body, the term for the exchange energy is given by

$$E_{ex} = \epsilon \int_\Omega |\nabla m(x)^2 \, \mathrm{d}x, \tag{4.25}$$

where $\epsilon > 0$. The exchange energy represents the ability for a specimen to create domain structure (regions of uniform magnetization), by penalizing spatial changes of m. To see this, consider the Pauli Exclusion Principle. Two electrons having different spin can stay at the same orbital, which means to have the same angular state. But the closer electrons are to each to other, the stronger Coulomb repulsion they experience. On the other hand, if two electrons have the same spin, they occupy different orbits and so their relative Coulombic repulsion is lower. The Coulombic repulsion force the electron spins to be placed in different orbits, it is to say to be parallel within as large region as other effects enable.

If there was only an exchange part of the energy, the sample would adopt the single domain structure and would behave as a block magnet, which exhibits an external magnetic field with certain energy. This energy can be minimized by decreasing the external magnetic field by dividing the material into domains, see Figure 4.5. Adding extra doma-

ins increases the exchange energy because the domains can have parallel magnetization. However the total energy is decreased as the magnetostatic energy is the dominant effect. The contribution of the energy of the generated magnetic field to the total energy can be reduced to zero by a closed domain structure which does not leave any external field.

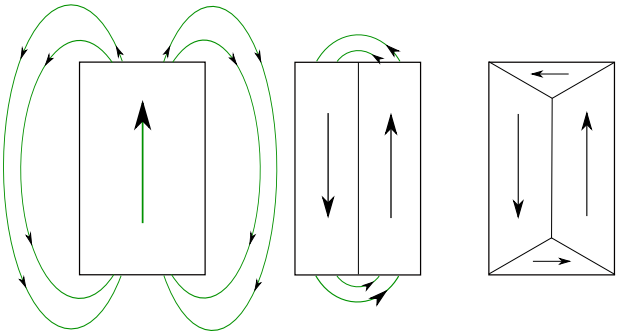

Figure 4.5: Adopting the domain structure leads to minimization of the magnetostatic energy of the specimen.

In order to describe this effect, the magnetostatic energy corresponding to the energy of the magnetic field $h \in L^2(\mathbb{R}^3, \mathbb{R}^3)$ generated by magnetized body with magnetization m, need to be introduced. The induced field has to be a solution of Maxwell's equations of magnetostatics (no free currents and no electric field is concerned).

$$\begin{aligned} \text{curl } h &= 0 \\ \text{div } (\mu_0 h + m\chi_\Omega) &= 0 \end{aligned}$$

in $\mathbb{R}^3$, where $\chi_\Omega : \mathbb{R}^n \to \{0, 1\}$ is the characteristic function of Ω and μ_0 is the vacuum permeability. Hence h is a curl-free field, and there exists a scalar function $u_m : \mathbb{R}^3 \to \mathbb{R}$ called scalar magnetic potential of spatially located magnetic dipoles so that

$$h = -\nabla u_m.$$

u_m is then governed by

$$\text{div}(-\mu_0 \nabla u_m + m\chi_\Omega) = 0. \tag{4.26}$$

The magnetostatic energy is the main reason for arising the domain structure.

But crystalline solids are rather anisotropic. This has the energy functional to reflect, otherwise the magnetization would always vanish if no magnetic field is applied, which does not corresponds to the observation. In magnetic crystal, there exist preferred directions,

so-called easy axis, along which the physical properties could vary dramatically from others. This effect is modeled through an even, non-negative anisotropy density $\phi : B_1 \to [0, +\infty)$. $\phi(x)$ vanishes along easy axis and thereby the directions of easy magnetization are determinate. The anisotropy energy is then given by

$$E_{ani} = \int_\Omega \phi(m)\,\mathrm{d}x. \tag{4.27}$$

The anisotropy energy can be minimized by adopting domain structure with magnetization point along the easy axis. The ideal magnetic material has an easy axis perpendicular to one another in order to minimize both the magnetostatic and anisotropic energy (see figure 4.5 (left)). In the regions bordering the domains, so-called domain walls, there is a change in the direction of the magnetization and so magnetization is not aligned along easy axes. Hence, structure with large domains with few domain walls tend to decrease the anisotropy energy.

The interaction energy is work needed for magnetization of a specimen by a certain external magnetic field $H : \mathbb{R}^3 \to \mathbb{R}^3$ in certain direction

$$E_{int} = -\int_\Omega H \cdot m\,\mathrm{d}x, \tag{4.28}$$

where we assume $H \in L^2(\Omega)$.

The total potential energy of the ferromagnetic body, the so-called Helmholtz energy, subjected to an external magnetic field is then given by

$$I_m(m) \;=\; \epsilon \int_\Omega |\nabla m|^2 \;+\; \int_\Omega \phi(m) \;-\; \int_\Omega H \cdot m \;+\; \frac{\mu_0}{2} \int_{\mathbb{R}^3} |\nabla u_m|^2, \tag{4.29}$$

and in accordance with the spirit of Hamilton's variation principle, the state of the ferromagnetic body corresponds to the minimizer of the Helmholz energy functional. The constant scaling the magnetostatic energy is vacuum permeability [4].

Our task is to find $m_0 \in \mathcal{M}$, where $\mathcal{M} = \{m \in W^{1,2}(\Omega, \mathbb{R}^3) : |m(x)| = 1 \text{ a.e.}\}$, so that

$$I(m_0) = \inf \{I(m) : m \in \mathcal{M}\}.$$

[4]The value of vacuum permeability is $\mu_0 = 4\pi \cdot 10^{-7} NA^{-2}$

The Helmholz free energy minimizer existence

Before we approach to prove the existence of the minimizer, it is necessary to define a few terms and give several statements, which we use hereinafter. For more a detailed introduction to the issue, see [30].

Definition 4.6.1. *Let X be a Banach space and let $f : X \to \mathbb{R} \cup \{\infty\}$*

1. *f is said to be convex if*

$$\lambda f(x) + (1-\lambda) f(y) \geq f(\lambda x + (1-\lambda) y).$$

for every $x, y \in X, \lambda \in [0,1]$

2. *f is said to be (sequentially) lower semicontinuous if*

$$\liminf_{x_n \to \widetilde{x}} f(x_n) \geq f(\widetilde{x}).$$

3. *f is said to be (sequentially) weakly lower semicontinuous over X if*

$$\liminf_{n \to \infty} f(x_n) \geq f(x) \quad \text{whenever} \quad x_n \rightharpoonup x \quad \text{in} \quad X.$$

4. *f is said to be coercive over X if*

$$f(x) \geq \alpha \|x\| + \beta$$

for every $x \in X$ and for some $\alpha > 0, \beta \in \mathbb{R}$.

Lemma 4.6.2. ***(Korn's inequality.)*** *Let Ω be an open, connected domain in $\mathbb{R}^3$ and $u \in W^{1,2}$. Then*

$$\int_\Omega e_{ij}(u) e_{ij}(u) dx \quad \geq \quad \frac{1}{2} \int_\Omega \frac{\partial u_i}{\partial x_j} \frac{\partial u_i}{\partial x_j} dx. \tag{4.30}$$

The Einstein summation convention is being used here.

Proof. Because $W^{1,2}(\Omega) = \overline{D(\Omega)}$ [5] we may assume, that u $\in D(\Omega)$. Hence

$$\frac{1}{4} \int_\Omega \left(\frac{\partial u_i}{\partial x_j} + \frac{\partial u_i}{\partial x_j} \right) \left(\frac{\partial u_i}{\partial x_j} + \frac{\partial u_i}{\partial x_j} \right) dx = \frac{1}{2} \int_\Omega \frac{\partial u_i}{\partial x_j} \frac{\partial u_i}{\partial x_j} dx + \frac{1}{2} \int_\Omega \frac{\partial u_i}{\partial x_j} \frac{\partial u_j}{\partial x_i} dx.$$

[5] $D(\Omega)$ is a space of functions with compact support.

But for the second integral on the right side, we get (by using the integration by parts)

$$\frac{1}{2}\int_\Omega \frac{\partial u_i}{\partial x_j}\frac{\partial u_j}{\partial x_i}dx = \frac{1}{2}\int_\Omega \left(\frac{\partial u_i}{\partial x_j}\right)^2 dx \geq 0.$$

Using this and the equation above, we obtain the statement.

Lemma 4.6.3. ***(Poincaré inequality.)*** *Assume that $1 < p < \infty$ and that Ω is a bounded open subset of $\mathbb{R}^n$ having Lipschitz boundary. Then there exists $C \in \mathbb{R}$ such that, for every function $u \in W^{1,p}(\Omega)$*

$$\|u - u_\Omega\|_{L^p(\Omega)} \leq C\|\nabla u\|_{L^p(\Omega)},$$

where

$$u_\Omega = \frac{1}{|\Omega|}\int_\Omega u(y)\,\mathrm{d}y$$

is the average value of u over Ω, with $|\Omega|$ standing for the Lebesgue measure of the domain Ω.

Theorem 4.6.4. *Let X be a reflexive Banach space and let $I : X \to \mathbb{R} \cup \{\infty\}$ be weakly lower semicontinuous and coercive over X. Assume also that there exists $\widetilde{u} \in X$ with $I(\widetilde{u}) < \infty$. Then there exists at least one $u_0 \in X$ such that*

$$I(u_0) = \inf\{I(u) : u \in X\} \tag{4.31}$$

Proof. Let u_n be a minimizing sequence for $\inf\{I(u) : u \in X\}$, i.e.

$$I(u_n) \to \inf I.$$

From hypotheses, we have that $\beta \leq \inf I(u) \leq I(\widetilde{u}) < \infty$. Using the coercivity of I, we may then deduce that there exists $K > 0$, independent of n, such that

$$\|u_n\| \leq K.$$

Since X is reflexive, we can extract a weakly convergent subsequence still denoted u_n, such that

$$u_n \rightharpoonup u_0 \quad \text{in} \quad X.$$

$I(u)$ is lower weakly semicontinuous, which means

$$\liminf_{n\to\infty} I(u_n) \geq I(u_0)$$

But because $\liminf_{n\to\infty} I(u_n) = \inf I$ then $\inf I = I(u_0)$.

Let us turn our attention back to the Helmholtz energy functional. We show that functional (4.29) takes the value of its infimum. In the first step, we prove that $\|m_k\|_{W^{1,2}} \leq C$. After that, in second step, we show that I_ϵ is weakly lower semicontinues and that there exists $m_0 :\ I(m_0) = \inf\{I(m) : m \in \mathcal{M}\}$.
Step 1

The fact that $|m(x)| = 1$ implies $m \in L^\infty$ and therefore $m \in L^2$. Let m_k be a minimizing sequence:

$$I_\epsilon(m_k) = \epsilon \int_\Omega |\nabla m_k|^2 \ + \ \int_\Omega \phi(m_k) \ - \ \int_\Omega H \cdot m_k \ + \ \frac{\mu_0}{2} \int_{\mathbb{R}^3} |\nabla u_m|^2.$$

the function ϕ is non-negative and so $\int_\Omega \phi(m_k) \geq 0$. For interaction energy holds estimation $\int_\Omega H \cdot m_k \leq \|H\|_{L^2} \|m\|_{L^2}$.

For the estimation of magnetostatic energy, we apply an arbitrary testing function $v : \mathbb{R}^3 \to \mathbb{R} : \lim_{x\to\infty} v(x) = 0$ on equation (6.2)

$$\operatorname{div}(m\chi_\Omega - \mu_0 \nabla u_m) v = 0$$

$$\operatorname{div}(m\chi_\Omega)\ v - \mu_0 \Delta u_m\ v = 0.$$

After integration over all of $\mathbb{R}^3$ and integration by parts

$$\int_{\partial\Omega} mv - \int_\Omega m \cdot \nabla v = \lim_{r\to\infty} \mu_0 \int_{S_r} v \nabla u_m - \mu_0 \int_{\mathbb{R}^3} \nabla u_m \cdot \nabla v,$$

where S_r stands for the sphere with radius r and is centered at the origin. According to behavior of the testing function, boundary items vanish. Specially for $v = u_m$ we obtain

$$\mu_0 \|\nabla u_m\|_{L^2}^2 = \int_\Omega m \cdot \nabla u_m \leq \|m\|_{L^2} \|\nabla u_m\|_{L^2}$$

$$\|\nabla u_m\|_{L^2} \leq \|m\|_{L^2}.$$

Considering $|m_k(x)| \leq 1$, we gain $0 \leq \int_\Omega |m_k(x)|^2 \leq |\Omega|$ and so

$$I_\epsilon(m_k) \geq \epsilon \|\nabla m_k\|^2_{L^2} + C_1.$$

Furthermore, using Poincaré inequality

$$\frac{1}{\epsilon} I_\epsilon(m_k) + C_2 \geq \|\nabla m_k\|^2_{L^2} \geq C_3 \|m_k\|^2_{L^2},$$

where $C_1, ..., C_3$ are constants. So we may then deduce that $I(m_k)$ is coercive and

$$\|m_k\|_{W^{1,2}} \leq C.$$

Since $\|m_k\|_{W^{1,2}}$ is bounded and $W^{1,2}$ is reflexive, we may (see Theorem C.3) extract a subsequence (still denoted m_k) such that

$$m_k \rightharpoonup m_0 \in W^{1,2}$$

Considering that the space $W^{1,2}$ is compact nesting in L^2, we have

$$m_k \to m \in L^2.$$

This is equivalent to $\int_\Omega |m_k - m_0|^2 \to 0 \Leftrightarrow |m_0| = 1$ a.e.
Step 2

The functionals $\int_\Omega |\nabla m_k|^2$ and $\int_\Omega |\nabla u_m|^2$ are both convex and so according to Dacorogna [6] (see Theorem C.1), they are weakly lower semicontinuous.

Because $m_k \to m \in L^2$ and ϕ is continuous, $\phi(m_k) \to \phi(m_0)$ a.e. Furthermore, ϕ is bounded, so using Lebesgue's Theorem we obtain $\int \phi(m_k) \to \int \phi(m_0)$ a.e. The same is valid for the interaction energy by using Hölder's inequality

$$\int_\Omega H \cdot (m_0 - m_k) \leq \|H\|_{L^1} \|m_0 - m_k\|_{L^\infty} \to 0,$$

i.e. $\int_\Omega H \cdot m_k \to \int_\Omega H \cdot m_0$ a.e., which is stronger than the assumption of weakly lower semicontinuity required in the proof of Theorem 4.6.4.

Thus, the energy functional $I_\epsilon(m)$ is weakly lower semicontinuous and so, according to Theorem 4.6.4, there exists m_0 such that $I_\epsilon(m_0) = \inf \{I_\epsilon(m) : m \in \mathcal{M}\}$.

4.7 Minimizer existence for linear elasticity

The proof of the minimizer's existence of the potential energy in the linear elasticity is very similar to the previous proof. Let us recall the problem. For $\Omega \subset \mathbb{R}^3$, a bounded domain and $\Gamma_1, \Gamma_2 \subset \partial\Omega$, $u^0 \in W^{1,2}(\Gamma_2; \mathbb{R}^3)$ we denote

$$\mathcal{U} = \left\{ u \in W^{1,2}(\Omega; \mathbb{R}^3) : \tau\nu = g \text{ on } \Gamma_1,\ u = u^0 \text{ on } \Gamma_2 \right\},$$

where u stands for field of displacement, τ for the stress tensor and g represents the contact force.

We study the minimizing problem of the free energy functional

$$I(u) = \frac{1}{2}\int_\Omega \langle \mathbb{C}e(u), e(u)\rangle \,\mathrm{d}x - \int_\Omega f \cdot u \,\mathrm{d}x - \int_{\Gamma_1} g \cdot u \,\mathrm{d}S, \quad u \in \mathcal{U} \tag{4.32}$$

where f stands for a vector field of body force, $\mathbb{C} : \mathbb{R}^{3^4} \times \mathbb{R}^{3^4} \to \mathbb{R}$ is the elasticity tensor (in orthogonal coordinates represented by positively defined matrix) and $e : \mathbb{R}^3 \times \mathbb{R}^3 \to \mathbb{R}$ is the small-deformation tensor. The small deformation is connected with the displacement through

$$e = \frac{1}{2}(\nabla u + (\nabla u)^T).$$

To prove that the free energy reaches the infimum, we will proceed similarly as before.

Let u_k be a minimizing sequence. Since $\mathbb{C}$ is positively defined

$$I(u_k) = \frac{1}{2}\int_\Omega \langle Ce(u_k)e(u_k)\rangle \,\mathrm{d}x - \int_\Omega f \cdot u_k \,\mathrm{d}x \;\geq\; \alpha \left\|e(u_k)\right\|_{L^2}^2 - \left\|f\right\|_{L^2} \left\|u_k\right\|_{L^2}.$$

After applying Korn's and Poincaré inequalities, we obtain

$$I(u_k) + \left\|f\right\|_{L^2} \left\|u_k\right\|_{L^2} \;\geq\; \alpha \left\|e(u_k)\right\|_{L^2}^2 \;\geq\; \alpha \left\|\nabla u_k\right\|_{L^2}^2 \geq \widetilde{\alpha} \left\|u_k\right\|_{L^2}^2.$$

So again we obtain the result

$$\left\|u_k\right\|_{W^{1,2}} \leq C.$$

Taking advantage of the properties of the spaces $W^{1,2}$ or L^2 (reflexivity and $W^{1,2} \hookrightarrow\hookrightarrow L^2$, see Theorem C.3 and Theorem C.4) we gain

$$u_k \rightharpoonup u \in W^{1,2}$$

$$u_k \to u \in L^2.$$

Further proceed is analogous to magnetism. Since the first part of (4.32) is convex and for the second part the Hölder's inequality is valid, the functional $I(u)$ is lower semicontinuous and coercive. And so, owing to Theorem 4.6.4, the free energy functional reaches its infimum, i.e. there exists u_0 such that $I(u_0) = \inf\{I(u) : u \in \mathcal{U}\}$.

Chapter 5

The stationary model for FSMA

In the following chapter, we will study the magnetostrictive materials, which means the combination of both effects - linear elasticity and magnetism. Generally, magnetostriction is the ability of some ferromagnetic materials to change their shape owing to an external magnetic field or to embody magnetization in consequence of deformation.

Such behavior makes us enlarge the potential energy model with the term of energy wells. This brings mathematical difficulties in to the minimizer existence argumentation because the resulting energy functional is not weakly lower semicontinuous at all. Therefore we introduce the quasiconvex formulation of the problem in section 5.1. The existence of the minimizer of a simplified magneto-elastic problem is solved in the successive section 5.2.

5.1 The quasiconvex problem formulation

The free energy of a magneto-elastic material at a fixed temperature below the Curie's temperature is, in general, given by

$$I(u,m) = \int_\Omega \Phi(u(x), m(x), \nabla u(x), \nabla m(x))dx.$$

We denote

$$\mathcal{UM} = \left\{[u,m] \in W^{1,2}(\Omega, \mathbb{R}^6)\right\}$$

for $\Omega \subset \mathbb{R}^6$ a bounded domain, $\Gamma \subset \partial\Omega$. We suppose, that $\mathcal{UM} \neq \emptyset$.

As described above, we may associate the stable phase of the material with the minimum

of the energy. This leads to the following problem:

$$\min \{ \ I(u,m); \ [u,m] \in \mathcal{UM}\}. \tag{5.1}$$

The difference between magneto-elasticity and the situations described in the previous two chapters lies in the assumption of existence of several local minimizers, the so-called energy wells. Each well represents a stable phase of the specimen. The point is that the phase in which the specimen could be found may locally differ, and the laminating structure might occur.

The energy density $\Phi(u(x), m(x), \nabla u(x), \nabla m(x))$ is invariant under material symmetry transformations

$$\Phi(Qu, Qm, Q(\nabla u)Q^T, Q(\nabla m)Q^T) = \Phi(u, m, \nabla u, \nabla m) \quad \forall Q \in \mathrm{SO}(3),$$

where $\mathrm{SO}(3) = \left\{Q \in \mathbb{R}^{3\times 3} : \det Q = 1, QQ^T = Q^TQ = I\right\}$. If $[e(u_0), m_0)]$ corresponds to the minimizer of (5.1), then $[Qe(u_0)Q^T, Qm_0]$ corresponds to the minimizer of (5.1) as well as to each $Q \in \mathrm{SO}(3)$. We suppose that every energy minimizer is generated from only one minimizer by means of symmetry transformations. Hence, the set of minimizers associated with $\int_\Omega \Phi \, \mathrm{d}x$ has the structure

$$\mathcal{W} = \bigcup_{i=1}^{N} [e(u_{0i}), \pm m_{0i}],$$

and for each $i = 1, ..., n$ there exists a symmetry transformation $Q \in \mathrm{SO}(3)$ such that

$$[e(u_{0i}), \pm m_{0i}] = [Qe(u_{01})Q^T, Qm_{01}]. \tag{5.2}$$

Each couple $[e(u_{0i}), m_{0i}]$ is then called the energy well. Thus there are $N = 2n$ energy wells. It turns out that in real materials the positions of energy wells cannot be stationed arbitrarily. The set $\mathcal{W}$ of the energy wells embodies symmetry properties reflecting symmetry of atomic structure of the concerned ferromagnetic material. This is usually called the pairwise compatibility of energy wells.

Definition 5.1.1. *(Pairwise compatibility conditions) The set* $\mathcal{W} = \bigcup_{i=1}^{N} [e(u_{0i}), \pm m_{0i}]$ *consists of* N *pairwise compatible magneto-elastic wells if there exist unit vectors* n_{jk}*, and*

vectors a_{jk}, $j,k = 1,...,N$ *such that*

$$e_j - e_k = \frac{1}{2}(a_{jk} \otimes n_{jk} + n_{jk} \otimes a_{jk}) \tag{5.3}$$
$$(m_j - m_k) \cdot n_{jk} = 0, \tag{5.4}$$

for all $j,k = 1,...,N$.

The structure of pairwise compatible magneto-elastic wells is in fact the consequence of kinematic compatibility condition for solid-to-solid transformation and its application on magnetically active material. This was introduced by James and DeSimone in [8] and is briefly outlined in following paragraph.

It is known (see [9]) that for a diffusionless solid-to-solid phase transformation the kinematic compatibility condition between the strain tensors e_j and e_k is satisfactory if there exists a 180° rotation Q such that

$$Qe_kQ^T = e_j, \quad Q = -I + 2b \otimes b, \tag{5.5}$$

where b denotes the axis of rotation of Q. Assuming (5.5) and letting
$a = 4[(e_k \cdot b \otimes b)b - e_k b]$, we obtain

$$e_j - e_k = \frac{1}{2}(a \otimes b + b \otimes a).$$

Therefore a planar interface can be formed to separate regions of the body deformed according to e_k and e_j, either with normal $n_I = b$ or with normal $n_{II} = a$. In the former case $Qn_I = n_I$ and the region is of type I, while in the latter case $Qn_{II} = n_{II}$ and the region of the body is of type II. In addition to this, let us assume, that Q is a symmetry transformation satisfying (5.2) and there exists a unique easy magnetic direction associated with each e_j, so that

$$m_j = \pm Qm_k. \tag{5.6}$$

Then the magnetic compatibility between k-*th* and j-*th* variant become a consequence of their elastic compatibility. In the case that $m_j = +Qm_k$

$$(m_j - m_k) \cdot n_I = (m_k - m_k) \cdot Qn_I = 0$$

and magneto-elastic compatibility can be achieved by taking $a_{jk} = a, n_{jk} = n_I = b$. If

$m_j = -Qm_k$, then

$$(m_j - m_k) \cdot n_{II} = (m_k \cdot Qn_{II} - m_k) \cdot Qn_{II} = 0$$

and we take $a_{jk} = b, n_{jk} = n_{II} = a$.

The preceding given derivation assumes existence of rotation Q satisfying (5.5) and existence of unique magnetic direction for each $\mathbf{e}_j$, so that equations (5.5) and (5.6) hold simultaneously. Despite these presumptions are not universally valid, they are sufficiently usable in most cases of practical interest.

Let us turn back our attention to the minimizing problem (5.1). Generally, no solution of (5.1) exists, i.e. $I(u, m)$ does not have to reach the minimizer. To demonstrate the aforementioned situation, let us look at the following one-dimensional example.

example 5.1.2. *(Dacorogna)*

$$\text{Minimize } J(y) = \int_0^1 y^2(x) \ + \ (y'^2(x) - 1)^2 dx, \ y \in W^{1,4}([0,1]), \ y(0) = y(1) = 0.$$

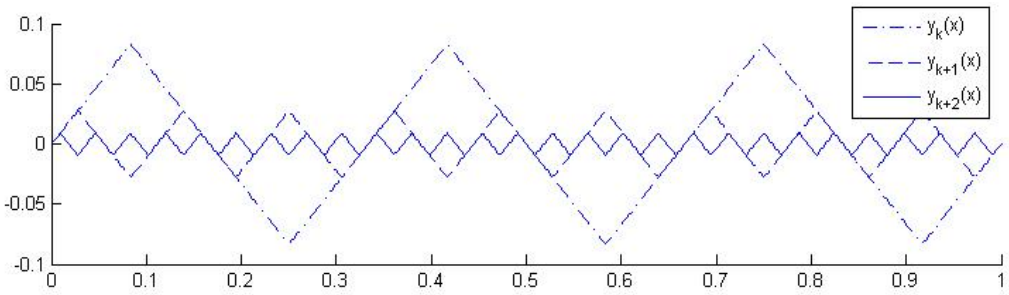

Figure 5.1: Construction of minimizing sequence y_k for J. As one can see $\lim J(y_k) = \inf J = 0$, however $J(w - \lim y_k) = J(0) > 0$.

It is easy to see that sequences of functions depicted on Figure 4.1 are the minimizing sequence for J and that $\lim J(y_k) = \inf J = 0$. However, $J(w - \lim y_k) = J(0) > 0$ and so the minimum is never reached. The point is that the functional J is not sequentially weak lower semicontinues, which is the same problem we face in the model of magnetostriction. This is sometimes called double/multiple-well model (spacial oscillations among various variants of solid phase). The situation is schematically depicted on Figure 5.2.

On the other hand we saw that in linear elasticity or simply magnetism, the stable state (energy minimizer) is being reached. It is necessary to answer the question, what is the property of the energy density Φ which prevents such behavior. This condition is called quasiconvexity.

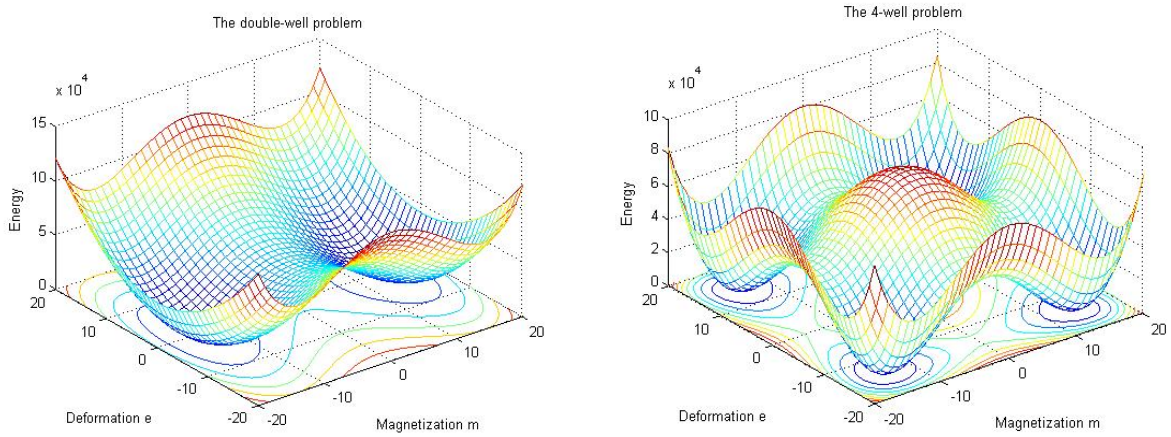

(a) Double-well problem (b) Multiple-well problem

Figure 5.2: Schematic illustration of double-well and multiple-well problem. The energy functional of 1D specimen (e.g. wire) made from magnetostrictive material embodies two (a) four (b) local minimums.

Definition 5.1.3. *$f : \mathbb{R}^{m\times n} \to \mathbb{R}$ is said to be quasiconvex if for any matrix $A \in \mathbb{R}^{m\times n}$ and any smooth function $\phi : \Omega \subset \mathbb{R}^n \to \mathbb{R}^m, \phi(x) = Ax$, for $x \in \partial\Omega$ holds that*

$$\int_\Omega f(\nabla\phi(x))dx \geq f(A)\ |\Omega|.$$

We can see that we deal with density which is not quasiconvex. Suitable extension (relaxation) of the problem, which would provide solvability, was introduced by Dacorogna (see Appendix Theorem C.2 or [6], Section 5.1). For the rest of this Section, let us denote the couple $[u, m] = v$, then we can reformulate the minimizing problem to

$$\min\left\{I_Q = \int_\Omega Q\Phi(v(x), \nabla v(x))dx; \quad v \in \mathcal{UM}\right\}, \tag{5.7}$$

where $Q\Phi(v, \cdot)$ is the quasiconvex envelope of $\Phi(v, \cdot)$ defined by

$$Q\Phi(v, \cdot) = \sup\{f \leq \Phi(v, \cdot); f \text{ quasiconvex}\}.$$

In such a case, I_Q is sequentially weakly lower semicontinuous and the problem (4.2) has a solution. That is to say that there is $v_0 \in \mathcal{UM}$ such that

$$I_Q(v_0) = \min\{I_Q(v) : v \in \mathcal{UM}\} \equiv \min(4.2).$$

The illustration of the idea of the quasiconvex envelope for energy functionals showed in 5.2 can be found in Figure 5.3.

The relaxed problem is connected with the original one via relaxation theorem introduced by Dacorogna, which says that under several growth conditions:

(i) $\inf(5.1) = \min(4.2)$,

(ii) if $v_0 \in \mathcal{UM}$ is a solution to (4.2) then there is a minimizing sequence $\{v_k\}_{k=1}^{\infty} \subset \mathcal{UM}$ converging weakly to v_0 in $W^{1,2}(\Omega, \mathbb{R}^3)$ and $\lim_{k\to\infty} I(v_k) = I_Q(v_0)$,

(iii) any minimizing sequence of (4.1) converges weakly to the minimizer of (4.2).

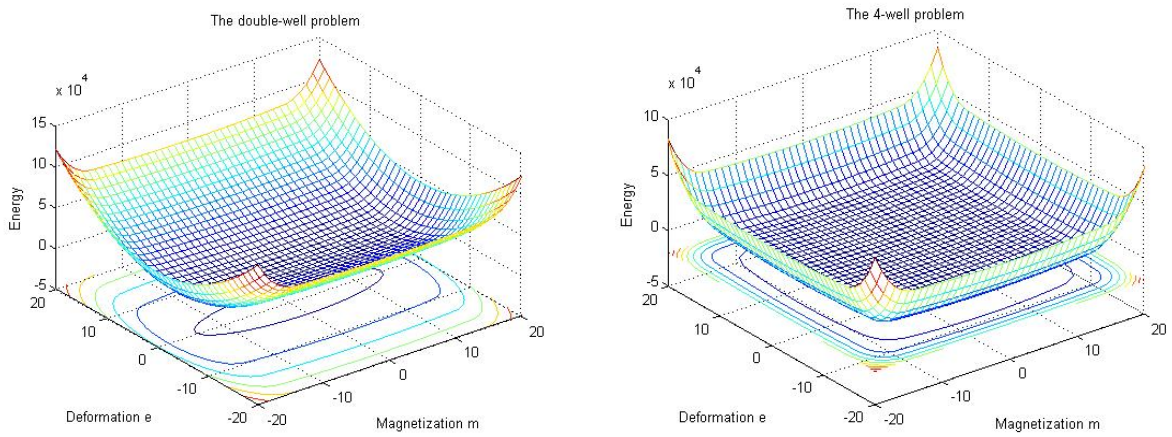

(a) Double-well problem

(b) Multiple-well problem

Figure 5.3: The quasiconvex envelope of the energy functional of 1D specimen made from magnetostrictive material introduced in figure 5.2.

5.2 The mathematical model of ferromagnetic shape memory alloy

Consider a magneto-elastic material having N martensitic variants. Each variant is characterized by a stress-free deformation, which is a symmetric $n \times n$ tensor ($n = 2, 3$ is the dimension), and by an easy axis prescribing two preferred directions of the magnetization $\pm m$. So, we actually face a $2N$-well problem. As a characterizing quantity, we choose $v : \Omega \to \mathbb{R}^{n(n+1)/2+n}$ as a conjunction of independent components of the symmetric tensor $e(u)$ and the magnetization m. For $n = 3$, we have

$$v = (e_{11},\ e_{22},\ e_{33},\ e_{12},\ e_{13},\ e_{23},\ m_1,\ m_2,\ m_3)$$

$$|m| = m_1^2 + m_2^2 + m_3^2 = 1$$

The i-*th* well is then described by the vector $v^i \in \mathbb{R}^{n(n+1)/2+n}$ where the first $n(n+1)/2$ components stay for the symmetric strain and the last n components stay for the magnetization. We assume that the set of v^i satisfies the pairwise compatibility conditions. We can group v^i, $i = 1, \dots, 2N$ so that v^{2j-1} differs from v^{2j} by the sign of the last n components $j = 1, \dots, N$.

We suppose that all variants have the same "magneto-elastic" moduli and that the magneto-elastic energy density of the i-*th* variant is given by

$$W_i(v) = \frac{1}{2}\left\langle \mathbb{C}(v - v^i), (v - v^i) \right\rangle \ ,$$

where $v \in \mathbb{R}^{n(n+1)/2+n}$ is the given configuration and $\mathbb{C}$ stands for the magneto-elastic tensor. The magneto-elastic tensor is an extension of the elasticity tensor, which denotes the response of a magneto-elastic material to both deformation and external magnetic field. We presume that $\mathbb{C}$ is positively defined. The overall energy is then

$$W(v) = \min_{1 \le i \le 2N} W_i(v) \ .$$

Notice that we know v if we know the displacement $u : \Omega \to \mathbb{R}^n$ of the body and its magnetization $m : \Omega \to \mathbb{R}^n$, $|m| = 1$ a.e. Hence, we set up the energy functional

$$I(u, m) = \int_\Omega W(v(x))\,\mathrm{d}x - \int_\Omega f \cdot u \mathrm{d}x - \tag{5.8}$$

$$- \int_{\Gamma_1} g \cdot u \mathrm{d}S - \int_\Omega H \cdot m + \frac{\mu_0}{2}\int_{\mathbb{R}^n} |\nabla u_m|^2\,\mathrm{d}x. \tag{5.9}$$

When compared with (4.29), we can see that the magnetic exchange energy was neglected. In this correction we take into consideration scaling analysis for the large body introduced by DeSimone in [7].

However, due to nonconvexity of W and because of the nonconvex constraint $|m| = 1$, the minimum of I does not necessarily exist for $u \in W^{1,2}(\Omega; \mathbb{R}^n)$, $u = u^0$ on Γ_0 and $m \in L^2(\Omega; \mathbb{R}^n)$, $|m| = 1$ because I is not sequentially weakly lower semicontinuous. Hence, we look for a weakly lower semicontinuous extension $\bar{I}$ of I which is, generally, very difficult

to find.

Following Govindjee, Mielke (see [11]) we estimate the effective energy density $\bar{W}$ by

$$\bar{W}(\lambda, v) = \sum_{i=1}^{2N} \lambda_i W_i(v) + \frac{1}{2} \sum_{i=1}^{2N} (\lambda_i^2 - \lambda_i) \left\langle \mathbb{C} v^i, v^i \right\rangle \ ,$$

where $\lambda_i : \Omega \to \langle 0, 1 \rangle : \ 0 \leq \lambda_i, \ \sum_i \lambda_i = 1$ are the volume fractions of particular variants. Function $\lambda_i(x)$ expresses the relative representation of i-th phase in an infinitesimal surrounding of point x. It is easy to see that

$$\bar{W}(\lambda, v) = \frac{1}{2} \left\langle \mathbb{C}(v - \sum_{i=1}^{2N} \lambda_i v^i), (v - \sum_{i=1}^{2N} \lambda_i v^i) \right\rangle \ ,$$

$\lambda = (\lambda_1, \ldots, \lambda_{2N})$. Moreover, we relax the constraint $|m| = 1$ to $|m| \leq 1$.

Assuming $f \in L^2(\Omega)$,$g \in L^2(\Gamma_1)$ and $H \in L^2(\Omega)$, we define the relaxed free energy functional

$$\begin{aligned} \bar{I}(\lambda, u, m) &= \int_\Omega \bar{W}(\lambda(x), v(x)) \, \mathrm{d}x - \int_\Omega f \cdot u \mathrm{d}x - & (5.10) \\ &- \int_{\Gamma_1} g \cdot u \mathrm{d}S - \int_\Omega H \cdot m + \frac{\mu_0}{2} \int_{\mathbb{R}^n} |\nabla u_m|^2 \, \mathrm{d}x. & (5.11) \end{aligned}$$

The task is to minimize it for $|m| \leq 1$, $m \in L^2(\Omega; \mathbb{R}^n)$, $\lambda \in L^\infty(\Omega; \mathbb{R}^{2N})$, $u \in W^{1,2} : \ u = u^0$ on Γ.

To show the existence means to apply the same procedure as before. Notice that the first term of (5.10) which contains $\mathbb{C}$ is strictly convex if $\mathbb{C}$ is positively defined. Then for $\int_\Omega \bar{W}(\lambda, v) \mathrm{d}x$ the following estimation is valid:

$$\begin{aligned} \int_\Omega \bar{W}(\lambda, v) \mathrm{d}x &\geq \alpha \left\| v - \sum_{i=1}^{2N} \lambda_i v^i \right\|_{L^2}^2 \geq \\ &\geq \alpha \left| \|v\|_{L^2} - \left\| \sum_{i=1}^{2N} \lambda_i v^i \right\|_{L^2} \right|^2 \geq \alpha \|v\|_{L^2}^2 - c \|v\|_{L^2}. \end{aligned}$$

For the remaining terms of $\bar{I}(\lambda, u, m)$ we use estimations introduced in the previous chapter, i.e.

$$\begin{aligned}\int_\Omega H\cdot m\mathrm{d}x+\int_\Omega f\cdot u\mathrm{d}x &\leq c_m\left\|m\right\|_{L^2}+c_u\left\|u\right\|_{L^2}\leq\\ &\leq c_m\left\|m\right\|_{L^2}+\tilde{c}_u\left\|\nabla u\right\|_{L^1}\leq c\left\|v\right\|_{L^2},\end{aligned}$$

where $c_m, c_u, \tilde{c}_u, c\in\mathbb{R}$. So finally

$$\bar{I}(\lambda,u,m)\geq\alpha\|v\|_{L^2}^2-\widetilde{c}\|v\|_{L^2}.$$

Let us consider the set

$$\mathcal{H}=\left\{(\lambda,u,m):|m|\leq 1, m\in L^2(\Omega;\mathbb{R}^n),\lambda\in L^\infty(\Omega;\mathbb{R}^{2N}),u\in W^{1,2}\right\}$$

and $(\lambda_k,u_k,m_k)\in\mathcal{H}$, the minimizing sequence for $\inf\bar{I}$, i.e.

$$\bar{I}(\lambda_k,u_k,m_k)\longrightarrow\inf\bar{I}.$$

We assume that $\lambda_k\to\lambda$ and $m_k\to m$. Considering estimations made above, we may deduce that $\bar{I}(\lambda_k,u_k,m_k)$ is coercive and that there exists $K\geq 0$, independent of k, such that

$$\|u_k\|_{W^{1,2}}\leq K\ ,\ \|m_k\|_{L^2}\leq K.$$

Since L^2 is reflexive Banach space and $W^{1,2}\hookrightarrow\hookrightarrow L^2$ we can extract weakly convergent subsequence (still denoted u_k) such that

$$u_k\rightharpoonup u \text{ in } W^{1,2}\quad\text{and}\quad u_k\to u \text{ in } L^2.$$

The terms $\int_\Omega\bar{W}(\lambda,v)$ and $\frac{\mu_0}{2}\int_{\mathbb{R}^n}|\nabla u_m|^2\,\mathrm{d}x$ are convex and so, according to Dacorogna, weakly lower semicontinuous. The remaining terms of (5.10) are continuous functionals, and u_k and m_k converge strongly. Therefore $\int_\Omega f\cdot u_k\mathrm{d}x\to\int_\Omega f\cdot u\mathrm{d}x$, $\int_\Omega H\cdot m_k\mathrm{d}x\to\int_\Omega H\cdot m\mathrm{d}x$ and $\int_\Gamma g\cdot u_k\mathrm{d}S\to\int_\Gamma g\cdot u\mathrm{d}S$. Hence $\bar{I}$ is sum of weakly lower semicontinuous functionals, it is weakly lower semicontinuous as well. Considering Theorem 4.6.4, we obtain the required statement, i.e.

$$\inf\bar{I}=\bar{I}(\lambda,u,m).$$

Chapter 6

The evolutionary model for FSMA

In this chapter we introduce evolutionary model of FSMA. The model is again build on a suitable extremum principle. We take advantage of the relaxed concept formulated in the Section 5.1. While in the steady case we were interested in the stored energy (described by an appropriate thermodynamical potential) only, in the case of time evolution we also want to take the effect of hysteresis into account. Therefore, two energy functionals are used: $\mathcal{E}$ describes the stored energy corresponding to a particular martensitic phase and $\mathcal{D}$ prices the phase transformation into a different martensitic phase.

Firstly, we introduce the concept of rate-independent processes is general in Section 6.1. Secondly, we apply the the general framework to the FSMA in Section6.2 and formulate the evolutionary model. Finally, we discuss the solution existence of the rate-independent process in Section 6.3.

6.1 Rate-independent process and energetic formulation

Let X be a Banach space, $y(t) : [0,T] \to X$ a state variable(s) describing the system at time t. A family of states $(y(t))_{[}0,T]$ is called a process. The rate-independence of the process means that the process is invariant with respect to any time rescaling. That is to say, if $y(t)$ is a process corresponding to some loading $\mathcal{L}$ and τ is any strictly monotone time reparametrization, then $y(\tau t)$ is a process corresponding to the loading $\mathcal{L}(\tau t)$.

The rate-independent process is defined through two energy functionals:

- the time-dependent energy-storage

$$\mathcal{E} : [0,T] \times X \to [0,\infty],$$

- the dissipation distance

$$\mathcal{R} : X \to [0, \infty].$$

The fact that the process is rate-independent implies that $\mathcal{R}$ is 1-homogeneous and weakly lower semi-continuous functional. The dissipation potential influences the evolution via the dissipation distance $\mathcal{D} : X \times X \to [0, \infty]$ defined by $\mathcal{D}(y_1, y_2) = \mathcal{R}(y_1 - y_2)$. We denote the total amount of energy dissipated within the process y during a time interval $[0, T]$ by $\mathrm{Diss}_{\mathcal{D}}$, with

$$\mathrm{Diss}_{\mathcal{D}}(y; [0, T]) = \sup\{\sum_{j=1}^{N} \mathcal{D}(y(t_{j-1}), y(t_j)), N \in \mathbb{N}, 0 = t_0 < ... < t_N = T\}.$$

Having the two constitutive functionals we may formulate the evolution law for a material. Following [27] we use an extremum principle formulated e.g. in [23]. The principle states that the change in the state occurs when it is thermodynamically admissible. In terms of energy, the energy gain caused by transition from y to $\hat{y}$ is greater than (or equal to) energy dissipation connected with this transition. Simultaneously the first law of thermodynamics has to be satisfied within every process, i.e. the sum of energy dissipated within a process and work done by external forces (loading) is equal to the energy obtained through the process.

Now, we are ready to define reasonably the solution for the evolutionary problem. Such a formulation is sometimes called the energetic concept.

Definition 6.1.1. *A process (function) $y(t) : [0, T] \to X$ is called energetic solution to the rate-independent model associated with $\mathcal{E}$ and $\mathcal{R}$, if the mapping $t \mapsto \partial_t \mathcal{E}(t, y(t))$ lies in $L^1((0, T), \mathbb{R})$ and if for all $t \in [0, T]$:*

$$\textbf{Stability}: \quad \forall \hat{y} \in X : \mathcal{E}(t, y(t)) \leq \mathcal{E}(t, \hat{y}(t)) + \mathcal{D}(y(t), \hat{y}), \tag{6.1}$$

$$\textbf{\textit{Energy Balance:}} \quad \mathcal{E}(t, y(t)) + \mathrm{Diss}_{\mathcal{D}}(y, [0, t]) = \mathcal{E}(0, y(0)) + \int_0^t \partial_\tau \mathcal{E}(\tau, y(\tau)) \, \mathrm{d}\tau. \tag{6.2}$$

The natural way to treat the evolutionary problem is to employ a time discretization $0 \leq t_0 <\leq t_1 \dots t_{N-1} \leq t_N = T$. Thus, the evolution is represented by sequence of time-incremental minimization problems

$$\text{Find minimizer } y_k \in X \text{ of functional } \mathcal{E}(t_k, y) + \mathcal{D}(y_{k-1}, y).$$

The aim of our effort is to show that sets of incremental problem solutions converge to

the solution of the evolutionary problem. Consequently, this strategy is a guideline to a straightforward numerical implementation of the model.

It is worth mentioning that the evolutionary problem might be formulated in alternative (local) way. We might search for $y(t)$ satisfying differential inclusion

$$-\mathrm{D}\mathcal{E}(t, y(t)) \in \partial\mathcal{R}(\dot{y}(t)), \tag{6.3}$$

where ∂ stands of subdifferential of a convex function. However, the formulation via (6.3) requires $\mathcal{E}$ to be strictly convex in order to obtain time continuous solutions. The energetic formulation has not such property. Additionally, the derivative of $t \to y(t)$ nor $z \to \mathcal{E}(t, y(t)$ does not need to be provided. Nevertheless, it was observed in [26] that energetic formulation is equivalent to (6.3) if $\mathcal{E}$ is quadratic and convex functional. So it might be understood as a weak form of the inclusion (6.3).

6.2 FSMA energetic model

We shall be concerned with evolution of FSMA body within time interval [0,T]. The sample is represented by domain $\Omega \in \mathbb{R}^3$. In the case of FSMA, the state variable $y(t)$ is compound of displacement $u(t)$, magnetization $m(t)$ and volume fraction $\lambda(t)$. To model the evolution of FSMA we take advantage of the relaxed stationary formulation considering that all variables are time-dependent now.

At each time level $t \in [0, T]$ we require $u(t)$ to satisfy boundary conditions

$$u = 0 \quad \text{on} \quad \Gamma_0, \qquad \sigma n = g \quad \text{on} \quad \Gamma_1,$$

where $\Gamma_0 \in \partial\Omega$ denotes non-empty part of the boundary, n stands for unit outer normal to the boundary $\partial\Omega$ and $\Gamma_1 = \Omega \setminus \Gamma_0$. Hence, we define the set of admissible displacements

$$\mathcal{U} = \left\{ u \in W^{1,2}(\Omega, \mathbb{R}^3), \quad u = 0 \text{ on } \Gamma_0 \right\}$$

and the set of of admissible magnetizations

$$\mathcal{M} = \left\{ m \in W^{1,2}(\Omega, \mathbb{R}^3);\ |m| \leq 1 \text{ a.e. in } \Omega \right\}.$$

We allow the volume fraction to belong to

$$\mathcal{L} = \left\{ \lambda \in W^{1,1}(\Omega, \mathbb{R}^{2N}),\ \lambda_i \geq 0,\ i = 1...2N,\ \sum\nolimits_{i=1}^{2N} \lambda_i = 1 \right\}.$$

Let for given $t \in [0,T]$ $f(t) \in L^\infty(\Omega, \mathbb{R}^3)$, $g(t) \in L^\infty(\Gamma_1, \mathbb{R}^3)$ be the mechanical volume and surface loading respectively and $H(t) \in L^\infty(\Omega, \mathbb{R}^3)$ be the external magnetic field. We might define the loading functional at time t

$$\langle \ell(t), v \rangle = \int_\Omega f(t) \cdot u \mathrm{d}x + \int_{\Gamma_1} g(t) \cdot u \mathrm{d}S + \int_\Omega H(t) \cdot m \, \mathrm{d}x.$$

The stored energy is described by functional $\mathcal{E} : [0,T] \times \mathcal{U} \times \mathcal{M} \times \mathcal{L} \to [0,\infty]$ which reads as

$$\begin{aligned} \mathcal{E}(t,u,m,\lambda) = &\int_\Omega \bar{W}(\lambda, v)\ \mathrm{d}x - \left\langle \ell(t), v \right\rangle \\ &+ \epsilon \int_\Omega |\nabla m|^2 \, \mathrm{d}x + K^\lambda \int_\Omega |\nabla \lambda| \, \mathrm{d}x + \frac{\mu_0}{2} \int_{\mathbb{R}^n} |\nabla u_m|^2 \ \mathrm{d}x. \end{aligned} \tag{6.4}$$

Recall that $v = (e, m)$ and $\bar{W}(\lambda, v)$ denotes the relaxed magneto-elastic energy density

$$\bar{W}(\lambda, v) = \frac{1}{2} \left\langle \mathbb{C}(v - \sum_{i=1}^{2N} \lambda_i v^i), (v - \sum_{i=1}^{2N} \lambda_i v^i) \right\rangle.$$

Again, at each the magnetostatic potential u_m is associated with magnetization through Maxwell's equations, namely

$$t \in [0,T] \quad \mathrm{div}(-\mu_0 \nabla u_m(t) + m(t)\chi_\Omega) = 0.$$

Contrary to 5.10 a term containing gradient of λ was added. The term (scaled by positive constant K^λ) penalizes martensitic phase oscillations. Since the volume fraction is necessarily not continues, sharp interfaces between particular martensitic phases may occur.

The energy dissipation is set by the dissipation functional

$$\mathcal{R}(\dot{\lambda}(t)) = R^\lambda \int_\Omega |\dot{\lambda}(t)| \, \mathrm{d}x, \tag{6.5}$$

which naturally determinate the dissipation distance $\mathcal{D} : \mathcal{L} \times \mathcal{L} \to [0, \infty]$.

$$\mathcal{D}(\lambda_1, \lambda_2) = R^\lambda \int_\Omega |\lambda_1 - \lambda_2| \, \mathrm{d}x, \tag{6.6}$$

with $R^\lambda > 0$ and for all $\lambda_1, \lambda_2 \in \mathcal{L}$.

It is worth pointing out that our considerations are still based on the magnetostatic version of Maxwell's equations. That is to say, no cross coupling phenomena between magnetic and electric field is involved as the time step goes to zero. Such a huge assumption might be justified only when the relaxation processes within the material are fast compared to evolution rate of the applied loading.

In order to make the notation well-arranged, let us define the sets $\mathcal{S}(t)$ of stable states at time t:

$$\begin{aligned}\mathcal{S}(t) = \big\{ (u, m, \lambda) \in \mathcal{U} \times \mathcal{M} \times \mathcal{L} : \mathcal{E}(t, u, m, \lambda) < \infty \text{ and} \\ \forall (\hat{u}, \hat{m}, \hat{\lambda}) : \mathcal{E}(u, m, \lambda) \leq \mathcal{E}(\hat{u}, \hat{m}, \hat{\lambda}) + \mathcal{D}(\hat{u}, \hat{m}, \hat{\lambda}) \big\}\end{aligned}$$

and the stable graph $\mathcal{S}_{[0,T]} = \bigcup_{[0,T]} (t, \mathcal{S}(t)) \subset [0, T] \times \mathcal{U} \times \mathcal{M} \times \mathcal{L}$.

The task is to find the energetic solution for the functionals $\mathcal{E}$ and $\mathcal{R}$, that is to say for a given initial state $(u_0, m_0, \lambda_0) \in \mathcal{S}(0)$ and given loading $(f(t), g(t), H(t))$ find $(u(t), m(t), \lambda(t)) \in \mathcal{U} \times \mathcal{M} \times \mathcal{L}$ such that $(u(0), m(0), \lambda(0)) = (u_0, m_0, \lambda_0)$, and $\forall t \in [0, T]$: $(u(0), m(0), \lambda(0)) \in \mathcal{S}(t)$ and the energy balance (6.2) is satisfied.

6.3 Energetic solution existence

In this section we prove the existence of the energetic solution for the rate independent FSMA model (described via functionals $\mathcal{E}$ and $\mathcal{D}$). Our reasoning is based on now classical theory for energetic solutions, see e.g. [26],[25]. We formulate the existence theorem for the particular case of FSMA and show that it is a corollary of the existence result presented in [28].

Theorem 6.3.1 (Existence for the FSMA model)**.** *Let us assume that the loading is* $f \in C^1([0, T], L^\infty(\Omega, \mathbb{R}^3))$, $H \in C^1([0, T], L^\infty(\Omega, \mathbb{R}^3))$ *and* $g \in C^1([0, T], L^\infty(\Gamma_1, \mathbb{R}^3))$, *and* $(u_0, m_0, \lambda_0) \in \mathcal{S}(0)$. *Then there exists an energetic solution for the rate independent model*

of FSMA determined by (6.4) *and* (6.5) *with*

$$u \in \mathrm{B}([0,T], W^{1,2}(\Omega,\mathbb{R}^3)),\ m \in \mathrm{B}([0,T], W^{1,2}(\Omega,\mathbb{R}^3)) \quad \textit{and}$$

$$\lambda \in L^\infty([0,T], W^{1,1}(\Omega,\mathbb{R}^{2N})) \cap BV([0,T], L^1(\Omega,\mathbb{R}^{2N})).$$

Proof. The existence proof is based on a time-incremental minimization problem. Assume an arbitrary partition of the time interval $0 = t_0 < ... < t_N = T$. Considering the 1-homogeneity of the dissipation distance $\mathcal{D}$, we are asked on each discrete time level to solve a following problem:

$$\begin{gathered}\text{For } k \in 1,\dots,N \text{ and given } (u_0, m_0, \lambda_0) \in \mathcal{S}(0) \text{ find on } \mathcal{U}\times\mathcal{M}\times\mathcal{L}\\ \text{minimizer } u_k, m_k, \lambda_k \text{ of functional } \mathcal{E}(t_k,u,m,\lambda) + \mathcal{D}(\lambda,\lambda_{k-1}).\end{gathered}$$

Step 1: Incremental problem solution

Lemma 6.3.2. *Let the functionals $\mathcal{E}$ and $\mathcal{D}$ be defined via* (6.4) *and* (6.5)*, with loading qualification as in theorem . Then for every $k \in 1,\dots,N$ there exists a minimizer (u_k, m_k, λ_k) of the functional $\mathcal{E}(t,u,m,\lambda) + \mathcal{D}(\lambda,\lambda_{k-1})$ on $\mathcal{U}\times\mathcal{M}\times\mathcal{L}$. That is to say, on every time level there exists a a solution of the time incremental problem.*

Proof. Following the procedure showed in the steady state, we have

$$\begin{aligned}&\mathcal{E}(t,u,m,\lambda) + \mathcal{D}(\lambda,\lambda_{k-1})\\ &\quad= \int_\Omega \bar{W}(\lambda,v)\ \mathrm{d}x - \Big\langle \ell(t), v\Big\rangle + \epsilon\,\|\nabla m\|_{L^2}^2 + \frac{\mu_0}{2}\,\|\nabla u_m\|_{L^2}^2 + K^\lambda\,\|\nabla\lambda\|_{L^1} + R^\lambda\,\|\lambda-\lambda_{k-1}\|_{L^1}\\ &\quad\geq \alpha\|v\|_{L^2}^2 - c_1\|v\|_{L^1} - c_2\,\|v\|_{L^2} + c_3\,\|\lambda\|_{W^{1,1}}\,.\end{aligned}$$

Therefore, we have coercivity:

$$\mathcal{E}(t,u,m,\lambda) + \mathcal{D}(\lambda,\lambda_{k-1}) \to \infty \text{ for } \|u\|_{W^{1,2}} + \|m\|_{W^{1,2}} + \|\lambda\|_{W^{1,1}} \to \infty.$$

Both functionals $\mathcal{E}$ and $\mathcal{D}$ are convex and lower semi-continuous. Hence, they are weakly lower semi-continuous. The minimizer existence is then guaranteed by the fundamental lemma of calculus of variations.

□

Lemma 6.3.3. *Let the presumptions of the theorem 6.3.2 are fulfilled. Then for $\mathcal{E}(t,u,m,\lambda)$ given by (6.4) there exist $c_E^0, c_E^1 > 0$ such that*

$$\mathcal{E}(t,u,m,\lambda) < \infty \quad \Longrightarrow \quad |\partial_t \mathcal{E}(t,u,m,\lambda)| \leq c_E^1(c_E^0 + \mathcal{E}(t,u,m,\lambda)). \tag{6.7}$$

Proof. Let us recall

$$\begin{aligned}\mathcal{E}(t,u,m,\lambda) &= \int_\Omega \bar{W}(\lambda, v)\,\mathrm{d}x - \left\langle \ell(t), v \right\rangle + \epsilon \left\|\nabla m\right\|_{L^2}^2 + K^\lambda \left\|\nabla \lambda\right\|_{L^1} + \frac{\mu_0}{2}\left\|\nabla u_m\right\|_{L^2}^2 \\ &\geq \frac{\alpha}{2}\left\|v\right\|_{L^2}^2 - C(1 + \left\|\ell(t)\right\|_{L^\infty}\left\|v\right\|_{L^2}) \geq \tilde{C}\left\|v\right\|_{L^2} - \frac{1}{2\alpha}\left(\tilde{C} + C(1+\left\|\ell(t)\right\|_{L^\infty})\right)^2,\end{aligned}$$

where $C > 0$,Using this estimate and qualification of the loading, we arrive with

$$|\partial_t \mathcal{E}(t,u,m,\lambda)| \leq \left\|\dot{\ell}(t)\right\|_{L^\infty}\left\|v\right\|_{L^2} \leq \frac{\left\|\dot{\ell}(t)\right\|_{L^\infty}}{\tilde{C}}\left(\mathcal{E}(t,u,m,\lambda) + \frac{1}{2\alpha}\left(\tilde{C} + C(1+\left\|\ell(t)\right\|_{L^\infty})\right)^2\right).$$

As one can see $c_E^1 = \frac{\left\|\dot{\ell}(t)\right\|_{L^\infty}}{\tilde{C}}$ and $c_E^0 = \frac{1}{2\alpha}\left(\tilde{C} + C(1+\left\|\ell(t)\right\|_{L^\infty})\right)^2$. □

In fact, the Lemma 6.3.3 says that $t \mapsto \mathcal{E}(t,u,m,\lambda)$ is uniformly bounded and differentiable on $[0,T]$. Consequently, the lemma secures the uniform continuity of $t \mapsto \mathcal{E}(t,u,m,\lambda)$ on sublevels of $\mathcal{E}$: take $t_1, t_2 \in [0,T]$:

$$\begin{aligned}\mathcal{E}(t_2,u,m,\lambda) &= \mathcal{E}(t_1,u,m,\lambda) + \int_{t_1}^{t_2} \partial_\tau \mathcal{E}(\tau,u,m,\lambda)\,\mathrm{d}\tau \\ c_E^0 + \mathcal{E}(t_2,u,m,\lambda) &\leq \mathcal{E}(t_1,u,m,\lambda) + c_E^0 + \int_{t_1}^{t_2} c_E^1(c_E^0 + \mathcal{E}(\tau,u,m,\lambda)) \\ \mathcal{E}(t_2,u,m,\lambda) &\leq (\mathcal{E}(t_1,u,m,\lambda) + c_E^0)e^{c_E^1|t_2-t_1|} - c_E^0, \end{aligned} \tag{6.8}$$

where we used the 6.7 and Gronwall's lemma respectively.

Additionally, the loading functions f, g, H are localy Lipschitz in time because they are assumed to have continouos time derivative. Furthermore, $\mathcal{E}$ satisfied strenghened version of 6.7: $\forall E > 0\ \exists$ modulus of continuity $\omega_\mathcal{E} : [0,t] \mapsto [0,\infty)$:

$$\mathcal{E}(0,u,m,\lambda) < E \quad \Longrightarrow \quad \forall t_1, t_2 \in [0,T] : |\partial_t \mathcal{E}(t_1,u,m,\lambda) - \partial_t \mathcal{E}(t_2,u,m,\lambda)| \leq \omega_E(t_1 - t_2).$$

Step 2: A priori estimates

Having an energy minimizer at each time level (i.e an incremental problem solution), we wish to show that it is coherent with the energetic formulation. Following lemma shows that energy minimizers have appropriate qualities and additionally it provides suitable a priori estimates.

Lemma 6.3.4. *let* $(u_0, m_0, \lambda_0) \in \mathcal{S}(0)$*, then every solution of the incremental problem satisfies the discrete version of the stability condition* (6.1)

$$u_k, m_k, \lambda_k \in \mathcal{S}(t_k) \tag{6.9}$$

and the discrete version of the energy balance (6.2)*:*

$$\int_{t_{k-1}}^{t_k} \partial_t \mathcal{E}(\tau, u_k, m_k, \lambda_k)\,\mathrm{d}\tau \le \mathcal{E}_k + \mathcal{D}_k - \mathcal{E}_{k-1} \le \int_{t_{k-1}}^{t_k} \partial_t \mathcal{E}(\tau, u_{k-1}, m_{k-1}, \lambda_{k-1})\,\mathrm{d}\tau, \tag{6.10}$$

for all $k \in \{1, \dots, N\}$*. We denote* $\mathcal{E}_k = \mathcal{E}(t_k, u_k, m_k, \lambda_k), \mathcal{E}_{k-1} = \mathcal{E}(t_{k-1}, u_{k-1}, m_{k-1}, \lambda_{k-1})$ *and* $\mathcal{D}_k = \mathcal{D}(\lambda_k, \lambda_{k-1})$*. Furthermore, following a priori estimates are fulfilled*

$$\mathcal{E}_k \le \left(\mathcal{E}_0 + c_E^0\right) e^{c_E^1 t_k} - c_E^0 \quad \textit{and} \quad \sum_{j=1}^{N} \mathcal{D}_j \le \left(\mathcal{E}_0 + c_E^0\right) e^{c_E^1 T}. \tag{6.11}$$

Proof. The discrete stability condition follows from the definition of a minimizer and the fact that $\mathcal{D}$ satisfies the triangle inequality

$$\mathcal{E}_k + \mathcal{D}_k \le \mathcal{E}(t_k, u, m, \lambda) + \mathcal{D}(\lambda, \lambda_{k-1}) \le \mathcal{E}(t_k, u, m, \lambda) + \mathcal{D}_k + \mathcal{D}(\lambda, \lambda_k).$$

The upper estimate in the discrete energy balance (6.10) comes from minimality of (u_k, m_k, λ_k) tested by $(u, m, \lambda) = (u_{k-1}, m_{k-1}, \lambda_{k-1}$

$$\begin{aligned}\mathcal{E}_k + \mathcal{D}_k &\le \mathcal{E}(t_k, u_{k-1}, m_{k-1}, \lambda_{k-1}) + \mathcal{D}(\lambda_{k-1}, \lambda_{k-1}) \\ &\le \mathcal{E}(t_{k-1}, u_{k-1}, m_{k-1}, \lambda_{k-1}) + \int_{t_{k-1}}^{t_k} \partial_t \mathcal{E}(\tau, u_{k-1}, m_{k-1}, \lambda_{k-1})\,\mathrm{d}\tau.\end{aligned}$$

To justify the lower estimate in (6.10), one has to test the stability of $(u_{k-1}, m_{k-1}, \lambda_{k-1})$

by (u_k, m_k, λ_k)

$$\mathcal{E}_{k-1} \leq \mathcal{E}(t_{k-1}, u_k, m_k, \lambda_k) + \mathcal{D}_k = \mathcal{E}_k + \mathcal{D}_k - \int_{t_{k-1}}^{t_k} \partial_t \mathcal{E}(\tau, u_k, m_k, \lambda_k)\, \mathrm{d}\tau. \tag{6.12}$$

The a priori estimates are direct consequence of the upper estimate (**??**) combined with (**??**). Using Gronwall's lemma in a same as in we arrive with

$$\mathcal{E}_k + \mathcal{D}_k \leq (\mathcal{E}_{k-1} + c_E^0)(e^{c_E^1(t_k - t_{k-1})} - 1) = (\mathcal{E}(t_{k-1} + c_E^0) e^{c_E^1(t_k - t_{k-1})} - c_E^0.$$

If we consider $\mathcal{D}_k \geq 0$, the induction over $j = 1, \dots k$ gives

$$\mathcal{E}_k + c_E^0 \leq (\mathcal{E}_0 + c_E^0) \prod_{j=1}^{k} e^{c_E^1(t_j - t_{j-1})} = (\mathcal{E}_0 + c_E^0) e^{c_E^1(t_k)},$$

for $k = 1, \dots, N$. This is exactly the first estimate in (6.11). Show the second one, we take the advantage of (6.12), namely we evaluate the dissipation distance $\mathcal{D}_j$ between two time levels t_j and $t_j - 1$ and sum over $j = 1, \dots k$, the rest of the computation is straightforward

$$\begin{aligned}
\sum_{j=1}^{k} \mathcal{D}_j &\leq \mathcal{E}_0 - \mathcal{E}_k + \sum_{j=1}^{k} (\mathcal{E}_{j-1} + c_E^0)(e^{c_E^1(t_j - t_{j-1})} - 1) \\
&\leq (c_E^0 + \mathcal{E}_0) - (c_E^0 + \mathcal{E}_k) + (c_E^0 + \mathcal{E}_0) \sum_{j=1}^{k} (e^{c_E^1 t_j} - e^{t_{j-1}}) \\
&\leq (c_E^0 + \mathcal{E}_0) + (c_E^0 + \mathcal{E}_0)(e^{c_E^1 t_k} - 1) = (c_E^0 + \mathcal{E}_0) e^{c_E^1 t_k}.
\end{aligned}$$

□

At this stage we are ready to define piecewise constant interpolant and show that it satisfies the a priori bounds.

Lemma 6.3.5. *For given time partition* $\Pi^N = \left\{0 = t_0 < t_1^N \dots < t_{N-1}^N < t_N^N = T\right\}$ *we define the piecewise interpolant* $(u^N, m^N, \lambda^N) : [0, t] \mapsto \mathcal{U} \times \mathcal{M} \times \mathcal{L}$ *of precise solution as*

$$\left(u^N(t), m^N(t), \lambda^N(t)\right) = \begin{cases} (u_k, m_k, \lambda_k) & \text{for} \quad t \in [t_k, t_{k+1}) \\ (u_N, m_N, \lambda_N) & \text{for} \quad t = t_N = T. \end{cases} \tag{6.13}$$

Such a defined function meets following bounds:

$$\mathcal{E}(t, u^N(t), m^N(t), \lambda^N(t)) \leq (\mathcal{E} + c_E^0)e^{c_E^1 t} - c_E^0,$$
$$\mathrm{Diss}_{\mathcal{D}}(\lambda^N; [0,T]) = \sum_{j=1}^{N} \mathcal{D}(\lambda_j, \lambda_{j-1}) \leq (\mathcal{E} + c_E^0)e^{c_E^1 T}.$$

Proof. The second inequality follows directly from (6.11). To obtain the first one, consider $t \in [t_k, t_{k+1})$ and employ (6.7) together with (**??**) to

$$\mathcal{E}(t, u^N(t), m^N(t), \lambda^N(t)) = \mathcal{E}(t, u_k, m_k, \lambda_k) = \mathcal{E}(t_k, u_k, m_k, \lambda_k) + \int_{t_k}^{t} \partial_\tau \mathcal{E}(\tau, u_k, m_k, \lambda_k)\,\mathrm{d}\tau$$

and follow the procedure leading to (6.11). □

Consequently, taking advantage of $\mathcal{E}$ coercivity on $[0,T] \times W^{1,2} \times W^{1,2} \times W^{1,1}$ and $\mathcal{D}$ coercivity on L^1 we may conclude

$$\left\|u^N\right\|_{L^\infty([0,T],W^{1,2})} \leq C, \quad \left\|m^N\right\|_{L^\infty([0,T],W^{1,2})} \leq C,$$
$$\left\|\lambda^N\right\|_{L^\infty([0,T],W^{1,1})} \leq C, \qquad \mathrm{Var}_{\mathrm{L}^1}(\lambda^N, [0,T]) \leq C.$$

Step 3: Subsequence selection

We choose a sequence $\left\{\Pi^N\right\}_{N=1}^{\infty}$ of the time interval parons in a way that $\forall N : \Pi^N \subset \Pi^{N+1}$ and $\tau^N \to 0$ for $N \to \infty$, where $\Delta^N = \max_{j=1\ldots N}(t_j - t_{j-1})$ stands for the largest time step of the N^{th} partition. The sequence of partitions generates a sequence of approximations $\{(u^N, m^N, \lambda^N)\}$. Taking advantage of a special version of Helly's selection theorem introduced in [1] we may select a subsequence $\left\{\lambda^{N_k}\right\}_{k\in\mathbb{N}}$ such that there exists $\lambda \in L^\infty([0,T], W^{1,1}) \cap \mathrm{BV}([0,T], W^{1,1}) : \forall t \in [0,T]$:

$$\lambda^{N_k}(t) \longrightarrow \lambda(t) \text{ weakly in } W^{1,1} \text{and strongly in } L^1.$$

Here, we use the compact embedding $W^{1,1} \Subset L^1$ which holds in three dimensions. Consequently, we might deduce that $\forall t \in [0,T]$ there exists $\delta(t)$ such that

$$\lim_{k\to\infty} \mathrm{Diss}_{\mathcal{D}}(\lambda^{N_k}, [0,t]) = \delta(t).$$

Let us denote $\theta^{N_k} = \partial_t \mathcal{E}(t, u^{N_k}(t), m^{N_k}(t), \lambda^{N_k}(t))$. The inequality 6.7 and the esti-

mate **??** imlies that θ^{N_k} is bounded in $L^\infty((0,T))$. Therefore, it is possible to extract a subsequence (still denoted by same index) such as

$$\theta^{N_k} \rightharpoonup^* \theta_* \text{ in } L^\infty((0,T)).$$

Simultaneously, we define $\theta : [0,T] \to \mathbb{R}$ as $\theta(t) = \limsup_{k\to\infty} \theta^{N_k}(t)$. Regarding the Fatou's lemma we have $\theta_*(t) \geq \theta(t)$ for a.e. $t \in [0,T]$.

Thus, for fixed $t \in [0,T]$ we might select sebsequence $N_l(t)$ of N_k, whereas the selection is dependent on the choice of t, such as

$$\begin{aligned}
\theta^{N_l(t)}(t) &\to \theta(t) \quad \text{for } l \to \infty,\\
u^{N_l(t)}(t) &\to u(t) \ \text{ weakly in } W^{1,2} \ \text{ for } l \to \infty,\\
m^{N_l(t)}(t) &\to m(t) \ \text{ weakly in } W^{1,2} \ \text{ for } l \to \infty.
\end{aligned}$$

Altogether, we obtain that for all $t \in [0,T]$:

$$(u^{N_k}(t), m^{N_k}(t)\lambda^{N_k}(t)) \rightharpoonup (u(t), m(t)\lambda(t)) \text{ in } W^{1,2} \times W^{1,2} \times W^{1,1}.$$

and we have to show that the limit function $(u(t), m(t)\lambda(t)) : [0,T] \to \mathcal{U} \times \mathcal{M} \times \mathcal{L}$ is a energetic solution. That is to say to verify the stability condition (6.1) and the energy balance (6.2).

Step 4: Stability of the limit function

The stability of $(u(t), m(t)\lambda(t))$ is secured due to the weak closeness of the stable graph in $W^{1,2} \times W^{1,2} \times W^{1,1}$. We have $(u^{N_k}(t), m^{N_k}(t)\lambda^{N_k}(t)) \in \mathcal{S}(\tau_k)$, with $\tau_k = \max\{\tau \in \Pi^{N_k} : \tau \leq t\}$, whereas $\tau_k \nearrow t$ for $k \to \infty$.

Take $(t_j, u_j, m_j, \lambda_j) \in \mathcal{S}_{[0,T]}$ with $t_j \to t$, $u_j \rightharpoonup u$ in $W^{1,2}$, $m_j \rightharpoonup m$ in $W^{1,2}$ and $\lambda_j \rightharpoonup \lambda$ in $W^{1,1}$. Since $\mathcal{D}$ is strongly continuous on L^1 (hence, weakly continuous on $W^{1,1}$ due to the compact embedding) and $\mathcal{E}$ is weakly lower semi-continuous, we have for all $(\hat{u}, \hat{m}, \hat{\lambda}) \in \mathcal{U} \times \mathcal{M} \times \mathcal{L}$:

$$\begin{aligned}
\mathcal{E}(t,u,m,\lambda) &\leq \liminf_{j\to\infty} \mathcal{E}(t_j, u_j, m_j, \lambda_j)\\
&\leq \liminf_{j\to\infty} \mathcal{E}(t_j, \hat{u}, \hat{m}, \hat{\lambda}) + \mathcal{D}(\lambda_j, \hat{\lambda}) = \mathcal{E}(t, \hat{u}, \hat{m}, \hat{\lambda}) + \mathcal{D}(\lambda, \hat{\lambda}).
\end{aligned}$$

Hence, we might conclude that for all $t \in [0,T]$ the limit function $(u(t), m(t)\lambda(t)) \in \mathcal{S}(t)$.

Step 5: Energy balance for the limit function

Lemma 6.3.6 (Upper energy estimate)**.** *Let $t \in [0,T]$. For the stored energy $\mathcal{E}$ and dissipation distance $\mathcal{D}$ defined via* (6.4) *and* (6.6)*, the following upper energy estimate holds*

$$\mathcal{E}(t,u(t),m(t),\lambda(t))+\mathrm{Diss}_{\mathcal{D}}(\lambda,[0,t]) \leq \mathcal{E}(0,u(0),m(0),\lambda(0))+\int_0^t \partial_\tau.\mathcal{E}(\tau,u(\tau),m(\tau),\lambda(\tau))\,\mathrm{d}\tau.$$

Proof. First of all, the weakly lower semi-continuity of $\mathcal{E}$ gives

$$\mathcal{E}(t,u(t),m(t),\lambda(t)) \leq \liminf_{k\to\infty} \mathcal{E}(t,u^{N_k}(t),m^{N_k}(t),\lambda^{N_k}(t)).$$

At the same time, the weak continuity on $W^{1,1}$ of $\mathcal{D}$ and stability condition imply

$$\begin{aligned}\mathcal{E}(t,u(t),m(t),\lambda(t)) &= \lim_{k\to\infty} \mathcal{E}(t,u(t),m(t),\lambda(t)) + \mathcal{D}(\lambda^{N_k}(t),\lambda(t)) \\ &\geq \limsup_{k\to\infty} \mathcal{E}(t,u^{N_k}(t),m^{N_k}(t),\lambda^{N_k}(t)).\end{aligned}$$

Altogether, we might conclude that $\mathcal{E}$ converges along the approximation sequence, i.e.

$$\mathcal{E}(t,u(t),m(t),\lambda(t)) = \lim_{k\to\infty} \mathcal{E}(t,u^{N_k}(t),m^{N_k}(t),\lambda^{N_k}(t)).$$

Since $\ell \in C^1([0,T],(W^{1,2})^*)$, we have $\partial_t\mathcal{E}(t,u,m,\lambda) = -\left\langle \dot{\ell}(t), v \right\rangle$. Hence, the time derivatives of the stored energy functional converge as well

$$\partial_t\mathcal{E}(t,u(t),m(t),\lambda(t)) = \lim_{k\to\infty} \partial_t\mathcal{E}(t,u^{N_k}(t),m^{N_k}(t),\lambda^{N_k}(t)).$$

The desired energy estimate on $[0,T]$ is a consequence of the discrete upper estimate (6.10). Considering the definition of approximate solution (6.13), we have

$$(u^{N_k}(t),m^{N_k}(t),\lambda^{N_k}(t)) = (u^{N_k}(\tau_k),m^{N_k}(\tau_k),\lambda^{N_k}(\tau_k)) \text{ with } 0 \leq t-\tau_k \leq \Delta_k.$$

Recall that Δ_k stands for the largest step of the time discretization Π^{N_k}, whereas $\Delta_k \to 0$

for $k \to \infty$. Thus, we obtain

$$\begin{aligned}\mathcal{E}(t, u^{N_k}(t), m^{N_k}(t), \lambda^{N_k}(t)) &+ \mathrm{Diss}_{\mathcal{D}}(\lambda^{N_k}; [0,T]) \\ &\leq \mathcal{E}(\tau_k, u^{N_k}(\tau_k), m^{N_k}(\tau_k), \lambda^{N_k}(\tau_k)) + \mathrm{Diss}_{\mathcal{D}}(\lambda^{N_k}; [0,T]) + C\Delta_k \\ &\leq \mathcal{E}(0, u(0), m(0), \lambda(0)) + \int_0^{\tau_k} \partial_s \theta^{N_k}(s)\,\mathrm{d}s + C\Delta_k \\ &\leq \mathcal{E}(0, u(0), m(0), \lambda(0)) + \int_0^{t} \partial_s \theta^{N_k}(s)\,\mathrm{d}s + 2C\Delta_k.\end{aligned}$$

Taking advantage of $\theta \rightharpoonup \theta_*$ and $\mathrm{Diss}_{\mathcal{D}}(\lambda^{N_k}; [0,T]) \to \delta(t)$, the limit passage gives

$$\mathcal{E}(t, u(t), m(t), \lambda(t)) + \delta(t) \leq \mathcal{E}(0, u(0), m(0), \lambda(0)) + \int_0^t \partial_s \theta_*(s)\,\mathrm{d}s.$$

However, $\theta_* \leq \theta = \partial_t \mathcal{E}(t, u(t), m(t), \lambda(t))$ and the energy dissipation is a lower semi-continuous function. Thus we arrive

$$\mathcal{E}(t, u(t), m(t), \lambda(t)) + \mathrm{Diss}_{\mathcal{D}}(\lambda, [0,t]) \leq \mathcal{E}(0, u(0), m(0), \lambda(0)) + \int_0^t \partial_\tau . \mathcal{E}(\tau, u(\tau), m(\tau), \lambda(\tau))\,\mathrm{d}\tau.$$

and the proof is completed. □

Lemma 6.3.7 (Lower energy estimate)**.** *Let $t \in [0,T]$. For the stored energy $\mathcal{E}$ and dissipation distance $\mathcal{D}$ defined via* (6.4) *and* (6.6)*, the following upper energy estimate holds*

$$\mathcal{E}(t, u(t), m(t), \lambda(t)) + \mathrm{Diss}_{\mathcal{D}}(\lambda, [0,t]) \geq \mathcal{E}(0, u(0), m(0), \lambda(0)) + \int_0^t \partial_\tau . \mathcal{E}(\tau, u(\tau), m(\tau), \lambda(\tau))\,\mathrm{d}\tau.$$

Proof. The estimate follows from the stability condition. Take a paron of the time interval $\Pi^M : 0 = t_0 < \ldots < t_M = T$ with the fineness Δ_M. The stability of $(u(t_{j-1}), m(t_{j-1}), \lambda(t_{j-1}))$ tested against $(u(t_j), m(t_j), \lambda(t_j))$, $j = 1, \ldots, M$ reads

$$\begin{aligned}\mathcal{E}(t_{j-1}, u(t_{j-1}), m(t_{j-1}), \lambda(t_{j-1})) &\leq \mathcal{E}(t_{j-1}, u(t_j), m(t_j), \lambda(t_j)) + \mathcal{D}(\lambda(t_j), \lambda(t_{j-1})) \\ \mathcal{E}(t_j, u(t_j), m(t_j), \lambda(t_j)) &+ \mathcal{D}(\lambda(t_j), \lambda(t_{j-1})) - \int_{t_{j-1}}^{t_j} \partial_t \mathcal{E}(s, u(t_j), m(t_j), \lambda(t_j))\,\mathrm{d}s.\end{aligned}$$

Summing over $j = 1, \dots, M$ gives

$$\begin{aligned}
&\mathcal{E}(t, u(t), m(t), \lambda(t)) + \mathrm{Diss}_{\mathcal{D}}(\lambda, [0,t]) + \mathcal{E}(t, u(s), m(s), \lambda(s)) \\
&\quad \le \sum\nolimits_{j=1}^{M} \int_{j-1}^{t_j} \partial_t \mathcal{E}(s, u(t_j), m(t_j), \lambda(t_j))\, \mathrm{d}s \\
&\quad = \sum\nolimits_{j=1}^{M} (t_j - t_{j-1}) \partial_t \mathcal{E}(s, u(t_j), m(t_j), \lambda(t_j))\, \mathrm{d}s + \sum\nolimits_{j=1}^{M} (t_j - t_{j-1}) \epsilon_j, \qquad (6.14)
\end{aligned}$$

where $\epsilon_j = \frac{1}{t_j - t_{j-1}} \int_{j-1}^{t_j} \left[\partial_t \mathcal{E}(s, u(t_j), m(t_j), \lambda(t_j)) - \partial_t \mathcal{E}(t_j, u(t_j), m(t_j), \lambda(t_j))\right] \mathrm{d}s$. However, the modulus of continuity (**??**) provides a uniform bound $|\epsilon_j| \le \omega_E(t_j - t_{j-1}) \le \omega_E(\Delta_j)$. This pushes the last sum in (6.14) to zero, since $w_E(\Delta_M)T \to 0$ as $\Delta_M \to 0$. Additionally, the first term in (6.14) in fact represents an approximation of the Lebesgue integral via Riemann sums. Therefore, passing the $\Delta_M \to 0$ we obtain the desired estimate. □

The lemma 6.3.6 and lemma 6.3.7 hold at the same time. Thus, we conclude that the limit function satisfies the energy balance and so it is a energetic solution. □

Chapter 7

Numerical simulations

In this chapter several we present several examples in order to demonstrate numerically the mathematical model developed in the previous chapter(s). The first section refers to chapter 5 by performing the steady state model. In the second section we demonstrate the evolutionary model developed in chapter 6. We are concerned with a magnetoelastic tablet, so our simulations are done in 2D.

Let us recall the problem and the notation we use. The sample is represented by a bounded domain Ω. The state of the sample at point $x \in \Omega$ is described by the value

$$v(x) = \begin{bmatrix} e(u(x)) \\ m(x) \end{bmatrix},$$

where $e(u(x))$ stands for the symmetric part of the displacement gradient at point x: $e(u(x)) = \nabla u(x) + \nabla u(x)^T$ and $m(x)$ is magnetization at x.

Our aim is to minimize the free energy of the sample, with respect to the existence of several preferred states - the martensitic phases. The free energy is given by

$$\begin{aligned} \bar{I}(\lambda, u, m) = & \int_\Omega \bar{W}(\lambda(x), v(x))\,\mathrm{d}x - \\ & - \int_\Omega f \cdot u \mathrm{d}x - \int_{\Gamma_1} g \cdot u \mathrm{d}S - \\ & - \int_\Omega H \cdot m + \frac{\mu_0}{2} \int_{\mathbb{R}^n} |\nabla u_m|^2 \,\mathrm{d}x, \end{aligned} \tag{7.1}$$

with magneto-elastic energy density

$$\bar{W}(\lambda, v) = \frac{1}{2}\left\langle \mathbb{C}(v - \sum_{i=1}^{2N} \lambda_i v^i), (v - \sum_{i=1}^{2N} \lambda_i v^i) \right\rangle \ .$$

The minimization is subjected to the constraints:

$$\sum_{i=1}^{2N} \lambda_i = 1 \quad |m| \leq 1. \tag{7.2}$$

In addition, the magnetostatic potential u_m satisfies

$$\mathrm{div}(-\mu_0 \nabla u_m + m\chi_\Omega) = 0. \tag{7.3}$$

Please consider that the following notation is being used

Ω	...	domain representing the sample
Γ_1	...	part of the domain boundary
f	...	loading: external body force
g	...	loading: external surface force onΓ_1
H	...	loading: external magnetic field
u_m	...	magnetostatic potential
v_i	...	the i-th martensitic variant
λ_i	...	volume fraction of the i-th martensitic variant
λ	...	$(\lambda_1, \ldots, \lambda_{2N})$.

To solve this minimizing problem, we use the software MATLAB, which provides the optimization toolbox. Concretely, we take advantage of the function FMINCON, which is designed for finding a minimum of constrained nonlinear multi-variable problem

$$\min_x f(x) \quad \text{such that} \begin{cases} c(x) \leq 0, & ceq(x) = 0 \\ A \cdot x \leq beq & Aeq \cdot x = beq \\ lb \leq x \leq ub & \end{cases},$$

where the right side of the vinculum assigns the constrictions. The functions $c(x)$ and $ceq(x)$ stand for nonlinear constrictions, the matrices A, Aeq with vectors b, beq give the linear constrictions, and lob and upb define a set of lower and upper bounds on the design variables in x.

The CD with all MATLAB source codes is attached to the thesis. In appendix A the list of all used functions is provided. Consequently, in appendix B several key MATLAB are listed.

7.1 Stationary 2D model

In this section we introduce the 2D numerical model. We presume all variables to be time-independent. We examine the response of a magnetostrictive tablet to external loading. In the first instance we apply magnetic field, afterwards we use external stress. Since we deal with two dimensional model, the unknown variables are

$$u(x) = \begin{bmatrix} u_1(x) \\ u_2(x) \end{bmatrix}, \quad m(x) = \begin{bmatrix} m_1(x) \\ m_2(x) \end{bmatrix}, \quad \lambda(x).$$

The aim is to find approximate minimizer of the free energy functional 7.1 with respect to constraints 7.2 and 7.1. For simplicity, we assume that the tablet represented by the domain Ω is a rectangle of size 0.2×0.1. We divide the domain into triangular elements following standard rules for triangulization, see the figure 7.2 on the left. Delaunay[1] triangulation $\mathcal{T}_\mathcal{D}$ is used here.

To construct approximative solution we use element-wise affine functions for the components of u and element-wise constant functions for components of m and λ.

$$\begin{aligned}
u \in V_1, \quad \text{where} \quad & V_1 = \left\{ v \in \mathcal{C}(\Omega); \quad v_i\big|_K \in P^1 \quad \forall K \in \mathcal{T}_\mathcal{D},\ i = 1,2 \right\} \\
m \in V_2, \quad \text{where} \quad & V_2 = \left\{ v : \Omega \to \mathbb{R}^2; \quad v_i\big|_K \in P^0,\ i = 1,2,\ |v\big|_K| \leq 1 \quad \forall K \in \mathcal{T}_\mathcal{D} \right\} \\
\lambda \in V_3, \quad \text{where} \quad & V_3 = \left\{ v : \Omega \to \mathbb{R}; \quad v\big|_K \in P^0,\ 0 \leq v\big|_K \geq 1 \quad \forall K \in \mathcal{T}_\mathcal{D} \right\}
\end{aligned}$$

Hence, the displacement u is evaluated in the vertexes of the grid and magnetization m and volume fraction λ are evaluated on elements. Since the components of u are element-wise affine, components of $e(u)$ are element-wise constant functions. To calculate values of

[1]The triangulization for set of points P is called Delanoy if no point from P is inside the circumcircle of any triangle in DT(P).

$e(u)$ at each element, the equation for the components of u at each element is needed. Let us take arbitrary element from $\mathcal{T}_\mathcal{D}$ with corners A,B,C. Being given values of $u_i, i = 1, 2$ in the corners, we may evaluate u_i in every point (x,y) of the element (except for the constant k which we use in order to make u continuous on Ω)

$$u_i(x,y) = \frac{y^{CA}u_i^{BA} - y_{BA}u_i^{CA}}{x^{BA}y^{CA} - x^{CA}y^{BA}}x + \frac{x^{BA}u_i^{CA} - x^{CA}u_i^{BA}}{x^{BA}y^{CA} - x^{CA}y^{BA}}y + k, \quad i = 1, 2,$$

where we denote $x^{BA} = B_x - A_x$, $x^{CA} = C_x - A_x$, $y^{BA} = B_x - A_x$, $y^{CA} = C_x - A_x$, $u_i^{BA} = u_i^B - u_i^A$, $u_i^{CA} = u_i^C - u_i^A$. To understand the notation see the figure 7.1.Then the value of $e(u)$ on the same element is

$$e(u) = \begin{pmatrix} \frac{y^{CA}u_1^{BA} - y^{BA}u_1^{CA}}{x^{BA}y^{CA} - x^{CA}y^{BA}} & \frac{x^{BA}u_1^{CA} - x^{CA}u_1^{BA}}{x^{BA}y^{CA} - x^{CA}y^{BA}} \\ \frac{y^{CA}u_2^{BA} - y^{BA}u_2^{CA}}{x^{BA}y^{CA} - x^{CA}y^{BA}} & \frac{x^{BA}u_2^{CA} - x^{CA}u_2^{BA}}{x^{BA}y^{CA} - x^{CA}y^{BA}} \end{pmatrix}.$$

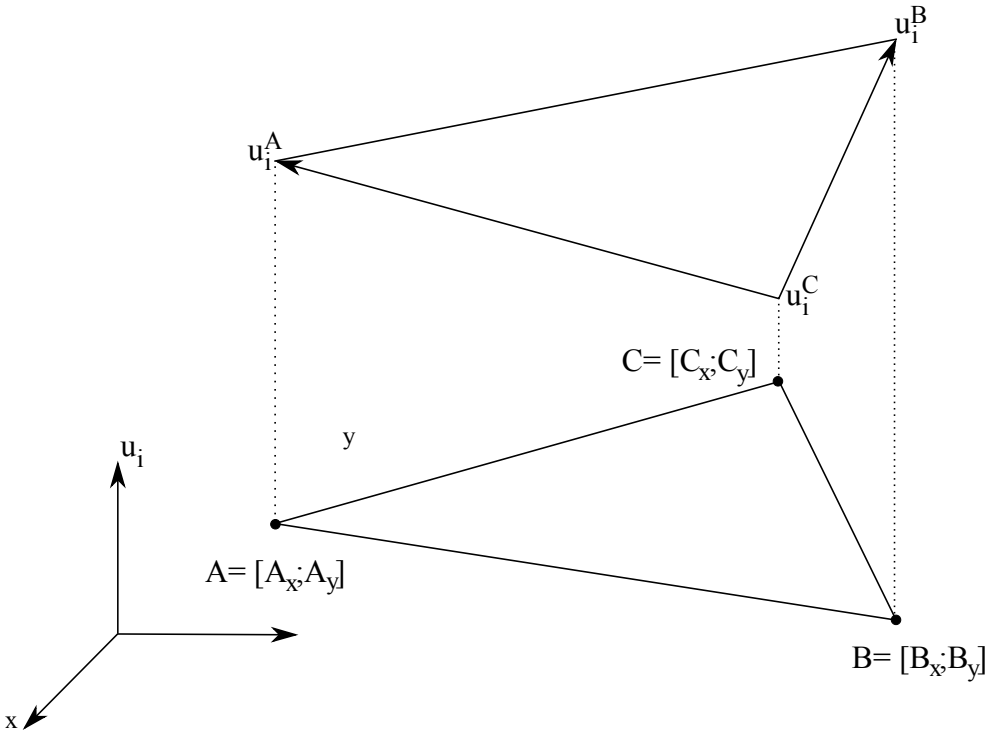

Figure 7.1: The triangle ABC is an arbitrary element of triangulization $\mathcal{T}_\mathcal{D}$, u_i is piece-wise affine function on ABC. Hence, u_i is determinated by three values of u_i^A,u_i^B and u_i^C. The equation describing u_i on the triangle ABC is equation of a plane passing through points $[A_x, A_y, u_i^A]$, $[B_x, B_y, u_i^B]$ and $[C_x, C_y, u_i^C]$

.

To handle the external loading f and g in 7.1 we take into consideration that

$$-\mathrm{div}T = f, \qquad Tn = g, \qquad T = T^T$$

where T stands for the Cauchy stress tensor. Therefore, we may write

$$\begin{aligned}\int_{\Gamma_1} g \cdot u \mathrm{d}S + \int_\Omega f \cdot u \mathrm{d}x &= \int_{\Gamma_1} Tn \cdot u \mathrm{d}S + \int_\Omega f \cdot u \mathrm{d}x \\ &= \int_\Omega \mathrm{div}T \cdot u + T \cdot \nabla u \mathrm{d}x + \int_\Omega f \cdot u \mathrm{d}x \\ &= \int_\Omega T \cdot e(u) \mathrm{d}x.\end{aligned}$$

The constrains 7.2 are implied in the choice of the spaces V_2 and V_3. The constrain 7.1 and consequently the last integral in 7.1 need to be treated separately. In each cycle of the minimization routine the equation 7.1 needs to be solved. Regarding the fact that m is piece-wise constant we can not search for approximation of u_m as a classical solution. However, taking advantage of Lax-Milgram lemma we know that equation 7.1 has a unique weak solution, i.e. u_m satisfies

$$-\mu_0 \int_{\mathbb{R}^2} \nabla u_m \nabla v \, \mathrm{d}x = \int_\Omega m \nabla v \, \mathrm{d}x \quad \forall v \in \mathcal{C}_0^\infty.$$

To calculate the integral over $\mathbb{R}^2$ we benefit from the fact that the magnetostatic potential decreases to zero being far enough from the source of the magnetic field. Thus, we set $u_m = 0$ on $\partial\tilde{\Omega}$, where $\bar{\Omega} \subset \tilde{\Omega}$, meas$\Omega$ << meas$\tilde{\Omega}$ and we wish to solve

$$-\mu_0 \int_{\tilde{\Omega}} \nabla u_m \nabla v \, \mathrm{d}x = \int_\Omega m \nabla v \, \mathrm{d}x \quad \forall v \in \mathcal{C}_0^\infty.$$

Hence, the finite element method might be used to find approximation of u_m. We take box (square 2×2 with centre in origin) as $\tilde{\Omega}$ and we construct the triangulization $\tilde{\mathcal{T}_\mathcal{D}}$ of $\tilde{\Omega}$ so that it matches with $\mathcal{T}_\mathcal{D}$ on Ω, see the figure 7.2 on the right. Again, we approximate u_m with piece-wise affine function with zero trace on $\partial\tilde{\Omega}$, that is to say

$$u_m \in \tilde{V}_1, \quad \text{where} \quad \tilde{V}_1 = \left\{ v \in \mathcal{C}(\tilde{\Omega}),\ v\big|_{\partial\tilde{\Omega}} = 0; \quad v\big|_K \in P^1 \quad \forall K \in \tilde{\mathcal{T}_\mathcal{D}} \right\}$$

.

At the moment all involved variables are defined on elements. Thus, we may proceed to

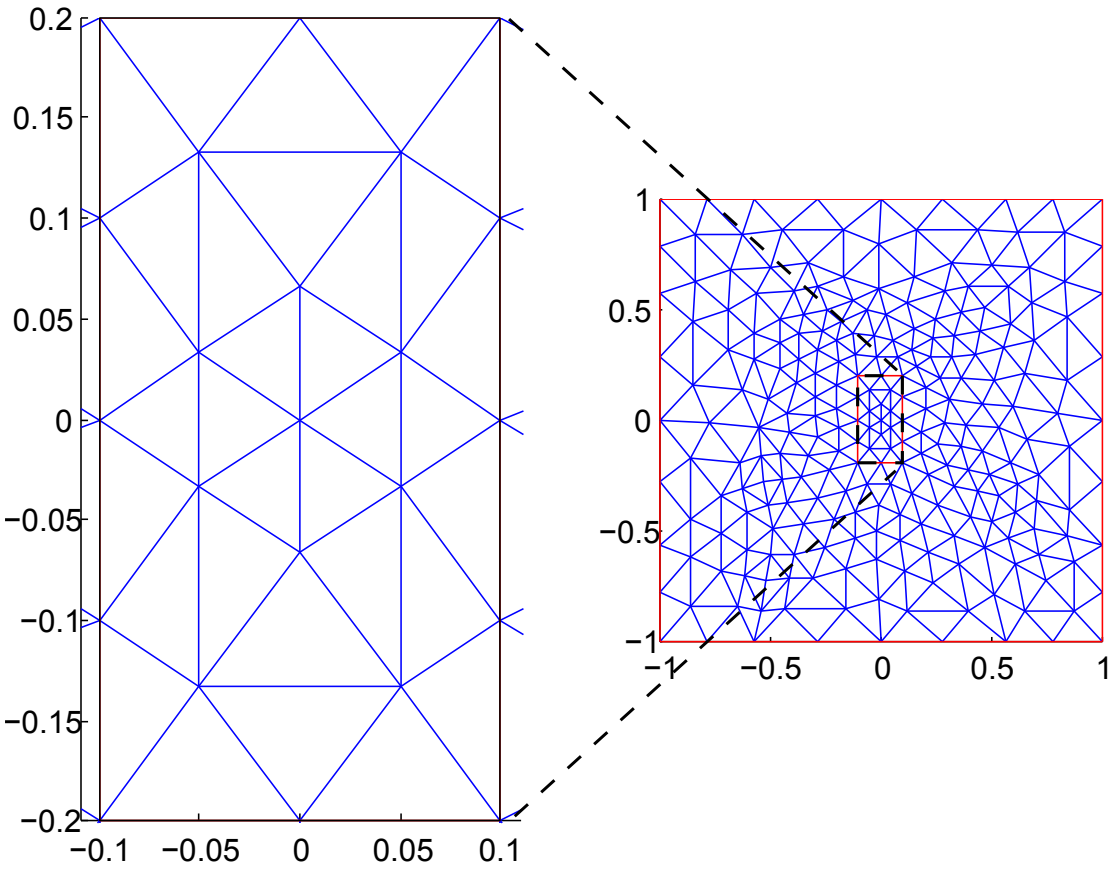

Figure 7.2: The triangulation of domains $\tilde{\Omega}$ (on the right) and Ω (on the left), $\Omega \subset \tilde{\Omega}$. The domain Ω represents the sample, the $\tilde{\Omega}$ corresponds to the area so that we may set $u_m\big|_{\partial\tilde{\Omega}} = 0$. In the following text we dentote the upper part of the rectangle border Γ_U and the lower part Γ_L.

the discretization of the energy functional 7.1. Let us denote $e^K(u) = e\big|_K(u)$, $m^K = m\big|_K$, $\lambda^K = \lambda\big|_K$, $T^K = T\big|_K$, $H^K = H\big|_K$, $\forall K \in \mathcal{T}_\mathcal{D}$ and $\nabla u_m^{\tilde{K}} = (\nabla u_m)\big|_{\tilde{K}}$, $\forall \tilde{K} \in \tilde{\mathcal{T}}_\mathcal{D}$. Considering that $u \in V_1$,$m \in V_2$, $\lambda \in V_3$,$u_m \in \tilde{V}_1$ we arrive with

$$\bar{\mathcal{E}}^d = \frac{1}{2}\sum_{K\in\mathcal{T}_\mathcal{D}} \left\langle \mathbb{C}(v^K - \lambda^K v^{01} - (1-\lambda^K)v^{02}), (v^K - \lambda^K v^{01} - (1-\lambda^K)v^{02}) \right\rangle - \\ - \sum_{K\in\mathcal{T}_\mathcal{D}} T^K \cdot e^K(u) - H^K \cdot m^K + \sum_{\tilde{K}\in\tilde{\mathcal{T}}_\mathcal{D}} |\nabla u_m^K|^2,$$

where K runs over all elements from $\mathcal{T}_\mathcal{D}$ and $\tilde{K}$ runs over all elements from $\tilde{\mathcal{T}}_\mathcal{D}$.

As described at the beginning of the chapter the minimization is implemented in MATLAB using the minimization toolbox, namely the function FMINCON . See the code

script for more detail. In the following we present responses of the FSMA tablet on several different types of loading. We also show behaviour of different martensitic phases.

Magnetic tension

Let the sample be homogeneous having two martensitic phases described by

$$v_1 = \begin{bmatrix} 0.05 & 0 \\ 0 & -0.05 \\ 1 & 0 \end{bmatrix} \quad \text{and} \quad v_2 = \begin{bmatrix} -0.05 & 0 \\ 0 & 0.05 \\ -1 & 0 \end{bmatrix}$$

As one can see the phase v_1 prefers the enlargement in x-direction at the expense of the y-direction, on the contrary v_2 supports the y-extension and x-shortening. The both martensitic phases are illustrated in figure 7.3.

We apply constant external magnetic field only. The direction of the field is contrary to y-axes. We set the boundary conditions $u_y = 0$ on Γ_U and $u_x = 0$ at the upper right corner of the sample (at the point $(x, y) = (0.1, 0.2)$). The results are plotted in the figure 7.1, the deformed configuration, magnetization are depicted in the figure , the distribution of the volume fraction is shown in the figure . For completeness' sake we add the figure 7.5 that shows the magnetostatic potential of the sample.

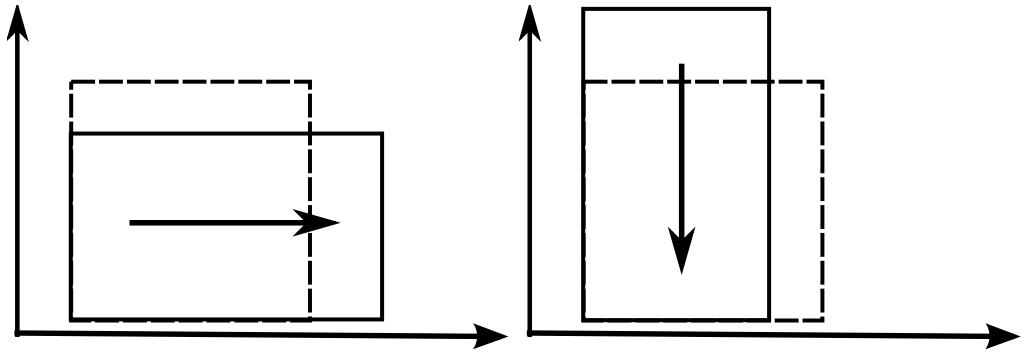

(a) The phase v_1 (b) The phase v_0

Figure 7.3: Magnetic tension - the ilustration of the two martensitic phases.

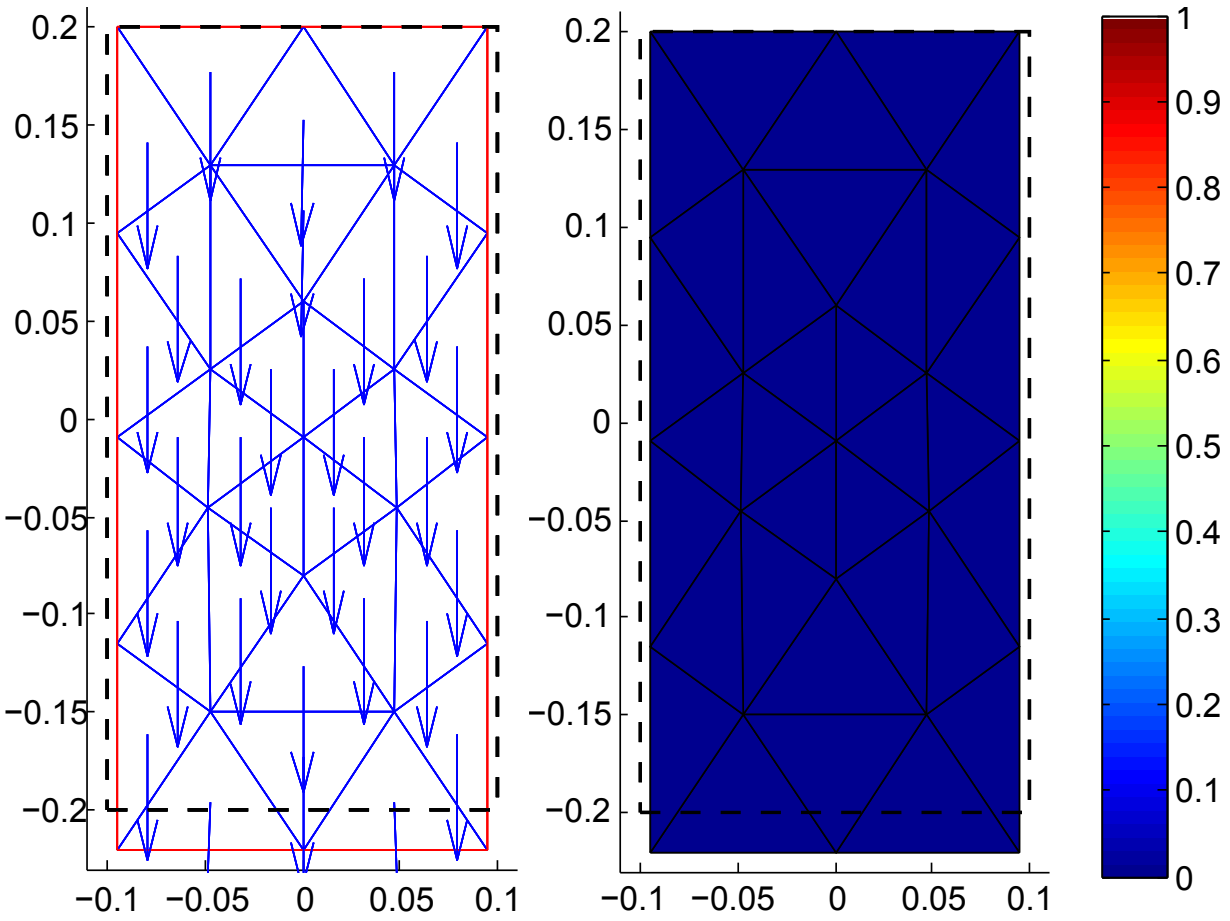

(a) Deformation and magnetization

(b) Volume fraction distribution

Figure 7.4: Magnetic tension - the FSMA in a shape of tablet exposed to the external magnetic field. The sample is loaded by magnetic field $H = [0 \ -0.2]$. The reference configuration is represented by the black rectangle. The magnetization and deformation of the sample are depicted on the left, the distribution of volume fraction is shown on the right. The value $\lambda = 1$ is associated with v_1 and $\lambda = 0$ with v_0. Used parameters: $\mathbb{C} = \mathbb{I}$, $\mu_0 = 1$

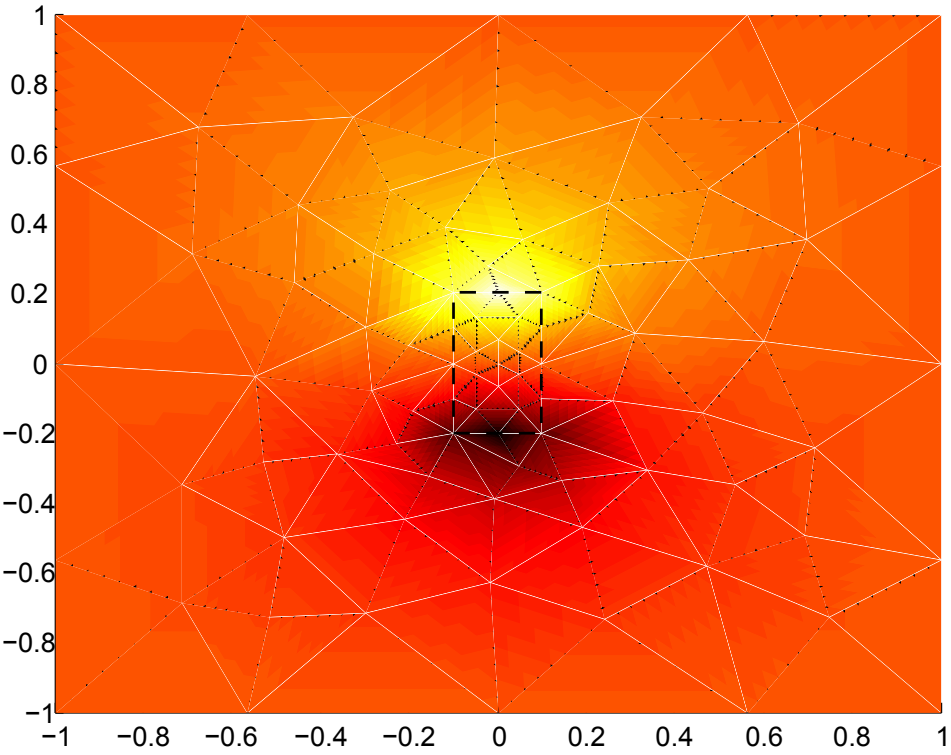

(a) Magnetostatic potential pictured by colormap

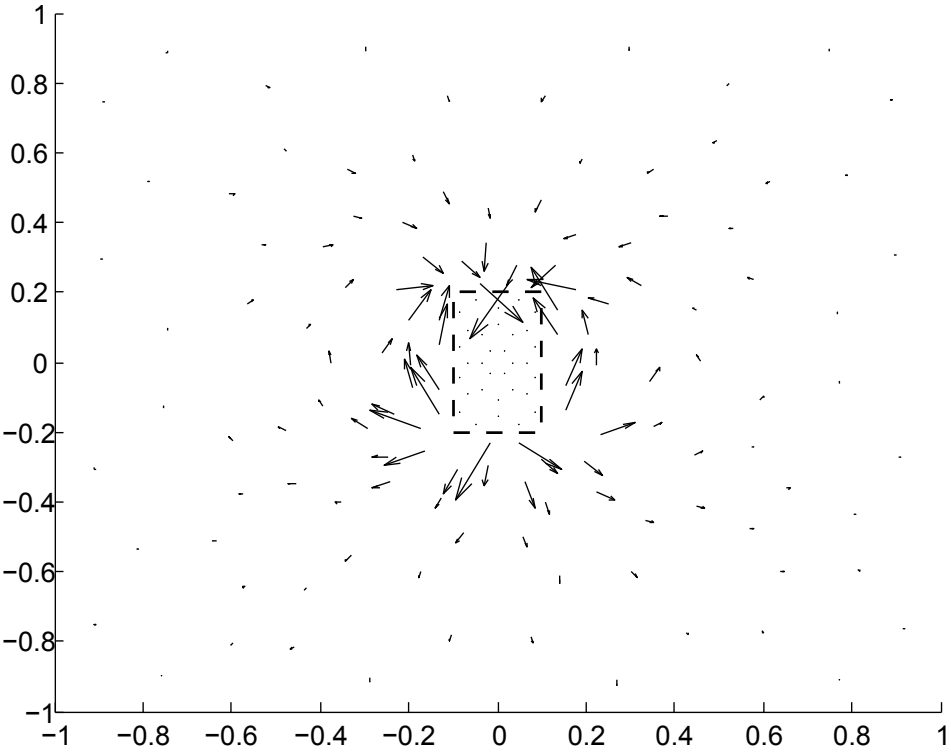

(b) Magnetostatic potential pictured by flux lines

Figure 7.5: Magnetic tension - the magnetostatic potential of the FSMA tablet exposed to the external magnetic field. The sample is loaded by magnetic field $H = [0 \ -0.2]$. The reference configuration is represented by the black rectangle. Used parameters: $\mathbb{C} = \mathbb{I}$, $\mu_0 = 1$

Mechanical bending

To demonstrate the response of the tablet to the mechanical loading we study bending of the sample by external force. Again, we take two martensitic phases, however here we use

$$v_1 = \begin{bmatrix} 0 & 0.05 \\ 0.05 & 0 \\ 1 & 1 \end{bmatrix} \quad \text{and} \quad v_0 = \begin{bmatrix} 0 & -0.05 \\ -0.05 & 0 \\ -1 & -1 \end{bmatrix}. \tag{7.4}$$

The phase v_1 corresponds to the upper right shear and v_2 referes to the upper left one, cf. figure 7.6. We considere the tablet completely fixed on upper and lower boundary, that is to

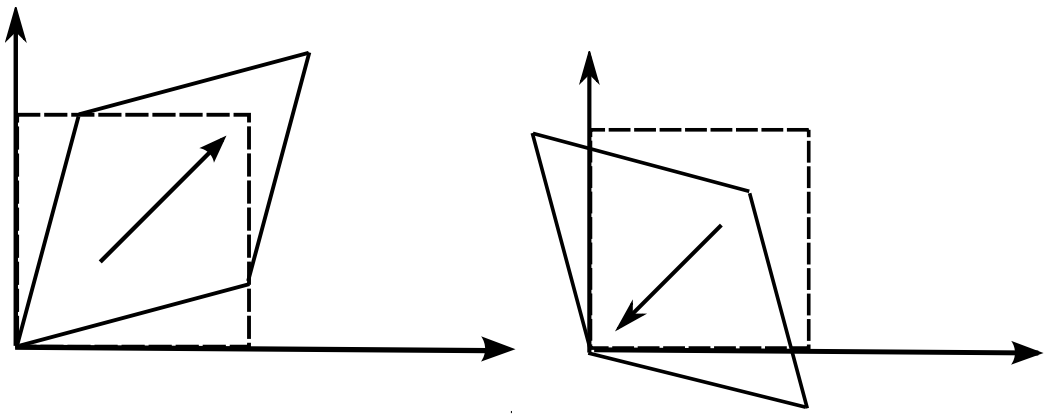

(a) The phase v_1 (b) The phase v_0

Figure 7.6: Mechanical bending - the ilustration of the two martensitic phases.

say $u\big|_{\Gamma_L} = u\big|_{\Gamma_U} = 0$. The sample is loaded by constant body force $F = [0.40]$. The results for the plotted in the figure 7.7. As one would expect, the sample bends in the direction of the applied force, see the figure 7.7(a). We observe that the volume fraction changes along the tablet. Whilst, in the upper part the phase v_0 is more energetically convenient for the material, in the lower part the phase v_1 is preferred, clarify the figure 7.7(b). For the illustration we also plot the magnetostatic potential in figure 7.8.

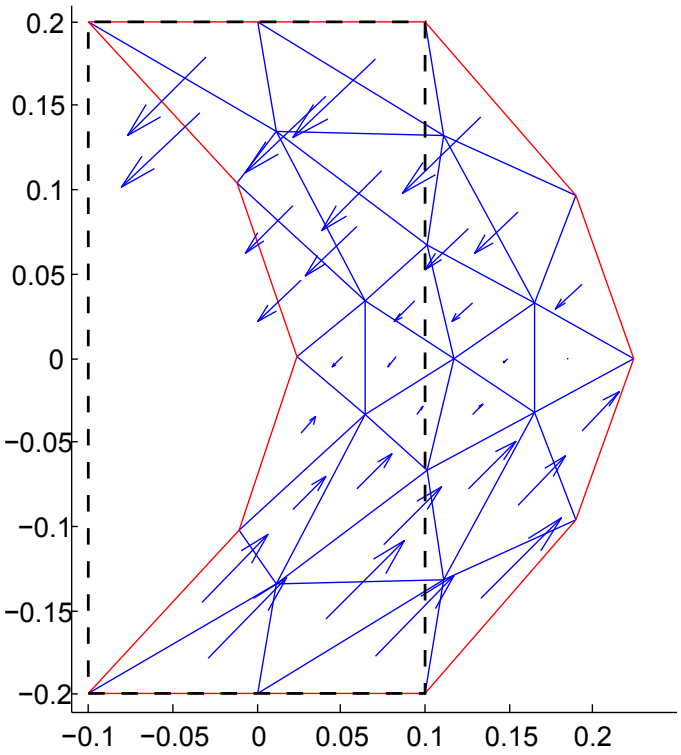

(a) Deformation and magnetization of the sample

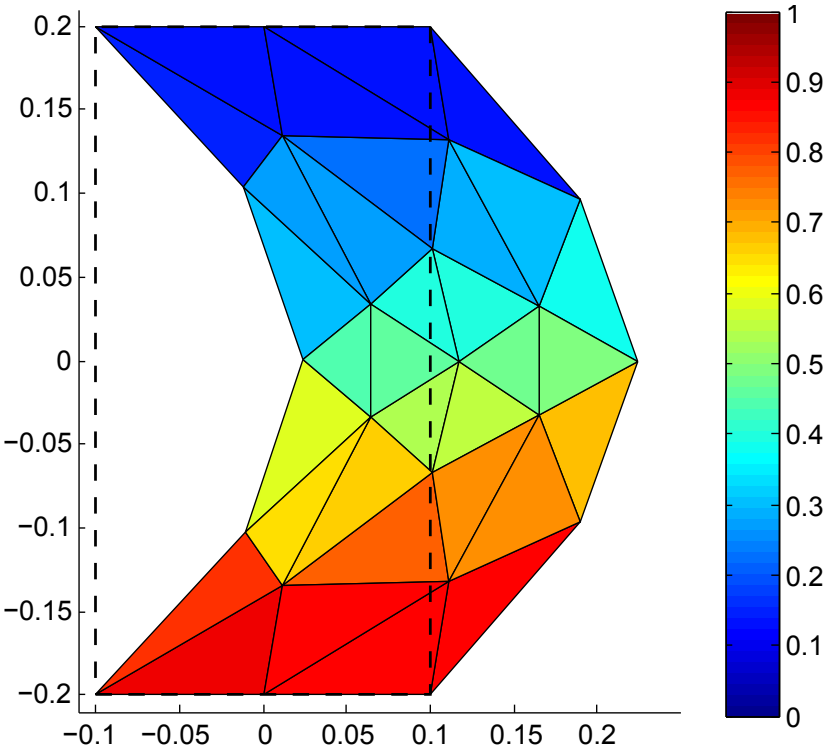

(b) Distribution of the colume fractin within the sample

Figure 7.7: Mechanical bending - volume fraction distribution. The FSMA in a shape of tablet loaded by external force $F = [0.20]$. The reference configuration is represented by the black rectangle. The value $\lambda = 1$ is associated with v_1 and $\lambda = 0$ with v_0. Used parameters: $\mathbb{C} = \mathbb{I}$, $\mu_0 = 1$

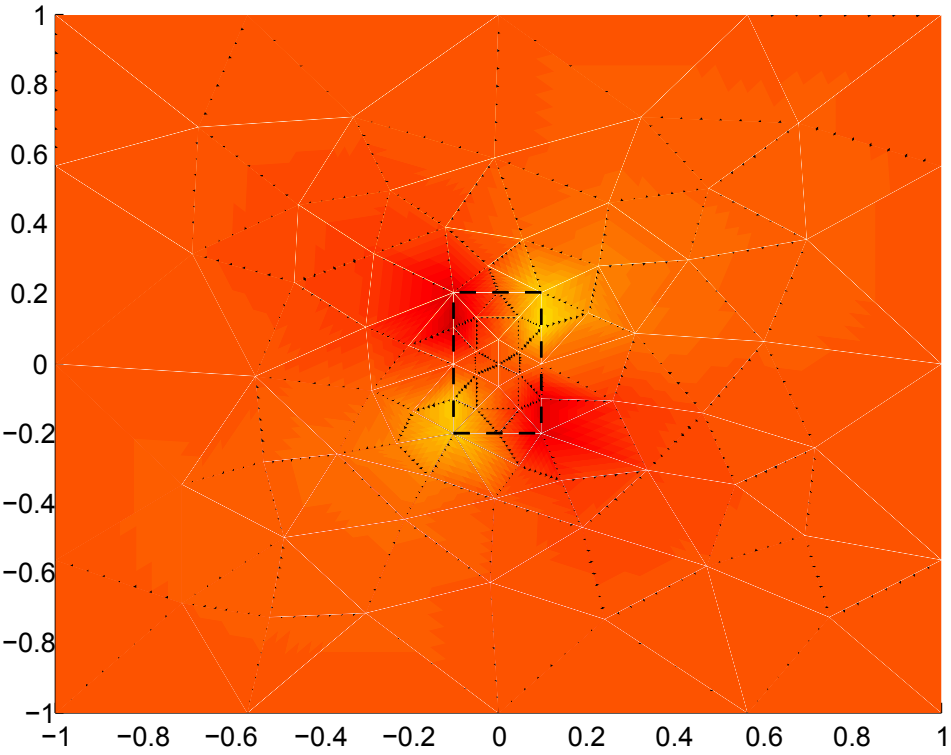

(a) Magnetostatic potential pictured by a colormap

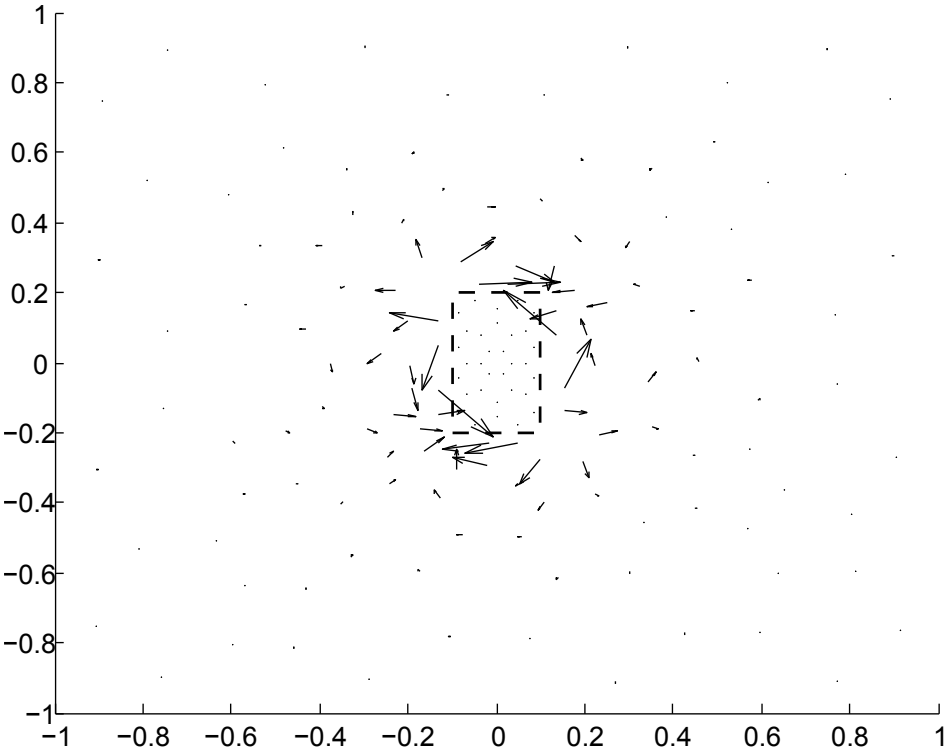

(b) Magnetostatic potential pictured by flux lines

Figure 7.8: Mechanical bending - the magnetostatic potential. The reference configuration is represented by the black rectangle. The FSMA in a shape of tablet loaded by external force $F = [0.2\ 0]$ Used parameters: $\mathbb{C} = \mathbb{I}$, $\mu_0 = 1$

7.2 Evolutionary 2D model

Contrary to the section 7.1 we now assume that the loading is time dependent. We take advantage of the energetic formulation introduced in chapter 6 since it offers direct way for implementation. We take discretization of the time interval $[0, T]$. At every time step we solve the time incremental problem which reads

$$\begin{gathered}\forall k \in 1, \dots, N \text{ and given } (u_0, m_0, \lambda_0) \in \mathcal{S}(0) \text{ we search for minimizer} \\ (u_k, m_k, \lambda_k) \in \mathcal{U} \times \mathcal{M} \times \mathcal{L} \text{ of functional } \mathcal{E}(t_k, u, m, \lambda) + \mathcal{D}(\lambda, \lambda_{k-1}).\end{gathered}$$

Since we work with piecewise affine and piecewise constant approximations of (u, m, λ) we actually deal with the approximate time incremental problem

$$\begin{gathered}\forall k \in 1, \dots, N \text{ and given } (u_0, m_0, \lambda_0) \in \mathcal{S}(0) \text{ we search for minimizer} \\ (u_k, m_k, \lambda_k) \in V_1 \times V_2 \times V_3 \text{ of functional } \mathcal{E}^d(t_k, u, m, \lambda) + \mathcal{D}^d(\lambda, \lambda_{k-1}),\end{gathered}$$

where $\mathcal{E}^d$, $\mathcal{D}^d$ stand for discretized versions of $\mathcal{E}$, $\mathcal{D}$ with respect to used triangulations $\mathcal{T}_\mathcal{D}$ and $\tilde{\mathcal{T}_\mathcal{D}}$.

$$\begin{aligned}\mathcal{E}^d &= \frac{1}{2} \sum_{K \in \mathcal{T}_\mathcal{D}} \left\langle \mathbb{C}(v^K - \lambda^K v^{01} - (1 - \lambda^K) v^{02}), (v^K - \lambda^K v^{01} - (1 - \lambda^K) v^{02}) \right\rangle - \\ &\quad - \sum_{K \in \mathcal{T}_\mathcal{D}} T^K \cdot e^K(u) - H^K \cdot m^K + \sum_{\tilde{K} \in \tilde{\mathcal{T}_\mathcal{D}}} |\nabla u_m^K|^2, \\ \mathcal{D}^d &= K^\lambda \sum_{K \in \mathcal{T}_\mathcal{D}} |\lambda^K - \lambda_{k-1}^K|.\end{aligned}$$

As in the previous section we are concerned with a sample that has shape of rectangular tablet, we set the dimension of the tablet to 0.2×0.4. We introduce both types (magnetic and mechanic) loading with various martensitic variants.

Mechanical bending

First, let us consider the martensitic phases as in 7.4, i.e.

$$v_1 = \begin{bmatrix} 0 & 0.05 \\ 0.05 & 0 \\ 1 & 1 \end{bmatrix} \quad \text{and} \quad v_0 = \begin{bmatrix} 0 & -0.05 \\ -0.05 & 0 \\ -1 & -1 \end{bmatrix}.$$

Additionally, we set the hysteresis constant to be 10^{-6}. We expose the sample to the external body force which time evolution is defined via

$$f(t) = \begin{bmatrix} F_x \sin(t) \\ 0 \end{bmatrix}.$$

For simplicity, we take the force to be spatial constant. We consider Dirichlet boundary conditions $u|_{\Gamma_U} = u|_{\Gamma_L} = 0$ and for the initial state ($t = 0$) we use $v = 0, \lambda = 0.5$. The resulting sequence of states which approximates the response of the sample in time is plotted in the following figures. The reference and the deformed configuration of the sample together with magnetization are plotted in the figure 7.9. The distribution of martensitic phases is shown in the figure 7.10. In both figures we plot 25 states which cover response to one cycle of the loading force $f_x = 1 \to -1 \to 1$.

Magnetic twisting

Secondly, we examine the response of the tablet to the changing magnetic field. Again, we use two preferred types of deformation (upper right shear and the lower left shear). However, for this case, let us assume that there are two different directions of magnetization. Thus, there are four matensitic phases

$$v_A = \begin{bmatrix} 0 & 0.05 \\ 0.05 & 0 \\ 1 & 1 \end{bmatrix}, v_B = \begin{bmatrix} 0 & 0.05 \\ 0.05 & 0 \\ -1 & -1 \end{bmatrix}, \quad v_C = \begin{bmatrix} 0 & -0.05 \\ -0.05 & 0 \\ -1 & 1 \end{bmatrix}, v_D = \begin{bmatrix} 0 & -0.05 \\ -0.05 & 0 \\ 1 & -1 \end{bmatrix}.$$

See figure 7.11 for an illustration. We load the sample by a spatially constant magnetic field which we allow to "rotate" in time. Being precise, the magnetic field is set by

$$H(t) = \begin{bmatrix} H_x \cos(t) \\ H_y \sin(t) \end{bmatrix},$$

where we use $H_x = 2, H_y = 2$. The numerical result is depicted in 7.12.

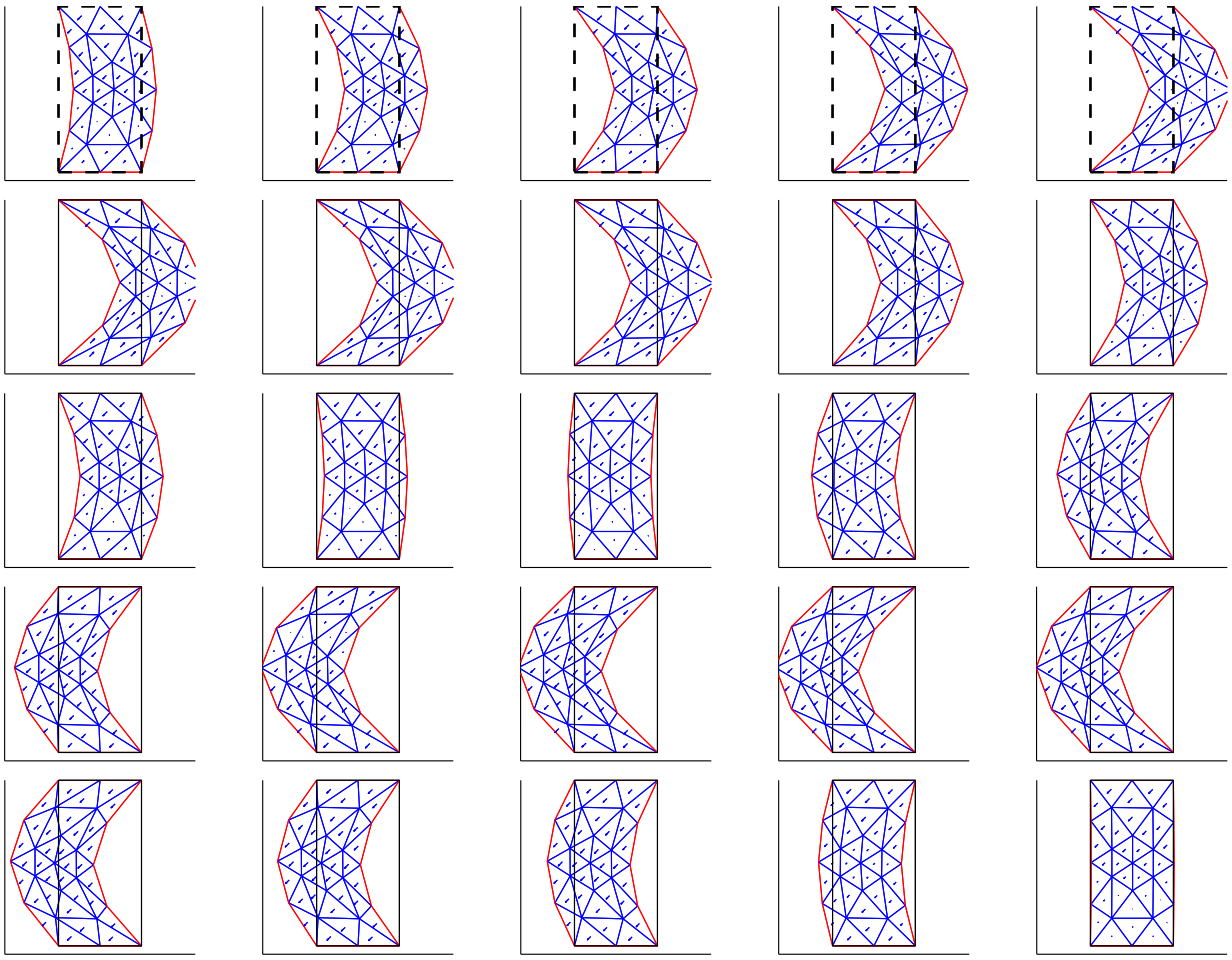

Figure 7.9: Mechanical bending - respose of the sample exposed to a changing body force. The sequence of 25 subfigures shows the evolution of the sample deformation and magnetization within one cycle of the force.

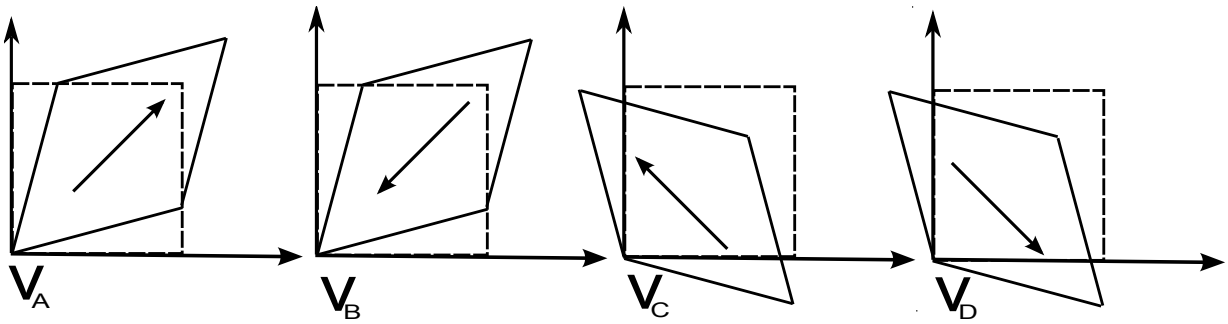

Figure 7.11: Four martensitic phases v_A, v_B, v_C, v_D used for magnetic twisting.

As might be seen in the figure 7.12, the magnetization of the sample follows the evolution

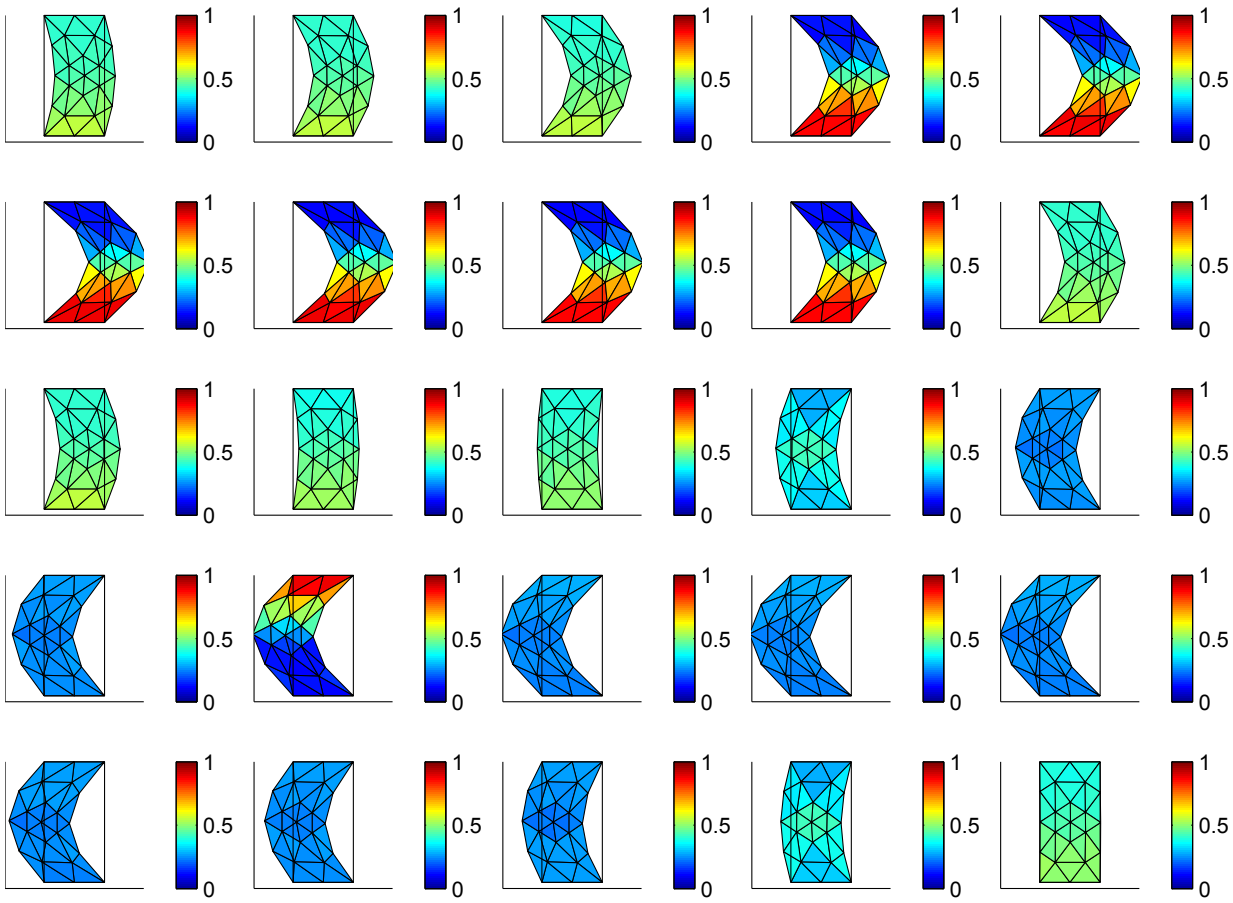

Figure 7.10: Mechanical bending - response of the sample exposed to a changing body force. The sequence of 25 subfigures shows the evolution of volume fraction distribution within one cycle of the force.

of the external magnetic field. It jumps from one phase to an other in order to let the magnetization be as aligned as possible with the external field. Consequently, the phase transformations are associated with spatial change. Thus, we observe slight shearing of the sample.

7.3 Magnetic Field-induced Strain Experiment

In order to demonstrate the qualitative agreement of the model with experimentally observed behaviour of FSMA, we wish simulate the FSMA loading sequence described in section

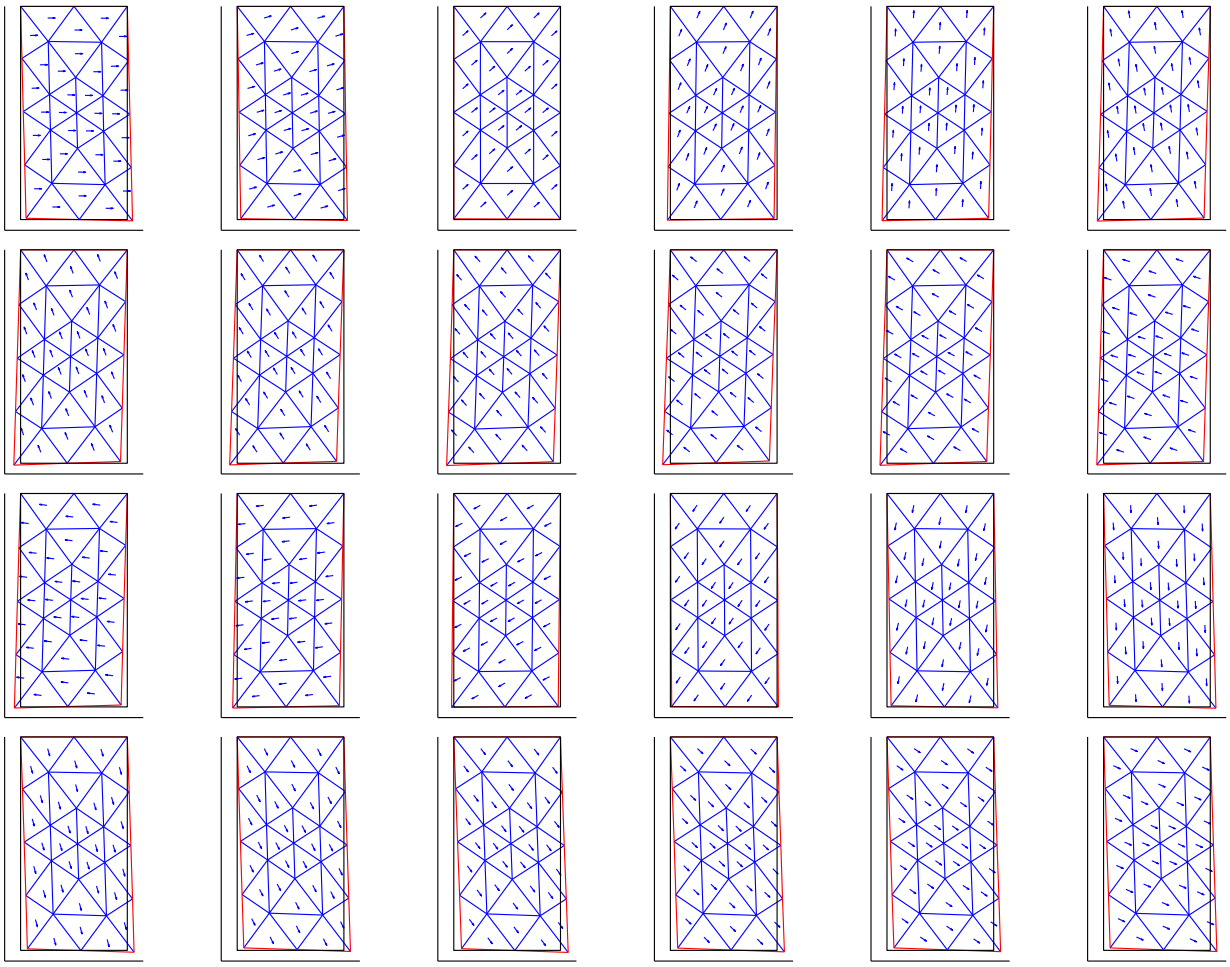

Figure 7.12: Magnetical twisting - response of the sample exposed to a rotating magnetic field. The sequence of subfigures shows the cycle.

2.3, clarify the figures 2.6 and 2.11. For this purpose we consider four energy wells

$$v_A = \begin{bmatrix} 0.05 & 0 \\ 0 & -0.05 \\ 0 & 1 \end{bmatrix}, v_B = \begin{bmatrix} 0.05 & 0 \\ 0 & -0.05 \\ 0 & 1 \end{bmatrix}, \quad v_C = \begin{bmatrix} -0.05 & 0 \\ 0 & 0.05 \\ 1 & 0 \end{bmatrix}, v_D = \begin{bmatrix} -0.05 & 0 \\ 0 & 0.05 \\ 1 & 0 \end{bmatrix}.$$

As in the previous examples we use the rectangular tablet 0.2×0.4. However, the non-trivial tensor of magnetoelastic constants $\mathbb{C}$ is considered. Since $\mathbb{C}$ is symmetric, it

has no more than 15 non-zero elements in the 2D case. Let us use $\mathbb{C}$ of the following form

$$\mathbb{C} = \begin{bmatrix} c_{11} & c_{12} & 0 & c_{14} & c_{15} \\ c_{12} & c_{11} & 0 & c_{15} & c_{14} \\ 0 & 0 & c_{33} & 0 & 0 \\ c_{14} & c_{15} & 0 & c_{44} & 0 \\ c_{15} & c_{14} & 0 & 0 & c_{55} \end{bmatrix}.$$

The choice of the tensor structure is motivated by crystallography considerations. Initially, the sample is loaded pressure in y-direction. Afterwards, the homogeneous time-dependent magnetic field is applied in x-direction. The results are plotted in figure 7.13.

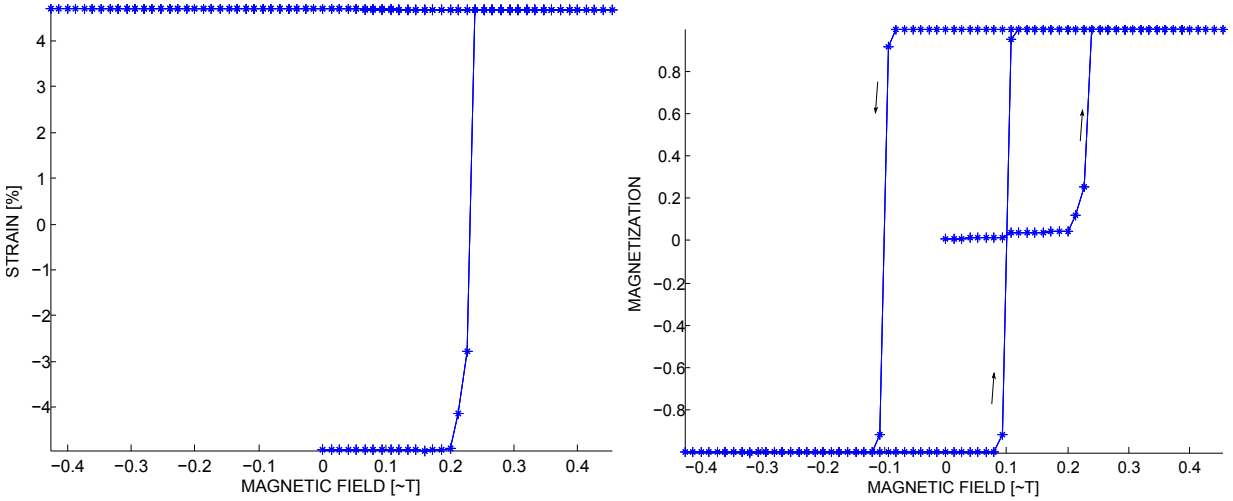

(a) Strain vs. magnetic field curve

(b) Magnetization vs. magnetic field curve

Figure 7.13: The response of the sample to the loading sequence described in section 2.3. The sample is loaded by pressure in y-direction of value 0.2. The magnetic loading runs $0 \to 0.4 \to -0.4 \to 0.4$. Magnetoelastic coefficients were set as follows: $c_{11} = c_{22} = c_{33} = c_{44} = c_{55} = 100, c_{12} = 10, c_{15} = -50, c_{14} = 0$. The value of C_{Hys} was set to 0.1. For the permeability of vacuum the physical value was used.

The above presented examples demonstrates that the model reacts reasonably with respect to the applied loading. However, the rigorous analysis of the model whether it is realistic or not can be done only through comparison with experimental data. The key ingredient for such analysis is complete set of experimental data, namely information about the volume fraction distribution is essential for correct calibration of the model.

Chapter 8

Conclusion

The thesis focuses on describing phenomenon of ferromagnetic shape memory alloys in terms of mathematical modelling. We studied the theory of linear elasticity and micromagnetism in order to analyse relevant physical effects and reflect them accordingly in the mathematical model. We formulated appropriate thermodynamic functionals of a linear elastic material as well as a ferromagnetic material, and combined them in order to model magneto-elastic behaviour.

Our primary goal is not to create a formally faultless model of a magnetostrictive material, but we aim to come up with a mathematical description of concerned phenomena with respect to practical usage and numerical implementation of the model (as shown in chapter 7). Thus, we show the complexity of the problem and then we introduce its simplifications with appropriate discussion about potential cost of quality of the obtained results. Such a simplification represents the usage of the volume fraction λ, whose qualification $\lambda \in L^\infty(\Omega, \mathbb{R})$ was postulated. It is a rather statistical than physical value, since $\lambda(x)$ characterizes the surrounding of the point x instead of giving precise information about the behaviour directly at point x.

This brings us to the issue how to potentially extend the work (in accordance with length and quality). Natural direction of further research would be to incorporate the temperature into the model, so that the austenite-to-martensite transformation could be described. Another possibility is to advance in the direction of mathematical theory, study methods of the calculus of variations and introduce other mathematical tools for dealing with the multiple-well problem, e.g. Young measures approach, see [20]. Finally, implementation of the 3D model for FSMAs would be very valuable. Since experimental data is always related to the real (3D) world, having 3D simulations of FSMA loading response would

enable physical calibration of the model via comparison with available experimental results.

In conclusion, the work lays out the procedure of extending the linear elasticity theory to magnetically active materials. Such a model is then applied to describe a special family of materials - ferromagnetic shape memory alloys. The author is aware of complexity and complicacy of the problem and considers the text as a prologue to future work.

The author is pleased to write that the thesis was awarded the first place in the students' research competition[1] in mathematics in 2011, which was organized by The Union of Czech Mathematicians and Physicists (JČMF).

[1]Studentská vysokoškolská odborná činnost (SVOČ 2011) organizována matematickou sekcí Jednoty českých matematiků a fyziků.

Chapter 9

Bibliography

[1] Mainik Andreas and Mielke Alexander. Existence results for energetic models for rate-independent systems. *Calc. Var. PDEs*, 22:73–99, 2005.

[2] S. Blundell and D. Thouless. *Magnetism in condensed matter*. Oxford University Press Oxford, UK, 2001.

[3] K.H.J. Buschow and F.R. Boer. *Physics of magnetism and magnetic materials*. Plenum Pub Corp, 2003.

[4] James H.; Butler George W. Calkins, Frederick T.; Mabe. Boeing's variable geometry chevron: morphing aerospace structures for jet noise reduction. *Smart Structures and Materials 2006: Industrial and Commercial Applications of Smart Structures Technologies.*, 6171:199–210, 2006.

[5] V.A. Chernenko and S. Besseghini. Ferromagnetic shape memory alloys: Scientific and applied aspects. *Sensors and Actuators*, 142:542–548, 2008.

[6] B. Dacorogna. *Direct methods in the calculus of variations*. Springer-Verlag, Berlin, 1988.

[7] A. DeSimone. Energy minimizers for large ferromagnetic bodies. *Archive for Rational Mechanics and Analysis*, 125(2):99–143, 1993.

[8] A. DeSimone and R.D. James. A constrained theory of magnetoelasticity. *Journal of the Mechanics and Physics of Solids*, 50(2):283–320, 2002.

[9] J.L. Ericksen. On kinematic conditions of compatibility. *Journal of Elasticity*, 26(1):65–74, 1991.

[10] A. Paoluzi L. Morellon P. A. Algarabel M. R. Ibarra L. Righi F. Albertini, L. Pareti. Composition and temperature dependence of the magnetocrystalline anisotropy in ni2+xmn1+yga1+z (x+y+z=0) heusler alloys,. *Applied Physics Letters*, 81 (21):4032–4034, 2002.

[11] S. Govindjee, A. Mielke, and G.J. Hall. The free energy of mixing for n-variant martensitic phase transformations using quasi-convex analysis. *Journal of the Mechanics and Physics of Solids*, 50(4):1897–1922, 2002.

[12] M.E. Gurtin. *An introduction to continuum mechanics*. Academic Press. New York, 1981.

[13] Oleg Heczko and Ladislav Straka. Compositional dependence of structure, magnetization and magnetic anisotropy in ni–mn–ga magnetic shape memory alloys. *Journal of Magnetism and Magnetic Materials*, 272-276 (Part 3):2045–2046, 2004.

[14] A. Hubert and R. Schäfer. *Magnetic domains: the analysis of magnetic microstructures*. Springer Verlag, 1998.

[15] K. Ullakko E. Pagounis I. Suorsa, J. Tellinen. Voltage generation induced by mechanical straining in magnetic shape memory materials. *Journal of Applied Physics*, 95(12):8054–8058, 2004.

[16] I. Jääskeläinen Aaltio K. Ullakko J. Tellinen, I. Suorsa. Basic properties of magnetic shape memory actuators. *Proceedings of the 8th International Conference ACTUATOR 2002, Bremen, Germany, 10-12 June*, pages 566–569, 2002.

[17] C. Kantner R. C. O'Handley K. Ullakko, J. K. Huang and V. V. Kokorin. Large magnetic-field-induced strains in ni2mnga single crystals. *Applied Physics Letters*, 69 (13):1966–1968, 1996.

[18] Bjoern Kiefer. *A phenomenological constitutuve model for magnetic shape memory alloys*. PhD thesis, Texas A&M University, 2006.

[19] C. Kittel. *Introduction to solid state physics*. Wiley New York, 1986.

[20] M. Kruzık. Variational models for microstructure in shape memory alloys and in micromagnetics and their numerical treatment. In *Proceedings of the Bexbach Kolloquium on Science*, 2000.

[21] G. N. Washington T. A. Lograsso L. E. Faidley, M. J. Dapino. Reversible strain in ni-mnga with collinear field and stress. *Proceedings of SPIE, Smart Structures and Materials: Active Materials: Behavior and Mechanics, San Diego, CA*, 5761:501–512, 6–10 March 2005.

[22] United States Naval Research Laboratory. *http://cst-www.nrl.navy.mil/lattice/struk/ltype.html.* accessed 12 July 2011.

[23] V.I. Levitas. Phase transitions in elastoplastic materials: continuum thermomechanical theory and examples of control, part 1 nad part 2. *Mech. Phys. Solids*, 45:923–947 and 1203–1222, 1997.

[24] J. Lukeš. *Úvod do funkcionální analýzy.* Karolinum, Praha, 2005.

[25] A. Mielke. Evolution in rate-independent systems (ch. 6). *In C. Dafermos and E. Feireisl, editors, Handbook of Differential Equations, Evolutionary Equations*, 2:461–559, 2005.

[26] A. Mielke and F. Theil. On rate independent hysteresis models. *Nonl. diff. Eqns. Appl (NoDEA)*, 11:151–189, 2004.

[27] A. Mielke, F. Theil, and V.I. Levitas. A variational formulation of rate-independent phase transformations using an extremum principle. *Archive for Rational Mechanics and Analysis*, 162:137–177, 2002.

[28] Alexander Mielke and Gilles Francfort. Existence results for a class of rate-independent material models with nonconvex elastic energies. *J. reine angew. Math.*, 595:55–91, 2006.

[29] P. Mohn. *Magnetism in the solid state: an introduction.* Springer Verlag, 2003.

[30] J. Nečas and I. Hlaváček. *Úvod do matematické teorie pružných a pružně-plastických těles.* statní pedagogické nakladatelstí, Praha, 1974.

[31] A.G. Olabi and A. Grunwald. Design and application of magnetostrictive materials. *Materials and Design*, 29:469–483, 2008.

[32] M. Pasquale. Mechanical sensors and actuators. *Sensors and Actuators A: Physical*, 106:142 – 148, 2003.

[33] A. E. Clark M. Wun-Fogle T. A. Lograsso R. A. Kellogg, A. B. Flatau. Temperatureand stress dependencies of the magnetic and magnetostrictive properties of fe0.81ga0.19. *Journal of Applied Physics*, 91 (10):7821–7823, 2002.

[34] M. Rokyta, John O., J. Málek, M. Pokorný, and J. Stará. Úvod do teorie parciálních diferenciálních rovnic. The unpublisched lectuare notes, http://www.karlin.mff.cuni.cz/ rokyta/vyuka/skripta-pdr/index.html.

[35] A. Sozinov, A. A. Likhachev, and K. Ullakko. Magnetic and magnetomechanical properties of ni-mn-ga alloys with easy axis and easy plane of magnetization. In *Storage and Retrieval for Image and Video Databases*.

[36] Dieter Stoeckel, Alan Pelton, and Tom Duerig. Self-expanding nitinol stents: material and design considerations. *European Radiology*, 14:292–301, 2004. 10.1007/s00330-003-2022-5.

[37] Minoru Taya Yuanchang Liang, Yasuo Kuga. Design of membrane actuator based on ferromagnetic shape memory alloy composite for synthetic jet applications. *Sensors and Actuators A: Physical*, 125(2):512–518, 2006.

Appendix A

List of Functions

There is a CD attached to the thesis. Besides the text it contains all matlab-codes which were used for numerical implementation of the model. To make it easier to read we provide a list of several functions and commentary on their particular role. The list does not contain all of the functions. The first free functions are used as command files. To give the reader an insight into the codes a listing of the command files is provided in appendix B.

- function [dl,corners, CORNERS, p, e, t, ti, iind, NumP, NumT, IinBox, PI, TI, BD1, BD2, LeftBoundaryIndex, RightBoundaryIndex, UpperBoundaryIndex, LowerBoundaryIndex] = Setting;
  The function prepares the setting of the computation. The values dl, $corners$ and $CORNERS$ specify the geometry. Variables p, e and t give information about the mesh.

- function [sm,teziste,BaseGradient,TS] = PrepMag;
  The function prepares the computation of the magnetostatic potential.

- function [U0,M0,L0,x0] = Initial;
  The function computes the inital values for the minimizetion procedure. The function assumes a material with two energy wells.

- function [U0,M0,L0,x0] = Initial4;
  The function computes the inital values for the minimizetion procedure. The function assumes a material with four energy wells.

- function [Aeq,beq,lob,upb]=constrains(case,U0,M0,L0,x0,UpperBoundaryIndex,...
  LowerBoundaryIndex,LeftBoundaryIndex,RightBoundaryIndex)

The function sets the linear constrains for the minimization procedure. The variable $case = 1 \ldots 6$ specifies the type. The function assumes a material with two energy wells.

- function [Aeq,beq,lob,upb]=constrains4(case,U0,M0,L0,x0,UpperBoundaryIndex,... LowerBoundaryIndex,LeftBoundaryIndex,RightBoundaryIndex)
  The function sets the linear constrains for the minimization procedure. The variable $case = 1 \ldots 6$ specifies the type. The function assumes a material with four energy wells.

- function [c,ceq,gradc,gradceq] = nonlincon(x) The function sets the nonlinear constrains for the minimization procedure. The function also computes gradients of the constrains. The function assumes a material with two energy wells.

- function [c,ceq,gradc,gradceq] = nonlincon4(x) The function sets the nonlinear constrains for the minimization procedure. The function also computes gradients of the constrains. The function assumes a material with four energy wells.

- function [E, Egrad] = Energie1(x)
  The function computes the value of free energy E of the whole sample associated with state specified in x. Additionally it computes vector of partial derivatives of E with respect to state variables. The function is designed for the mechanical loading. The material is assumed to have two energy wells.

- function [E, Egrad] = Energie2(x)
  The function computes the value of free energy E of the whole sample associated with state specified in x. Additionally it computes vector of partial derivatives of E with respect to state variables. The function is designed for the magnetic and mechanical loading. The mechanical loading has to be defined via stress tensor. The material is assumed to have four energy wells.

- function [E, Egrad] = Energie3(x)
  The function computes the value of free energy E of the whole sample associated with state specified in x. Additionally it computes vector of partial derivatives of E with respect to state variables. The function is designed for the magnetic loading. The material is assumed to have two energy wells.

- function [E, Egrad] = Energie34(x)
  The function computes the value of free energy E of the whole sample associated with state specified in x. Additionally it computes vector of partial derivatives of E with respect to state variables. The function is designed for the magnetic loading. The material is assumed to have four energy wells.

- function EE = EnergieElement(C,va,vb,vc,vd,trisurf,e1,e2,e12,e21,mx,my,...
  lam1,lam2,lam3,lam4,LoadH,LoadT)
  The function computes the value of free energy EE of one element. Two energy wells are assumed.

- function EE = EnergieElement4(C,va,vb,vc,vd,trisurf,e1,e2,e12,e21,mx,my,...
  lam1,lam2,lam3,lam4,LoadH,LoadT)
  The function computes the value of free energy EE of one element. Four energy wells are assumed.

- function [e11,e12,e21,e22] = GradU(x,y,ux,uy)
  The function computes the values of gradient of displacement. The components of displacement are assumed to be piece-affine functions.

- function C = MagElasTensor(pripad);
  The function computes the tensor of magnetoelastic constants. For $pripad = 1$, C is as in section 7.3. If $pripad = 2$, C is identity.

- function EGEU = EnergyGradElemU(x1,x2,x3,y1,y2,y3,ux1,ux2,ux3,uy1,uy2,uy3,...
  mx,my,lam,der,k,TS,f)
  The function computes the value of energy gradient with respect to u_1 or u_2 (specified by der). The function is designed for a material with two energy wells.

- function EGEM = EnergyGradElemM(C,v1,v2,trisurf,e11,e12,e21,e22,...
  mx,my,lam,der,H)
  The function computes the value of energy gradient with respect to m_1 or m_2 (specified by der). The function is designed for a material with two energy wells.

- function EGEL = EnergyGradElemL(C,v1,v2,trisurf,e11,e12,e21,e22,...
  mx,my,lam,lamPrev)
  The function computes the value of energy gradient with respect to λ. The function is designed for a material with two energy wells.

- function EnergyGradElemU4(x1,x2,x3,y1,y2,y3,ux1,ux2,ux3,uy1,uy2,uy3,...
  mx,my,lam1,lam2,lam3,lam4,der,k,TS,T)
  The function computes the value of energy gradient with respect to u_1 or u_2 (specified by *der*). The function is designed for a material with four energy wells.

- functionEGEM = EnergyGradElemM4(C,va,vb,vc,vd,trisurf,e11,e12,e21,e22,...
  mx,my,lam1,lam2,lam3,lam4,der,H)
  The function computes the value of energy gradient with respect to m_1 or m_2 (specified by *der*). The function is designed for a material with four energy wells.

- function EGEL = EnergyGradElemL4(C,va,vb,vc,vd,der,trisurf,e11,e12,e21,e22,...
  mx,my,lam1,lam2,lam3,lam4,lamPrev)
  The function computes the value of energy gradient with respect to λ. The function is designed for a material with four energy wells.

- function [U,NablaU] = MagnetoStatics(M)
  For given magnetization of the material the function computes the magnetostatic potential U nad its gradient *nablaU*. As explained in section 7.1 the magnetostatic potential is computed on square 2×2 with centre in $(0, 0)$. For computation finite element method is used.

Appendix B

Details on numerical simulation

```
clear all;clc;cla;
t1 = cputime;
global p e t ts ti TI PI C v1 v2 T H f  alpha corners CORNERS ...
    NumP NumT sm BaseGradient  IinBox TS pin iind
% SPECIFY THE SETTING AND CREATE MESH
[dl,corners, CORNERS, p,e,t,ti,iind,NumP,NumT,IinBox,...
PI,TI,BD1,BD2,ts,LeftBoundaryIndex,RightBoundaryIndex,...
          UpperBoundaryIndex,LowerBoundaryIndex] = Setting;
[sm,teziste,BaseGradient,TS] = PrepMag;
%SET THE MINIMIZATION INITAL VALUES
casse = 2;
[U0,M0,L0,x0] = Initial;
[Aeq,beq,lob,upb]=constrains(casse,U0,M0,L0,x0,...
                    UpperBoundaryIndex,LowerBoundaryIndex);
%RUN THE MINIMIZATION RUTINE
%material properties v = [e1 e2 e12 e21 mx my]
C = eye(6);
%v1 = [ 0.05 -0.05 0  0 1  1];
%v2 = [-0.05  0.05 0  0 -1 -1];
v1 = [ 0  0  0.1  0.1  1  1];%lambda = 1 , cervena
v2 = [ 0  0 -0.1 -0.1 -1 -1];%lambda = 0 , modra
alpha = 0.1;
%DEFININE LOADING
ZATEZ = 3;
Hx = 2;
Hy = 0;
f = [0 0];
T = zeros(4,size(TI,2));
T(2,:) = 0*ones(1,size(TI,2));
H(1,:)= ones(1,size(TI,2))*Hx;
H(2,:) = ones(1,size(TI,2))*Hy;
%result = zeros(N,size(x0,2));
%lamPrev = x0(numel(x0)-size(TI,2)+1:numel(x0));
```

```
34 Hess = HessFun;%napocita hessian
35 options = optimset('GradObj','on','GradConstr','on','TolFun',10^(-13),...
36     'TolCon',10^(-13),'HessPattern',Hess);
37 %CHECK THE TYPE OF THE LOADING
38 if ZATEZ == 1;%zatizeni silou
39         [x,fval,exitflag,output,LAMBDA,grad,hessian] = ...
40                     fmincon(@Energie1,x0,[],[],Aeq,beq,lob,upb,@nonlincon);
41         result= x;
42 elseif ZATEZ == 2; %zatizeni popsano tenzorem napeti
43         [x,fval,exitflag,output,LAMBDA,grad,hessian] = ...
44                     fmincon(@Energie2,x0,[],[],Aeq,beq,lob,upb,@nonlincon);
45
46         %lambda(i,:) = lamPrev;
47 elseif ZATEZ == 3;%magneticka zatez
48        H(1,:) = ones(1,size(TI,2))*Hx;
49        H(2,:) = ones(1,size(TI,2))*Hy;
50        %rutine
51        [x,fval,exitflag,output,LAMBDA,grad,hessian] = ...
52             fmincon(@Energie3,x0,[],[],Aeq,beq,lob,upb,@nonlincon,options);
53 end
54 t2 = cputime;
55 time = t2-t1
```

Listing B.1: CommandFileSteadyState

```
1  clear all;clc;cla;
2  t1 = cputime;
3  global p e t ts ti TI PI C v1 v2 T  Chys alpha corners CORNERS ...
4  NumP NumT sm BaseGradient  IinBox TS pin iind lamPrev
5  % SPECIFY THE SETTING AND CREATE MESH
6  [dl,corners, CORNERS, p,e,t,ti,iind,NumP,NumT,IinBox,...
7  PI,TI,BD1,BD2,ts,LeftBoundaryIndex,RightBoundaryIndex,...
8          UpperBoundaryIndex,LowerBoundaryIndex] = Setting;
9  [sm,teziste,BaseGradient,TS] = PrepMag;
10 %SET THE MINIMIZATION INITAL VALUES
11 %casse==1 znamena dvoji vetknuti
12 %casse==3 znamena vetknuti nahore
13 casse = 1;
14 [U0,M0,L0,x0] = Initial;
15 [Aeq,beq,lob,upb]=constrains(casse,U0,M0,L0,x0,...
16                     UpperBoundaryIndex,LowerBoundaryIndex);
17 %RUN THE MINIMIZATION RUTINE
18 %material properties v = [e1 e2 e12 e21 mx my]
19 C = eye(6);
20 %v1 = [ 0.05 -0.05 0  0 0  1];
21 %v2 = [-0.05  0.05 0  0 0 -1];
22 v1 = [ 0  0  0.05  0.05  1  1];%lambda = 1 , cervena
23 v2 = [ 0  0 -0.05 -0.05 -1  -1];%lambda = 0 , modra
24 alpha = 0.1; %konstanata
25 Chys = 0; %konstanta hzstereze
26 N = 30;
27 %krok = linspace(-1,1,N);
```

```
%lamPrev = 0;
F =  1.5;
Hx = 0;
Hy = 0;
T = 0*ones(4,size(TI,2));
result = zeros(N+1,size(x0,2));

%lamPrev = x0(numel(x0)-size(TI,2)+1:numel(x0));
Hess = HessFun;
options = optimset('GradObj','on','GradConstr','on','TolFun',10^(-13),...
    'TolCon',10^(-13),'HessPattern',Hess);
%CHECK THE TYPE OF THE LOADING
laminitial = 0.5*ones(1,size(TI,2));
if sum(sum(abs(Hx)+abs(Hy))) == 0 && sum(sum(T))==0;
    for i = 1:N
        global f lamPrev
        f = [F*sin(2*pi*i/N) 0];
        if i == 1
            lamPrev = laminitial;
        else
            lamPrev = result(i-1,numel(x0)-size(TI,2)+1:numel(x0));
        end
        ff(i,:) = f;
        LL(i,:) = lamPrev;
        [x,fval,exitflag,output,LAMBDA,grad,hessian] = ...
                fmincon(@Energie1,x0,[],[],Aeq,beq,lob,upb,@nonlincon);
        result(i,:)= x;
        clear f lamPrev
    end
 elseif sum(sum(f)) == 0 && sum(sum(T))==0;
     for i = 1:N+1
        global H lamPrev
        if i == 1
            lamPrev = laminitial;
        else
            lamPrev = result(i-1,numel(x0)-size(TI,2)+1:numel(x0));
        end
         H(1,:) = ones(1,size(TI,2))*Hx*cos(i*2*pi/(N));
         H(2,:) = ones(1,size(TI,2))*Hy*sin(i*2*pi/(N));
         hh(i,:) = [H(1,1),H(2,1)];
         LL(i,:) = lamPrev;
         %rutine
         [x,fval,exitflag,output,LAMBDA,grad,hessian] = ...
                fmincon(@Energie3,x0,[],[],Aeq,beq,lob,upb,@nonlincon,
                    options);
         result(i,:)= x;
         clear H lamPrev
         %lambda(i,:) = lamPrev;
     end

end
```

```
78 t2 = cputime;
79 time = t2-t1;
```

Listing B.2: CommandFileEvolutionA

```
1  clear all;cla;
2  t1 = cputime;
3  global p e t ts tsin ti TI PI C va vb vc vd T  alpha corners CORNERS ...
4  NumP NumT sm BaseGradient  IinBox TS pin iind Chys lamPrev Hess
5  % SPECIFY THE SETTING AND CREATE MESH
6  [dl,corners, CORNERS, p,e,t,ti,iind,NumP,NumT,IinBox,...
7  PI,TI,BD1,BD2,ts,LeftBoundaryIndex,RightBoundaryIndex,...
8           UpperBoundaryIndex,LowerBoundaryIndex] = Setting;
9  [sm,teziste,BaseGradient,TS] = PrepMag;
10 ITI = find(t(4,:)==2); %InnerTriangleIndex
11 tsin = zeros(1,numel(ITI));
12 for i = 1:length(ITI)
13     tsin(i) = ts(ITI(i));
14 end
15 %SET THE MINIMIZATION INITAL VALUES
16 casse = 5;
17 [U0,M0,L0,x0] = Initial4;
18 [Aeq,beq,lob,upb]=constrains4(casse,U0,M0,L0,x0,UpperBoundaryIndex,...
19                                LowerBoundaryIndex,LeftBoundaryIndex,
                                      RightBoundaryIndex);
20 %RUN THE MINIMIZATION RUTINE
21 %material properties v = [e1 e2 e12 e21 mx my]
22 C = MagElasTensor(1);
23
24 %  va = [ 0  0  0.0  0.0  1  1];%lambda = 1 , cervena
25 %  vb = [ 0  0  0.0  0.0 -1 -1];%lambda = 0 , modra
26 %  vc = [ 0  0 -0.0 -0.0 -1  1];%lambda = 1 , cervena
27 %  vd = [ 0  0 -0.0 -0.0  1 -1];%lambda = 0 , modra
28 va = [ -0.05  0.05  0  0  1  0];%lambda = 1 ,
29 vb = [ -0.05  0.05  0  0  0 -1];%lambda = 0 ,
30 vc = [  0.05 -0.05  0  0  0  1];%lambda = 1 ,
31 vd = [  0.05 -0.05  0  0 -1  0];%lambda = 0 ,
32 ZATEZ = 1;
33 alpha = 10^(-6); %konstanata
34
35 Chys = 0.1; %konstanta hzstereze
36 n = 30;
37 N = 2*(n+1);
38 %krok = linspace(-1,1,N);
39 %lamPrev = 0;
40 %f =  [0;
41 Hx = 0.4*10^(0);
42 Hy = 0;
43 T = zeros(4,size(TI,2));
44 T(2,:) = -0.2*10^(0)*ones(1,size(TI,2));
45 result = zeros(N,size(x0,2));
46
```

```
47 H(1,:)= ones(1,size(TI,2))*Hx;
48 H(2,:) = ones(1,size(TI,2))*Hy;
49 %lamPrev = x0(numel(x0)-size(TI,2)+1:numel(x0));
50 Hess = HessFun4;
51 %options = optimset('Algorithm','Active-Set','GradObj','on','GradConstr','on
       ');
52 % options = optimset('Algorithm','interior-point','Display','iter','GradObj
       ','on',...
53 %                    'GradConstr','on','Hessian','user-supplied','HessFcn',
       @HESSIAN);
54 %options=optimset('GradObj','on','GradConstr','off','Algorithm','trust-
       region-reflective');
55 options = optimset('GradObj','on','GradConstr','on','TolFun',10^(-13),'
       TolCon',10^(-13),'HessPattern',Hess);
56 %CHECK THE TYPE OF THE LOADING
57 %options = optimset('Algorithm','interior-point','Hessian','fin-diff-grads
       ',...
58  %              'SubproblemAlgorithm','cg','GradObj','on','GradConstr','on');
59
60 if ZATEZ == 1
61     for i = 1:N+3*(n+1)
62         i
63         global H lamPrev
64         if i<=n+1
65             H(1,:) = ones(1,size(TI,2))*Hx*(i-1)/n;
66         elseif i>3*(n+1)
67             H(1,:) = ones(1,size(TI,2))*(Hx*(i-1)/n-4*Hx);
68         else
69             H(1,:) = ones(1,size(TI,2))*(2*Hx-Hx*(i-1)/n);
70         end
71 %         rutine
72         if i == 1
73             [x,fval,exitflag,output,LAMBDA,grad,hessian] = ...
74             fmincon(@Energie2a,x0,[],[],Aeq,beq,lob,upb,@nonlincon4);
75         else
76             lamPrev = result(i-1,numel(x0)-4*size(TI,2)+1:numel(x0));
77             [x,fval,exitflag,output,LAMBDA] = ...
78             fmincon(@Energie2,x0,[],[],Aeq,beq,lob,upb,@nonlincon4,options);
79             LL(i-1,:) = lamPrev;
80             exitflag
81         end
82         result(i,:)= x;
83         hh(i,:) = [H(1,1),H(2,1)];
84         clear H lamPrev
85     end
86  elseif ZATEZ == 2
87      for i = 1:N
88         global H lamPrev
89         if i == 1
90             lamPrev = laminitial;
91         else
```

```
92                lamPrev = result(i-1,numel(x0)-size(TI,2)+1:numel(x0));
93            end
94            i
95             H(1,:) = ones(1,size(TI,2))*Hx*cos(i*2*pi/(N));
96             H(2,:) = ones(1,size(TI,2))*Hy*sin(i*2*pi/(N));
97             hh(i,:) = [H(1,1),H(2,1)];
98             LL(i,:) = lamPrev;
99             rutine
100            [x,fval,exitflag,output,LAMBDA,grad,hessian] = ...
101                   fmincon(@Energie34,x0,[],[],Aeq,beq,lob,upb,@nonlincon4);
102            result(i,:)= x;
103
104             clear H lamPrev
105            lambda(i,:) = lamPrev;
106       end
107
108 end
109 %Pllt(result);
110 %save('vysledek1', 'Ux', 'Uy','mx','my','lambda','H')
111 t2 = cputime;
112 time = t2-t1
113 PlotTest1(result,hh);
```

Listing B.3: CommandFileEvolutionB

Appendix C

Used statements

Several important theorems were mentioned and used witin the thesis, however no precise formulation was given. Therefore we include these into the Appendix to make the work more comprehensive and transparent. We state theorems without proofs. The reader is supposed to use links referring to individual theorem. More information about relaxation theory as well as proof of the theorem C.2 might be found in [6], for the proof of the theorem C.3 see [24]. For the proof of theorem C.4 clarify [34].

Theorem C.1. *Let X be a Banach space and let $I : X \to \bar{\mathbb{R}} = \mathbb{R} \cup +\infty$ be convex and lower semicontinuous, then I is weakly lower semicontinuous.*

Definition C.1. *$f : \mathbb{R}^{m\times n} \to \mathbb{R}$ is said to be quasiaffine if f and $-f$ are quasiconvex (see the definition 5.1.3).*

Theorem C.2. *(The relaxation theorem)*
Let $\Omega \subset \mathbb{R}^n$ be a bounded open set with Lipschitz boundary. Let $f : \mathbb{R}^{nm} \to \mathbb{R}$ be continuous and satisfying

$$a + \sum_{i=1}^{N} b_i |\Phi_i(A)|^{\beta_i} \leq f(A) \leq c + \sum_{i=1}^{N} d_i |\Phi_i(A)|^{\beta_i}$$

for every $A \in \mathbb{R}^{nm}$ and for some $a, c \in \mathbb{R}$, $N \geq 1$, $\beta_i > 1$, $d_i \geq b_i > 0$ and where $\Phi_i : \mathbb{R}^{nm} \to \mathbb{R}$, $i = 1, ..., N$ are quasiaffine. Let $u \in W^{1,\infty}(\Omega, \mathbb{R}^m)$, then there exists $\{u^s\}_{s=1}^{\infty}$, $u_s \in W^{1,\infty}(\Omega, \mathbb{R}^m)$ such that

i) $u^s = u$ on $\partial\Omega$,

ii) $\Phi_i(\nabla u^s) \rightharpoonup \Phi_i(\nabla u)$ in $L^{\beta_i}(\Omega)$, $i = 1, ..., I$, as $s \to \infty$,

iii) $\int_\Omega f(\nabla u^s(x))\,\mathrm{d}x \to \int_\Omega Qf(\nabla u(x))\,\mathrm{d}x$ *as* $s \to \infty$,

where Qf *is quasiconvex envelope of* f.

Definition C.2. *Let* X^* *be dual space to normed vector space* X *over* $\mathbb{R}$ *(or* $\mathbb{C}$*) and* X^{**} *be dual space to Banach space* X^*. *We define continuous linear transformation* $\kappa : X \to X^{**}$

$$\kappa_f(x) = f(x) \quad \forall x \in X \text{ and } f \in X^*.$$

Since mapping κ *preserve the norm, it is injective. The space* X *is called reflexive, if* κ *is bijective.*

Theorem C.3. *(Equivalent definition of reflexive space)*
Let X *be a Banach space, then the following are equivalent*

1. *The space* X *is reflexive.*
2. *The dual space of* X *is reflexive.*
3. *Every bounded sequence in* X *has a weakly convergent subsequence.*
4. *Every continuous linear functional on* X *attains its maximum on the closed unit ball in* X.

Theorem C.4. *Let* $\Omega \in \mathbb{R}^n$ *be a bounded set with Lipschitz boundary,* $p \in \langle 1, n)$, *then*

$$\forall q \in \langle 1, p^*) \quad W^{1,p}(\Omega) \hookrightarrow\hookrightarrow L^q(\Omega),$$

where $p^* = \frac{pn}{n-p}$.